



Yago Chamoun Ferreira Soares

**Rheological and thermal properties of multifunctional
hexagonal boron nitride dispersions based in xanthan gum for use
in water-based drilling fluids**

Tese de Doutorado

Thesis presented to the Programa de Pós-graduação em Engenharia Mecânica of PUC-Rio in partial fulfillment of the requirements for the degree of Doutor em Engenharia Mecânica.

Advisor: Prof^a. Mônica Feijó Naccache
Co-advisor: Prof. Ricardo Jorge Espanhol Andrade

Rio de Janeiro
April 2024



Yago Chamoun Ferreira Soares

**Rheological and thermal properties of multifunctional
hexagonal boron nitride dispersions based in xanthan gum for use
in water-based drilling fluids**

Thesis presented to the Programa de Pós-graduação em Engenharia Mecânica of PUC-Rio in partial fulfillment of the requirements for the degree of Doutor em Engenharia Mecânica. Approved by the Examination Committee:

Prof^a. Mônica Feijó Naccache

Advisor

Departamento de Engenharia Mecânica – PUC-Rio

Prof. Ricardo Jorge Espanhol Andrade

Co-advisor

Engenharia de Materiais e Nanotecnologia, Escola de Engenharia, Universidade Presbiteriana Mackenzie

Prof. Guilhermino José Macêdo Fehine

Engenharia de Materiais e Nanotecnologia, Escola de Engenharia, Universidade Presbiteriana Mackenzie

Prof. Diogo Elias da Vinha Andrade

Departamento de Engenharia Mecânica – UFRGS

Dr. Ivan Rosa de Siqueira

Departamento de Engenharia Mecânica – PUC-Rio

Dr^a. Lorena Rodrigues da Costa Moraes

Departamento de Engenharia Mecânica – PUC-Rio

Rio de Janeiro, April 29th, 2024

All rights reserved.

Yago Chamoun Ferreira Soares

The author holds a bachelor's degree in Petroleum Engineering from the Universidade Federal Fluminense (UFF) in 2017. He has participated in several national and international congresses presenting his articles. In 2019, he obtained a M. Sc. Degree in Mechanical Engineering from Pontificia Universidade Católica do Rio de Janeiro (PUC-Rio). In the doctor's degree, developed research in the field of thermoscience focusing on rheological characterization of non-Newtonian fluids.

Bibliographic data

Soares, Yago Chamoun Ferreira

Rheological and thermal properties of multifunctional hexagonal boron nitride dispersions based in xanthan gum for use in water-based drilling fluids / Yago Chamoun Ferreira Soares ; advisor: Mônica Feijó Naccache ; co-advisor: Ricardo Jorge Espanhol Andrade. – 2024.

140 f. : il. color. ; 30 cm

Tese (doutorado)–Pontificia Universidade Católica do Rio de Janeiro, Departamento de Engenharia Mecânica, 2024.

Inclui bibliografia

1. Engenharia Mecânica – Teses. 2. Fluidos de perfuração. 3. Propriedades reológicas. 4. Nitreto de Boro hexagonal oxidado. 5. Goma Xantana. 6. Condições de alta pressão e alta temperatura. I. Naccache, Mônica Feijó. II. Andrade, Ricardo Jorge Espanhol. III. Pontificia Universidade Católica do Rio de Janeiro. Departamento de Engenharia Mecânica. IV. Título.

CDD: 621

I dedicate this work to my family, who provided the greatest emotional support and stood by my side at every stage of this journey. To friends who shared laughter, challenges, and victories, making this journey smoother and more meaningful. To mentors and teachers, who shared their wisdom with me, imparting knowledge for my personal and professional growth. To all who, in some way, contributed to this chapter of my life, I express my deep gratitude.

Acknowledgments

First and foremost, I express my gratitude to God for endowing me with wisdom and a family that facilitated my education, providing a solid foundation and enabling me to gain admission to the Pontifical Catholic University, renowned for its excellent academic standards.

My heartfelt appreciation extends to my parents for their unwavering encouragement and both psychological and financial support, pivotal in the successful completion of my Doctor's degree in Mechanical Engineering.

Special thanks to my mentor, Mônica Feijó Naccache, and my co-advisor, Ricardo Jorge Espanhol Andrade, for their invaluable support in crafting this work. Their guidance has imparted profound insights into a subject of exceptionally high international significance.

I would like to thank Dante Daiki Yokoyama, Lidiane Cristina Costa, Josué Marciano de Oliveira Cremonezzi, Monica Netto, Hélio Ribeiro, Nathália Maria M. Fernandes and Lara Schimith Berghe whose assistance in the experimental procedure and carrying out the tests contributed to the development of this work.

I extend my thanks to my friends, not solely from academia but throughout life, for their constant encouragement. Their steadfast support has been a source of strength through the challenges of my life journey.

This study was financed in part by the Coordenação de Aperfeiçoamento de Pessoal de Nível Superior - Brasil (CAPES) - Finance Code 001. I would also like to thank the support provided by Fundo Mackenzie de Pesquisa (MackPesquisa, Project Number 181009), Conselho Nacional de Desenvolvimento Científico e Tecnológico (CNPq, Projects Number: 409917/2018-4; 140241/2019-1; 305109/2022-7), Fundação de Amparo à Pesquisa do Estado do Rio de Janeiro (FAPERJ), Fundação de Amparo à Pesquisa do Estado do São Paulo (FAPESP, Grant No. 2012/50259-8), Petrobras, Agência Nacional do Petróleo, Gás Natural e Biocombustíveis (ANP), Financiadora de Estudos e Projetos (FINEP) and Ministério da Ciência, Tecnologia e Inovação (MCTI) through the ANP Human Resources Program for the Oil and Gas Sector – PRH-ANP/MCTI.

Abstract

Soares, Yago Chamoun Ferreira; Naccache, Mônica Feijó (Advisor); Andrade, Ricardo Jorge Espanhol (Co-advisor). **Rheological and thermal properties of multifunctional hexagonal boron nitride dispersions based in xanthan gum for use in water-based drilling fluids**. Rio de Janeiro, 2024. 140p. Tese de Doutorado – Departamento de Engenharia Mecânica, Pontifícia Universidade Católica do Rio de Janeiro.

In recent decades, the demand for oil and gas has surged, prompting the identification of new oil fields in challenging reservoir environments those characterized by high-pressure and high-temperature (HPHT) conditions. The development of high-performance aqueous-based drilling fluids with tailored properties aims to enhance extraction processes in the oil industry and reducing environmental contamination mainly caused by oil-based fluids. This study aims to investigate how variations in parameters such as temperature, pressure and concentration impact the thermal and rheological properties of xanthan gum suspensions with oxidized hexagonal boron nitride (hBN-oxi) nanostructures. The thermal conductivity was significantly increased by the addition of hBN-oxi nanoparticles (6.0 wt% suspension) to the base fluid, reaching an increase of up to 12 % at 70 °C. These nanostructures played a crucial role in preserving the thermal conductivity of xanthan gum suspensions even at elevated temperatures. The presence of nanoparticles at the highest concentration induced a yield stress in the fluid and when subjected to high shear rates, experienced a viscosity drop of only 16 % at 80 °C. These adverse effects of temperature and pressure on viscosity were mitigated by the interaction between the polymer matrix and hBN-oxi. Overall, the study highlighted the potential of boron nitride as a nanoadditive for conventional drilling fluids, showing that properly designed formulations can improve performance even in challenging conditions without causing harm to the environment, thanks to the material's high thermal and chemical stability.

Keywords

Drilling fluids; rheological properties; oxidized hexagonal boron nitride; xanthan gum; HPHT conditions.

Resumo

Soares, Yago Chamoun Ferreira; Naccache, Mônica Feijó (Advisor); Andrade, Ricardo Jorge Espanhol (Co-advisor). **Propriedades reológicas e térmicas de dispersões multifuncionais de nitreto de boro hexagonal à base de goma xantana para uso em fluidos de perfuração à base de água.** Rio de Janeiro, 2024. 140p. Tese de Doutorado – Departamento de Engenharia Mecânica, Pontifícia Universidade Católica do Rio de Janeiro.

Nas últimas décadas, a procura por petróleo e gás aumentou, levando à identificação de novos campos petrolíferos em ambientes de reservatórios desafiadores, caracterizados por condições de alta pressão e alta temperatura (HPHT). O desenvolvimento de fluidos de perfuração de base aquosa de alto desempenho com propriedades personalizadas visa aprimorar os processos de extração na indústria petrolífera e reduzir a contaminação ambiental causada principalmente por fluidos à base de óleo. Este estudo tem como objetivo investigar como variações em parâmetros como temperatura, pressão e concentração impactam nas propriedades térmicas e reológicas de suspensões de goma xantana com nanoestruturas de nitreto de boro hexagonal oxidado (hBN-oxi). A condutividade térmica foi significativamente aumentada pela adição de nanopartículas de hBN-oxi (suspensão de 6,0% em peso) ao fluido base, atingindo um aumento de até 12% a 70 °C. Estas nanoestruturas desempenharam um papel crucial na preservação da condutividade térmica das suspensões de goma xantana, mesmo em temperaturas elevadas. A suspensão com concentração mais alta apresentou tensão limite de escoamento e quando submetida a altas taxas de cisalhamento, sofreu uma queda de viscosidade de apenas 16 % a 80 °C. Estes efeitos adversos da temperatura e pressão sobre a viscosidade foram mitigados pela interação entre a matriz polimérica e o hBN-oxi. No geral, o estudo destacou o potencial do nitreto de boro como nanoaditivo para fluidos de perfuração convencionais, mostrando que formulações adequadamente projetadas podem melhorar o desempenho mesmo em condições desafiadoras sem causar danos ao meio ambiente, graças à alta estabilidade térmica e química do material.

Palavras-chave

Fluidos de perfuração; propriedades reológicas; Nitreto de Boro hexagonal oxidado; Goma Xantana; Condições de alta pressão e alta temperatura

Summary

1. INTRODUCTION	16
1.1 Objectives	20
1.1.1 Specific objectives	21
1.2 Justification and relevance of the study	21
1.3 Thesis Outline	23
2. THEORETICAL FRAMEWORK AND LITERATURE REVIEW	24
2.1 Rheology	24
2.1.1 Non-Newtonian Fluids	24
2.1.1.1 Generalized Newtonian Fluids	26
2.1.1.1.1 Rheological Models	27
2.1.1.1.2 Thixotropic Fluids	29
2.1.1.1.3 Viscoelastic Fluids	30
2.1.2 Rheometry	31
2.2 Characterization Techniques	32
2.2.1 X-Ray Diffraction (XDR)	33
2.2.2 Raman Spectroscopy	34
2.2.3 Thermogravimetric Analysis (TGA)	34
2.2.4 Transmission Electron Microscopy (TEM)	35
2.2.5 Fourier Transform Infrared (FTIR)	36
2.2.6 X-Ray Photoelectron Spectroscopy (XPS)	36
2.2.7 Dynamic Light Scattering (DLS)	37
2.2.8 Potential Zeta	38
2.2.9 Scanning Electron Microscopy (SEM)	38
2.2.9.1 Cryo-SEM	39
2.2.10 Modified Transient Plane Source (MTPS)	39
2.2.11 Rheological Characterization	40
2.3 Drilling Fluid	41
2.3.1 Functions of drilling fluids	42
2.3.2 Drilling fluids properties	43
2.3.3 Operational challenges	44
2.3.4 Types of drilling fluid	48
2.3.4.1 Water-Based Muds (WBM)	49

2.3.4.2. Oil-Based Muds (OBM)	51
2.3.4.3. Pneumatic Fluids	52
2.3.5. Drilling mud additives	52
2.3.5.1. Nanomaterials based drilling fluid	53
2.4. Thermal Conductivity of Nanofluids	57
2.4.1. Thermal Conductivity measurements methods	57
2.4.2. Parameters that affect Thermal Conductivity	58
2.5. Hexagonal Boron Nitride (hBN)	61
2.6. Previous experimental work studies on water-based drilling fluids under high pressure and high temperature conditions	67
2.7. Xanthan Gum	71
3. MATERIALS AND METHODS	76
3.1 Materials	76
3.2 HBN oxidation and exfoliation process	76
3.3 Nanofluid Preparation	77
3.4 Morphological and structural characterizations	79
3.5 Thermal measurements	80
3.6 Rheological measurements	80
4. RESULTS AND DISCUSSIONS	84
4.1 hBN-oxi nanoparticles characterization	84
4.2 Thermal conductivity of hBN-oxi Suspensions	92
4.2.1 Effect of concentration on thermal conductivity	92
4.2.2 Effect of temperature on thermal conductivity	93
4.3 Shear Rheology of hBN-oxi Suspensions	95
4.3.1 Effect of concentration on rheological properties	96
4.3.2 Effect of temperature on rheological properties	103
4.3.3 Effect of pressure on rheological properties	110
5. FINAL REMARKS	115
6. REFERENCES	118

List of figures

Figure 1.1 – Representative difference between flat rheology and conventional drilling fluid.....	18
Figure 2.1 – Plots of shear stress versus shear rate for non-Newtonian and Newtonian fluids: (a) time-independent (b) time-dependent fluids (Chhabra and Richardson, 2011).....	25
Figure 2.2 – (a) viscosity x shear rate for time-independent fluids and (b) viscosity x time for time-dependent fluid.....	29
Figure 2.3 - Schematic diagram of basic tool geometries for the rotational rheometer: (a) concentric cylinders (couette), (b) cone-plate, (c) parallel plates and (d) double-gap (Hackley, 2001).....	31
Figure 2.4 – Circulation of drilling fluid inside the well (Vryzas and Kelessidis, 2017).....	42
Figure 2.5 – Safer operating mud window (Naganawa, 2015).....	45
Figure 2.6 – Representation of lost circulation of drilling fluid in regions where there is fracture (Feng and Gray, 2017).....	46
Figure 2.7 – Representation of permeability changes caused by clay swelling and migration of fines (Yang et al., 2019).....	47
Figure 2.8 – Classification of drilling fluids.....	48
Figure 2.9 – Composition of a typical water-based drilling mud (WBM) and of the additives (Martin, 2022).....	50
Figure 2.10 – Common challenges of nanofluid development (Taha-Tijerina, 2018)	55
Figure 2.11 – Scheme of nanoparticles sedimentation over time (Ponticorvo et al., 2022).....	56
Figure 2.12 – Brownian motion of the particle (Taha-Tijerina, 2013).....	57
Figure 2.13 – Schematic diagram of methods for measuring the thermal conductivity of nanofluids (Gonçalves et al., 2021).....	58
Figure 2.14 – Parameters that affect the thermal conductivity of nanofluids (Gonçalves et al., 2021).....	59

Figure 2.15 – Crystalline structures of hBN and graphite (Hod, 2012).....	61
Figure 2.16 – Boron nitride crystal structures: (a) cubic, c-BN; (b) hexagonal, hBN; (c) wurtzite, wBN and (d) rhombohedral, rBN (Nikaido et al., 2022).....	63
Figure 2.17 – Schematic of the liquid exfoliation process (Nguyen et al., 2016).....	65
Figure 2.18 – Liquid exfoliation with ultrasound in “good” and “poor” solvents (Lin et al., 2017).....	66
Figure 2.19 – Structure unit of xanthan gum (Rosalam and England, 2006).....	73
Figure 2.20 – Schematic representation of the order-disorder conformation of xanthan gum (Adapted from Ardila, 2021).....	73
Figure 3.1 – HBN-oxi preparation method.....	77
Figure 3.2 – Nanofluid preparation.....	78
Figure 3.3 – (a) Physica rheometer MCR501 and (b) Haake Mars III.....	81
Figure 4.1 – (a) X-ray diffractograms of the as-received and oxidized hBN compared to the diffraction pattern of the PDF card n. 34-0421; SEM images of (b) as-received and (c) oxidized hBN; and (d) hBN-oxi particle size histogram.....	85
Figure 4.2 – TEM images of hBN bulk (a), and hBN-oxi from a 10 mg mL ⁻¹ dispersion (b-c).....	86
Figure 4.3 – Raman spectra of exfoliated hBN-oxi samples.....	87
Figure 4.4 – XPS extended spectra (a) and the high-resolution spectrum obtained in the region of the binding energy of B1s, N1s, and O1s respectively for hBN-oxi (b-d).....	88
Figure 4.5 – Average size and zeta potential of hBN (a,b) and hBN-oxi (c,d) suspensions 1 mg mL ⁻¹ in a mixture of 20 % by volume of IPA and 80 % DI water.....	89
Figure 4.6 – FTIR spectra of (a) hBN bulk and (b) exfoliated hBN-oxi samples.....	90
Figure 4.7 – Representative TGA analysis of hBN-oxi sample.....	91
Figure 4.8 – SEM observations at different scales of pure XG (a,b,c) and XG with hBN-oxi 60mg.mL (d,e,f).....	91
Figure 4.9 – Thermal conductivity of samples for different hBN-oxi concentrations.....	93

Figure 4.10 - Influence of temperature on thermal conductivity of samples for different concentrations of hBN-oxi.....	94
Figure 4.11 – Flow curves of XG + H ₂ O and XG + 20 % IPA/H ₂ O (a) viscosity and (b) shear stress as a function of the shear rate.....	95
Figure 4.12 – Flow curve of XG solution with 20%IPA/H ₂ O performed at 1, 6, 14, 23, and 30 days after sample preparation.....	96
Figure 4.13 – Flow curves of various concentrations of hBN-oxi nanoparticles (a) viscosity x shear rate and (b) shear stress x shear rate. Lines from C.0 to C.3 show the Carreau-Yasuda model and lines of C.4 and C.5 show the Herschel-Bulkley model (C.0 – pure, C.1 – 0.5 wt.%, C.2 – 1.0 wt.%, C.3 – 1.5 wt.%, C.4 – 3.0 wt.% and C.5 – 6.0 wt.%).....	97
Figure 4.14 – Viscosity as a function of concentration at 0.01 s ⁻¹	100
Figure 4.15 – (a) Storage (G') and (b) loss (G'') modulus as a function of strain for different concentrations.....	101
Figure 4.16 – Strain sweep of pure XG and XG+ hBN-oxi with 15 and 60 mg mL ⁻¹	102
Figure 4.17 – (a) Storage (G') and (b) loss (G'') modulus as a function of frequency for different concentrations.....	103
Figure 4.18 – Influence of temperature on flow curves for suspensions (a) pure XG, and with hBN-oxi concentration of (b) 15, (c) 30 and (d) 60mg.mL ⁻¹ ...	105
Figure 4.19 – Flow curves of pure XG (C.0) and XG with concentration of 60 mg.mL ⁻¹ hBN-oxi (C.5) (a) shear stress x shear rate and (b) viscosity x shear rate.....	107
Figure 4.20 – Variation of viscosity with temperature for each concentration at rates of (a) 1 and (b) 1,000 s ⁻¹	107
Figure 4.21 – Loss and storage modulus as a function of deformation at different temperatures of samples of (a) pure XG, and with hBN-oxi concentration of (b) 15, (c) 30 and (d) 60mg.mL ⁻¹	109
Figure 4.22 – Loss and storage modulus as a function of frequency at different temperatures of samples of (a) pure XG, and with hBN-oxi concentration of (b) 15, (c) 30 and (d) 60mg.mL ⁻¹	110
Figure 4.23 – Flow curve of pure XG analyzing (a) effect of temperature at 0.1 MPa (b) effect of temperature at 30 MPa (c) effect of pressure.....	112

Figure 4.24 – Flow curve of XG with hBN-oxi concentration of 30 mg.mL⁻¹ analyzing (a) effect of temperature at 0.1 MPa (b) effect of temperature at 30 MPa (c) effect of pressure.....113

Figure 4.25 – Flow curve of XG with hBN-oxi concentration of 60 mg.mL⁻¹ analyzing (a) effect of temperature at 0.1 MPa (b) effect of temperature at 30 MPa (c) effect of pressure.....114

List of tables

Table 2.1 – Main industrial applications of xanthan gum (adapted by García-Ochoa et al., 2000).....	75
Table 3.1. The concentration of the hBN-oxi suspensions used for rheological and thermal studies.....	77
Table 3.2. Nanofluid formulations to analyze effect of nanoparticle concentration, temperature and pressure.....	78
Table 3.3. The dimensions of concentric cylinders system.....	81
Table 3.4. Range of Shear Rates in a Drilling Circulating System (Guo and Liu, 2011).....	82
Table 4.1. Fitting parameters for the Carreau-Yasuda Model of nanofluids with an hBN-oxi concentration of 0 up to 15 mg.mL ⁻¹	98
Table 4.2. Fitting parameters for the Herschel-Bulkley Model of nanofluids with an hBN-oxi concentration of 30 and 60 mg.mL ⁻¹	99
Table 4.3. Fitting parameters for the Carreau-Yasuda Model of the pure xanthan gum suspension.....	106
Table 4.4. Fitting parameters for the Herschel-Bulkley Model of suspensions with an hBN-oxi concentration of 60 mg mL ⁻¹	106
Table 4.5. $ \Delta\mu $ % with respect to the viscosity at 20 °C.....	108

“Temos que continuar aprendendo. Temos que estar abertos. E temos que estar prontos para espalhar nosso conhecimento a fim de chegar a uma compreensão mais elevada da realidade. ”

Thich Nhat Hanh

1. INTRODUCTION

The exponential growth in energy consumption, driven by population growth and urban industrialization, has spurred a surge in demand for oil and natural gas, the primary fuel sources (Blkooor et al., 2023). As many existing oil fields reach maturity and struggle to meet production demands, the exploration and production industry is turning its attention to untapped areas and ultra-deep formations (Bardhan et al., 2024). Additionally, environmental concerns underscore the urgency for improved and more efficient processes.

Any water depth greater than 1500 feet is normally considered deepwater. When the depth exceeds 7000 feet, it becomes part of the ultra-deepwater category (Zamora et al., 2000). Extracting in ultra-deep waters has great difficulties, such as operations carried out using remotely operated vehicles (ROV), large distances (both between the platform and the field and from the platform to the coast) and the conditions of the marine environment.

Operational challenges and considerations associated with deeper offshore exploration encompass a range of factors, including environmental and safety concerns, as well as technical intricacies. These include ensuring stability under high-pressure conditions, managing narrow margins of pore/fracture pressure gradients, preventing gas hydrate formation, addressing challenges related to drilling in salt formations, mitigating loss of circulation issues, and facilitating efficient cuttings transport (Alcázar-Vara et al., 2018). All these difficulties make the project costly, risky and long-duration (Eia, 2016). The cost of drilling onshore is relatively lower than the cost of drilling offshore. Water depth, well depth, reservoir high pressure and temperature, field size, and distance from shore are some of the major cost factors for offshore drilling. Due to these complex conditions, some challenges such as decreasing density, viscosity and other rheological properties of the drilling fluid make it difficult to meet the drilling objectives and generate mechanical problems (Oseh et al., 2023).

Drilling fluids can account for 15% to 18% of the total cost of well drilling, however they may also be entirely responsible for drilling issues (Hossain and Al-Majed, 2015; Leffler et al., 2011). To minimize the cost of fluids and to ensure an efficient drilling program, fluid properties must be maintained continuously during

the drilling operation. Therefore, the selection of the best drilling fluid under the most complex conditions requires a lot of study and analysis as to the impact that each of these issues presented has on the operation.

Aside from these considerations, drilling operations at greater depths are characterized by heightened temperatures and pressures, posing significant challenges in maintaining the rheological properties of drilling fluids (Herzhaft et al., 2001). Bentonite has served as a key component for controlling the rheological behavior and filtration properties of these fluids. While increased viscosity facilitates efficient transport of cuttings from the wellbore to the surface, excessive use of bentonite can lead to complications such as elevated drill pipe torque due to friction and heightened risk of drill pipe entrapment within the wellbore. Consequently, alternative approaches have been explored to enhance fluid viscosity without escalating the concentration of bentonite. Among these approaches, the incorporation of xanthan gum (XG), a biopolymer, has gained prominence. XG stands out as one of the most effective viscosity enhancers for water-based drilling fluids, particularly due to its remarkable performance under high-temperature and high-salinity conditions (Souza et al., 2017).

Maintaining the rheological properties of drilling fluids poses a considerable challenge in ultra-deep water operations, compounded by the extreme temperatures and pressures encountered, along with the potential for salt contamination. The substantial temperature differential between the seabed and the bottom of the well further complicates efforts to regulate yield stress and fluid viscosity. Additionally, the geothermal heat emanating from underground sources can induce fluid degradation (Zamora et al., 2000; Hu et al., 2011).

A recent concept that has been aimed by the oil industry is the “flat rheology”, shown in Figure 1.1, where the rheological properties would remain constant throughout the drilling stage. Drilling fluids with flat rheology have been shown to have higher performance. This is possible by carefully balancing the use of emulsifiers, wetting agents, rheology modifiers, and viscosifiers (Alcázar-Vara et al., 2018).

The drilling fluid's primary functions include suspending the cuttings (drilled solids) and conveying them to the surface, controlling formation pressure to maintain well stability, cooling and lubricating the bit, minimizing reservoir damage, preventing the influx of formation fluids (water, oil, gas) into the well,

reducing environmental impact, and inhibiting gas hydrate formation (Saboori et al., 2019). Among these functions, the most critical is to minimize the accumulation of rock fragments around the bit and throughout the well. Failure to continuously remove cuttings from the fluid results in rapid loss of its cleaning ability in the annulus, obstructing fluid passage (Asme, 2005).

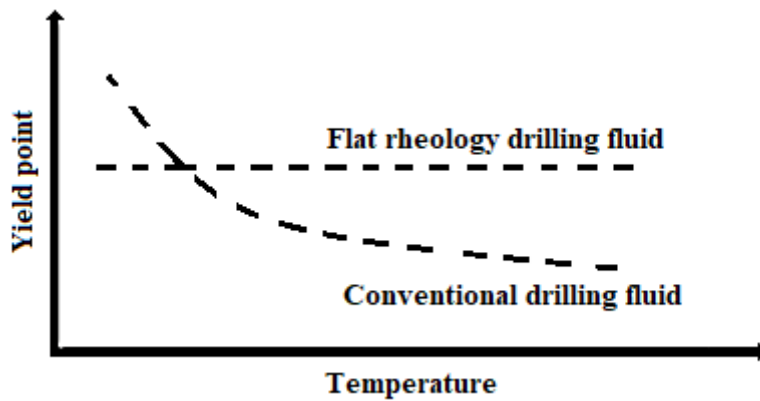


Figure 1.1 - Representative difference between flat rheology and conventional drilling fluid

The drilling fluid's primary functions include suspending the cuttings (drilled solids) and conveying them to the surface, controlling formation pressure to maintain well stability, cooling and lubricating the bit, minimizing reservoir damage, preventing the influx of formation fluids (water, oil, gas) into the well, reducing environmental impact, and inhibiting gas hydrate formation (Saboori et al., 2019). Among these functions, the most critical is to minimize the accumulation of rock fragments around the bit and throughout the well. Failure to continuously remove cuttings from the fluid results in rapid loss of its cleaning ability in the annulus, obstructing fluid passage (Asme, 2005).

Drilling fluid classification is primarily based on its composition, with the main criterion revolving around the continuous phase constituent. According to this classification, drilling fluids are categorized into oil-based drilling fluids (OBM) and water-based drilling fluids (WBM) (Tahr et al., 2023). OBM systems offer superior lubricating properties and boast advantages such as enhanced wellbore stability, reduced torque and drag, effective fluid loss control, and suitable rheological properties for borehole cleaning (Ozbayoglu et al., 2008). However,

they come with higher costs and environmental limitations. On the other hand, water-based drilling fluids (WBM) have been extensively utilized due to environmental concerns (Yang et al., 2023). Nonetheless, addressing the drawbacks related to the degradation of water-soluble polymers at elevated temperatures is necessary (Katende et al., 2019).

In recent years, the oil industry has increasingly embraced nanotechnology, with one of its applications being in drilling processes (Martin et al., 2023). This approach aims to tackle challenges by crafting high-performance fluids capable of functioning in high-pressure and high-temperature (HPHT) reservoirs while retaining their thermal and rheological properties and optimizing drilling hydraulics (Al-Yasiri and Al-Sallami., 2015). Moreover, the ability to produce tailored nanoparticles holds promise for developing customized fluids tailored to the requirements of each operator for addressing specific conditions. This underscores the significance of leveraging nanoparticles in formulating high-performance drilling fluids to overcome current and anticipated technical hurdles faced by the drilling industry (Vryzas and Kelessidis, 2017).

Nanotechnology has emerged as a transformative scientific field, driven by the recognition that the properties of materials are influenced not only by composition and structure, but also by shape and size. Nanoparticles exhibit improved physical and chemical properties compared to their particles at larger scales, made possible by innovative manufacturing technologies (Yu et al., 2009; Cao, 2004). These unique properties position nanoparticles as highly promising materials for engineering smart drilling fluids, tailored to meet the rigorous environmental demands associated with ultra-deepwater exploration.

Nanoparticles have unique properties, such as large surface area in relation to volume and size-dependent physical properties, which are capable of improving the properties of conventional fluids. (Taha-Tijerina, 2018; Kalhori et al., 2023). Suspension of nanometer-sized particles (from 1 to 100 nm) in a base-fluid define a nanofluid (Chai et al., 2018).

The emergence of nanofluids represents an advancement in thermal fluid technology, with the aim of improving heat transfer efficiency and potentially reducing energy costs (Ilyas et al., 2019). Choosing the appropriate material involves evaluating many properties. Therefore, experimental studies play a crucial role in building a comprehensive database of thermophysical properties, thereby

advancing understanding and outlining potential industrial applications (Rebello et al., 2023; Ibrahim et al., 2023).

Several materials such as ceramic oxides, nonmetallic solids (CuO, ZnO, TiO₂, SiO₂), metals (Cu, Ag, Au, Fe), carbon nanotubes (single and multiple wall) and graphene are used for the production of nanofluids (Taha-Tijerina, 2018). Carbon has the ability to combine with itself creating numerous stable compounds with different configurations (distinct molecular and structural forms) and physical properties (Farag and Helal, 2023). Boron nitride (BN) is a ceramic material with various crystalline structures, like to carbon (Lu et al., 2023). Among these structures, hexagonal boron nitride, hBN, stands out as the most stable, featuring a graphene-like arrangement formed by layers of sp²-hybridized atoms bonded hexagonally. Thanks to its chemical inertness and high in-plane thermal conductivity, hBN emerges as a promising material for drilling fluids (Ilhan, 2016; Lai et al., 2023). Its lubricating properties, coupled with exceptional thermal stability, oxidation resistance, and adsorption potential, make hBN superior to graphite for certain applications (Kostoglou et al., 2015; Ouyang, 2022; Huang et al., 2023; Mishra et al., 2023).

There are several polymers into which the nanoparticle can be inserted after its production and that are used in the petroleum industry as viscosifiers, shale stabilizers or filtrate controllers, such as carboxymethylcellulose (CMC), xanthan gum, guar gum, polyacrylamide, hydroxyethylcellulose (HEC), among others (Carico and Bagshaw, 1978). This study focuses on the incorporation of hBN-oxi into xanthan gum with an average molecular weight of 2×10^6 g.mol⁻¹. The choice of this biopolymer is due to its distinct and better properties compared to other polymers, such as resistance to mechanical degradation, excellent stability across a broad temperature range (0 to 100 °C) and pH (1 to 13), non-Newtonian behavior, high viscosity at low polymer concentrations and minimal viscosity sensitivity to salinity changes are among its notable features (Garcia-Ochoa et al., 2000; Vendruscolo et al., 2000).

1.1 Objectives

The development of more efficient drilling fluids through nanotechnology is capable of improving drilling processes in the petroleum industry as well as to

turn the process more sustainable and environment friendly. Therefore, the present work aims to investigate and evaluate the rheological and thermal properties of oxidized hexagonal Boron Nitride suspensions in xanthan gum, a biopolymer. The main objective of this work is to analyze how these suspensions behave with the variation of parameters such as: concentration of hBN nanoparticles used, temperature, pressure and time in order to obtain more efficient drilling fluids.

1.1.1 Specific objectives

- Produce oxidized hexagonal boron nitrite using the liquid exfoliation.
- Characterize and evaluate structurally and morphologically the 2D hBN-oxi nanolamellas produced through different characterization techniques.
- Prepare nanofluid composed of xanthan gum reinforced with hBN-oxi.
- Evaluate the thermal properties of hBN suspensions using the MTPS technique by varying parameters such as concentration and temperature in order to obtain characteristics of the sample's thermal behavior.
- Evaluate rheological parameters of suspensions with different concentrations as a function of temperature and pressure through flow curves and oscillatory measurements.

1.2 Justification and relevance of the study

From a scientific perspective, delving into the study of hBN suspensions in a simple base fluid with complex characteristics, especially in the context of non-Newtonian fluids, proves intriguing. This study is particularly crucial for technological advancements in the oil industry, necessitating a comprehensive understanding to enhance their applicability in the market.

The complete study of the mechanical behavior and nature of these fluids helps to investigate the rheological behavior of hBN suspensions since the

polymeric matrix has a rheological response dependent on particle-particle interactions with the polymeric chain, in determining its applications and in improving their properties, seeking to optimize the processes in which they are inserted (Taha-Tijerina, 2018).

The performance of drilling fluids is even more relevant in deepwater regions, where the technological challenges of drilling in these extreme conditions generate significant operational risks, as well as very high costs during the development of this type of field. Therefore, drilling deeper wells requires the development and use of exceptional drilling fluids, capable of continuous good performance even under the most complex conditions (Camero, 2000).

The drilling industry stands to gain substantial benefits from the advancements in nanotechnology. The most promising prospects lie in the utilization of nanoparticles in drilling fluids, aiming to formulate intelligent fluids that exhibit optimal properties across a broad range of operational conditions. Furthermore, the potential for crafting customized nanoparticles will play a crucial role in drilling fluid development, allowing the creation of tailored fluids that meet the specific needs of each operator to handle distinct conditions. This justifies the application of nanoparticles to formulate high-performance drilling fluids, which holds the potential to overcome current and future technical challenges faced and anticipated by the drilling industry (Vryzas and Kelessidis, 2017).

Despite several studies available (Ilhan et al., 2016; Navaneethakrishnan et al., 2019; Liu et al., 2019; Cheng et al., 2020; Ysiwata-Rivera et al., 2020; Urbaniak et al., 2022), hBN is relatively a recently explored nanoparticle that has already had some of its thermal, rheological and lubrication properties analyzed. Considering the fact that nanofluids containing hBN are promising candidates for application in the petroleum industry as multifunctional water-based drilling fluid even in aggressive environments to the detriment of their characteristics, there is a need to study how these nanosheets will affect the rheological and thermal characteristics of suspensions based on xanthan gum. Water-based offers a more ecological choice compared to oil-based, which has made companies opt for its use and as a result, some additives, such as nanoparticles, have been used to improve its performance in HPHT conditions.

In addition, there is a lack of studies on the viscoelastic properties of suspensions with this nanomaterial and how the thermal and rheological properties

of these nanofluids are affected at high temperatures and pressures. Therefore, this work aims to develop a complete rheological study about the hBN/xanthan gum system, varying some parameters such as concentration, temperature and pressure with values that simulate the conditions of an oil reservoir, in addition to performing thermal tests of these suspensions in order to develop more effective water-based drilling fluids, ensuring safer operations at reduced expenses.

1.3 Thesis Outline

This text is structured into four chapters. Chapter 1 provides an introduction to the work, outlining the objectives and the overall structure. Chapter 2 delves into important concepts in rheology, the operational modes of characterization techniques and a literature review is presented, covering the areas of study necessary for the research's development. Chapter 3 details the materials used, the method for obtaining oxidized hexagonal Boron Nitride, the nanofluid preparation by the two-step method and the techniques employed for the characterization of hBN-oxi suspensions. Experimental results are presented in Chapter 4. Chapter 5 offers conclusions drawn from the case study conducted in this work, along with suggestions for future research. The 6th and final chapter provides the bibliographic references that served as the foundation for this research.

2. THEORETICAL FRAMEWORK AND LITERATURE REVIEW

2.1 Rheology

Rheology is the scientific discipline dedicated to the study of material flow and deformational behavior under specific stresses during a defined timeframe and under particular thermodynamic conditions (Tanner and Walters, 1998). The significance of exploring this scientific realm lies in its broad impact on all material phases across various sectors. The rheological properties play a crucial role, influencing aspects ranging from the formulation's development and stability to the product's processing and performance. Understanding rheology is instrumental in designing equipment such as pumps, pipes, agitators, heat exchangers, and homogenizers. Furthermore, it contributes to quality control processes for intermediate and final products, including assessing expiration dates in sectors like food and cosmetics. Consequently, the importance of rheological techniques is underscored in diverse industrial segments, including cosmetics, food, polymers, petroleum, paints, pharmaceuticals, personal hygiene, and beyond.

2.1.1 Now-Newtonian Fluids

To describe different fluid behaviors, numerous mathematical models have been developed, each tailored to account for the unique characteristics of specific fluid types. Fluids, in general, fall into categories such as Newtonian or Non-Newtonian. Non-Newtonian or complex fluids are those that do not present a proportional relationship between shear stress and shear rate, as in the case of Newtonian fluids. The constitutive equation of the Newtonian fluid is given by: $\bar{\mathbf{T}} = \eta(\dot{\gamma})\bar{\mathbf{D}}$, where $\bar{\mathbf{T}}$ is the extra stress tensor, $\eta(\dot{\gamma})$ is the viscosity function and $\bar{\mathbf{D}}$ is the rate-of-strain tensor. Additionally, defined as: $\tau = \sqrt{(1/2)\bar{\mathbf{T}}^2}$ and $\dot{\gamma} = \sqrt{(1/2)tr\bar{\mathbf{D}}^2}$, τ and $\dot{\gamma}$ are, respectively, the second invariants of extra stress and rate-of-strain tensors. For a flow subject to simple shear the equation can be simplified as: $\tau = \eta\dot{\gamma}$, where τ is the shear stress and $\dot{\gamma}$ is the shear rate.

Different kinds of non-Newtonian fluids have different rheological behaviors, such as shear thinning, dilatant, viscoelasticity, thixotropy, among others (Irgens, 2014 and Krishnan et al., 2010). Selecting the correct rheological model is crucial and depends on the fluid category, as these models determine parameters like gel strength, apparent viscosity, plastic viscosity and yield point (Agwu et al., 2021). These properties define the behavior of the fluid, including its ability to suspend and transport cuttings from the wellbore to the surface, one of the main characteristics that a drilling fluid needs. Figure 2.1 illustrates the relationship between shear stress and shear rate for various types of fluids. This figure will be discussed in section 2.1.1.1. and 2.1.1.2.

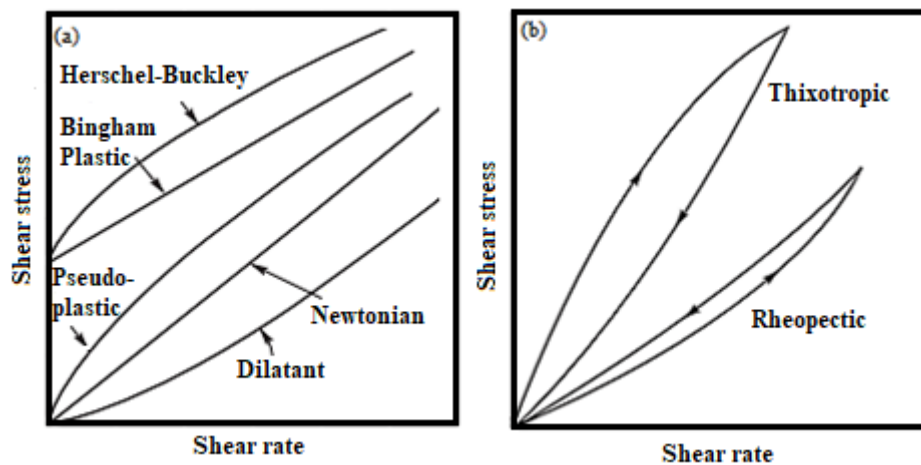


Figure 2.1 – Plots of shear stress versus shear rate for non-Newtonian and Newtonian fluids: (a) time-independent (b) time-dependent fluids (Chhabra and Richardson, 2011)

Some complex fluids can be modeled as Generalized Newtonian Fluids, these fluids are referred to as time-independent. Fluids in which the shear rate at any point is solely determined by the shear stress at that specific point and instant. Or more complex fluids are termed time-dependent fluids, like thixotropic, where the relationship between shear stress and shear rate is influenced not only by the current conditions but also by the duration of shearing and the kinematic history of the fluid. Moreover, another kind of time-dependency are the viscoelastic fluids, fluids that exhibit characteristics of both ideal fluids and elastic solids, showing partial elastic recovery after deformation (Chhabra and Richardson, 2011).

2.1.1.1. Generalized Newtonian Fluids

According to Deshpande (2010), for time-independent fluids that do not exhibit a minimum stress requirement, known as yield stress (τ_y), the viscosity can respond in three ways with increasing shear rate. In dilatant fluids, viscosity increases due to the disorder and approximation of molecules mechanism. In the case of Newtonian fluids, viscosity remains constant, while in pseudoplastic fluids, viscosity decreases. For suspensions where there are particles in the sample, this reduction in viscosity can be attributed to the fact that when the fluid is at rest, particles are randomly oriented and closely packed. As the shear rate increases, these particles align in the direction of flow, reducing resistance to flow (Breit, 2017).

The yield stress (τ_y) is a crucial rheological property used to assess the suitability of a material for various applications. However, there is no consensus on the definition of the yield point or on the techniques for measuring it. Therefore, establishing a unique value for the yield point is essential, yet challenging (Zakani and Grecov, 2020). A frequently used technique to measure yield stress involves extrapolating the shear stress versus shear rate curve to the point where it intersects the shear stress axis at zero shear rate. This value is known as the dynamic yield stress. The results obtained through this method can be significantly affected by the range of shear rates considered and the rheological model employed for the extrapolation. In contrast, the static yield stress refers to the shear stress required to start the flow of a fluid that is initially stationary (Parmar et al., 2008).

The viscoplastic fluid exhibits a distinctive trait, undergoing irreversible deformation once the minimum shear stress is surpassed initiating the flow of the fluid. This type of fluid has two non-Newtonian characteristics, yield stress and pseudoplasticity. As it is also a shear-thinning (or pseudoplastic) fluid, once the applied stress exceeds the yield stress, the fluid begins to flow and its viscosity decreases with increasing shear rate (Chhabra, 2010).

In the context of drilling fluids, the shear-thinning behavior plays a crucial role in facilitating the pumping of the fluid through the annular regions during drilling activities. Nonetheless, frequent shutdowns are required, and the drilling fluid must possess the capability to suspend cuttings, a feat made possible by the presence of the yield stress (Coussot et al., 2004.)

2.1.1.1.1. Rheological Models

In the literature, many mathematical models can be found describing the different rheological behaviors. The most common models to be used to describe the viscosity of time-independent materials are the power law, Carreau-Yasuda, Herschel-Bulkley and Bingham models and all equations will be shown below for a flow subject to simple shear.

The power-law model is an essential representation for describing the behavior of shear-thinning fluids without yield stress. This a mathematical relationship, depicted in Equation (1), correlates the apparent viscosity ($\eta(\dot{\gamma})$) with shear rate ($\dot{\gamma}$). Its simplicity is advantageous, making it a valuable tool in fluid dynamics analysis. The power-law model, as described by Morrison et al. (2001), comprises two parameters crucial for characterizing fluid behavior: K is the consistency coefficient and n the flow behavior index (dimensionless).

$$\eta(\dot{\gamma}) = K\dot{\gamma}^{n-1} \quad (1)$$

A model describing viscoplastic fluid behavior is the Bingham model, with its equation aligning with the Herschel-Bulkley model when n equals 1.

$$\eta = \begin{cases} \frac{\tau_y}{\dot{\gamma}} + \mu_p, & \text{if } \tau \geq \tau_y \\ \infty & , \text{if } \tau < \tau_y \end{cases} \quad (2)$$

Where μ_p = plastic viscosity (Pa.s) and τ_y = dynamic yield stress (Pa).

When the stress is below the yield stress, the fluid's viscosity tends toward infinity, signifying a state where it does not flow. The flow behavior of a viscoplastic fluid is delineated by two well-defined regions: the undeformed regions, where stresses are less than the yield stress; and the deformed regions, which manifest when stress levels surpass the yield stress. Categorizing these zones is crucial for discerning key flow attributes, including pressure drop across the flow and the volume of fluid that may stay immobile within a designated flow region. Consequently, investigating the flow pattern and evaluating its susceptibility to rheological and kinematic parameters holds fundamental significance.

The Herschel-Bulkley model is another mathematical representation that characterizes fluids experiencing a substantial alteration in material structure due to an initial stress (Herschel and Bulkley, 1926; Gavrilov et al., 2017). The equation for this model is provided below:

$$\eta = \begin{cases} \frac{\tau_y}{\dot{\gamma}} + K\dot{\gamma}^{n-1}, & \text{if } \tau \geq \tau_y \\ \infty & , \text{if } \tau < \tau_y \end{cases} \quad (3)$$

Where τ_y (Pa) represents the dynamic yield stress, η (Pa.s) denotes viscosity, $\dot{\gamma}$ (s^{-1}) represents shear rate, K (Pa.sⁿ) stands for the fluid consistency index, and n is the Power-Law index.

The consistency index indicates the degree of resistance to fluid flow, that is, the higher the K value, the more viscous the fluid will be when comparing for the same imposed shear rate.. A high value of K facilitates the transport of cuttings from the bottom of the well to the surface during drilling or circulation of fluid inside the well. The behavior index (n) indicates the degree of departure of the fluid from the Newtonian model. If the value of n is less than 1, we have a pseudoplastic fluid (exhibiting shear thinning), while a value greater than one indicates a dilatant (shear thickening) fluid. Pseudoplastic fluids present a reduction in viscosity with an increase in the shear rate (flow), which is interesting for drilling fluids, as lower viscosity values imply lower pressure loss values in the well (Machado, 2002).

The Carreau-Yasuda model is another empirical equation used to fit non-Newtonian data (Bird et al., 1987). This model describes pseudoplastic flow with asymptotic viscosities at zero (η_0) and infinite (η_∞) shear rates, and without yield stress. The Carreau-Yasuda model is suitable for fluids that are beginning to thin and can be used to describe polymeric emulsions and solutions.

$$\eta(\dot{\gamma}) = \eta_\infty + (\eta_0 - \eta_\infty)[1 + (\lambda\dot{\gamma})^a]^{\frac{n-1}{a}} \quad (4)$$

Where η_0 (Pa.s) is the theoretical dynamic viscosity at a zero rate of shear, η_∞ (Pa.s) is the viscosity at infinity shear rate, λ (s) is the characteristic relaxation time, n is the power-law index, and a is a parameter that is related to the breadth of the transition region between the zero-shear-rate and the power-law region.

2.1.1.2 Thixotropic Fluids

Materials exhibiting a variation in viscosity over time at a constant shear rate can be categorized as thixotropic or rheopectic fluids. These materials exhibit a specific time duration for the viscosity change, after which it remains constant regardless of the applied shear rate. This phenomenon is reversible, as the fluid returns to its initial configuration and regains its initial apparent viscosity upon the removal of shear stress. Thixotropic fluids experience a breakdown in their structure as the shearing time prolongs, leading to a reduction in viscosity. Conversely, rheopectic fluids demonstrate an increase in viscosity with extended shear time under constant conditions (Irgens, 2014).

Thixotropic effects are evident in numerous industrially relevant materials, including drilling fluids. The necessary conditions for achieving thixotropy can be met with various types of colloidal particles and are attainable at low concentrations for suspensions containing bentonite and synthetic laponite (Huynh et al., 2005 and Mewis et al., 2009). Thixotropic behavior becomes apparent in ramp tests of shear stress or shear rate. The resulting test outcome is termed a hysteresis area, providing a widely employed method for assessing and quantifying the material's thixotropic properties (Divoux et al., 2013).

An alternative means of depicting the rheological characteristics of shear-time-independent or dependent fluids is by plotting the apparent viscosity against the shear rate, as illustrated in figure 2.2.

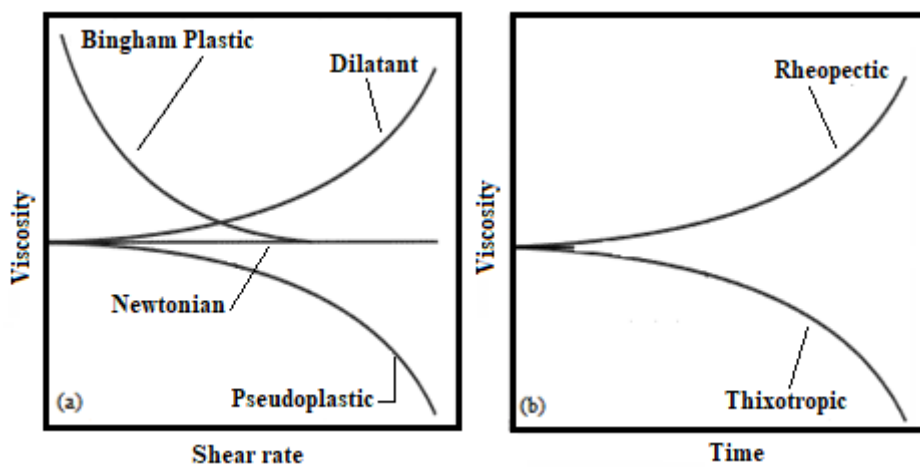


Figure 2.2 – (a) viscosity x shear rate for time-independent fluids and (b) viscosity x time for time-dependent fluid

2.1.1.3 Viscoelastic Fluids

Viscoelastic materials exhibit a mechanical behavior that lies between the Hookean characteristics of an elastic solid and the Newtonian behavior of a viscous fluid. In other words, these materials possess the capacity to dissipate energy during deformation through flow and subsequently recover their original shape when referring to a viscoelastic solid or recovering only a part of their original shape if it is a viscoelastic fluid. However, like any model, these definitions are idealized and may not fully capture the complexity of real materials. Many materials exhibit behavior that falls between that of elastic solids and viscous fluids, defining an intermediate response known as viscoelasticity.

According to Barnes et al. (1989), viscoelasticity is a time-dependent phenomenon exclusive to polymer systems. At the molecular level, when a constant stress is applied to the entangled structure of polymers, the molecules exhibit a resistant reaction to maintain a more stable conformation. Prolonged application of stress causes polymer chains to slide among each other, deforming the entangled structure. Upon stress removal, molecules in an elongated conformation tend to revert to their initial configuration, representing the most stable thermodynamic state.

The viscoelastic characteristics can be categorized into two domains: linear viscoelastic region (LVR) and non-linear viscoelastic. In the non-linear viscoelastic domain, substantial deformations are imposed, leading molecules to deviate from their equilibrium state. The structural composition experiences alterations as the fluid deforms, and the viscoelastic properties become influenced by both the shear rate and the deformation kinematics (Ferry, 1980).

Within the LVR, polymer molecules maintain proximity to their equilibrium state due to small and gradual deformations. This condition facilitates the structural characterization of the material. One crucial test in this regime is the small amplitude oscillatory shear (SAOS), which enables the evaluation of a material's viscoelasticity through two parameters: the storage modulus (G'), providing an elastic measurement of the material, and the loss modulus (G''), measuring the fluid's ability to dissipate energy in the form of heat (Ferry, 1980).

While subjecting the drilling fluid to deformation, the elastic property plays a crucial role in storing energy, impacting the pressure drop and fluid flow

behavior. Consequently, understanding viscoelasticity becomes essential, encompassing properties like solid suspension, gel structure, gel strength, and hydraulic sagging. To characterize the viscoelastic behavior of a drilling fluid mixture, a rheometer can perform tests, such as oscillatory tests, providing insights into the significance of viscoelastic properties (Bui et al., 2012).

2.1.2. Rheometry

Various rheological properties can be acquired using a rotational rheometer. This instrument measures the stress and deformation of materials subjected to a drag flow, which can be induced by a rotational (steady flow) or oscillating (oscillatory flow) movement, of a geometry at an angular velocity (Miri, 2011). Figure 2.3 depicts several geometries that can be attached to the rheometer, such as concentric cylinders (Couette), cone-plate, parallel plates, and double-gap. The selection of these geometries depends on the desired range of viscosity and shear rate for obtaining experimental measurements, as well as the nature of the fluid being studied.

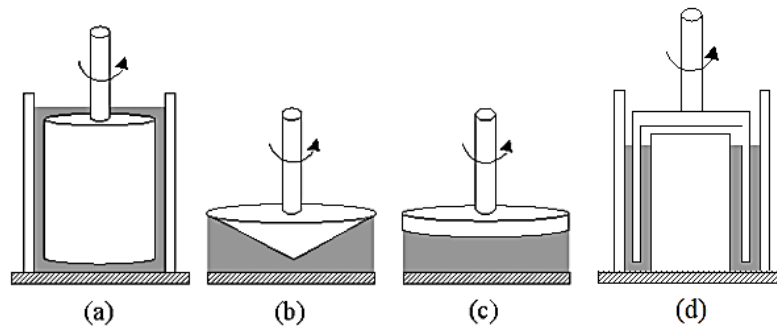


Figure 2.3 - Schematic diagram of basic tool geometries for the rotational rheometer: (a) concentric cylinders (couette), (b) cone-plate, (c) parallel plates and (d) double-gap (Hackley, 2001).

The geometries that were used in this work are cone-plate and concentric cylinders. Cone-plate rheometry offers the advantage of a well-defined flow, allowing for accurate interpretation. It requires a small sample volume and is easily cleaned. The primary benefit lies in the uniform application of shear rate throughout the sample. However, limitations exist, particularly concerning the size of particles within the sample, which should be restricted to 10–20% of the truncation height of

this geometry. Ideally, particles should be smaller than 5–20 μm to prevent jamming the gap and irregularities in data. Caution is necessary at high shear rates, as there is a risk of material escaping between the plates. Additionally, this geometry is highly susceptible to sedimentation (Miri, 2011).

Concentric cylinders systems feature a unique geometry that one cylinder is stationary and the other is set in motion with either a constant velocity or constant torque and ensures a substantial contact area between the sample and the surface of the geometry. This design enables testing with high torque resolution, especially for low-viscosity liquids (Ghanbari et al., 2020). The system's advantages include the expansive surface area it exposes with just a small amount of sample and its excellent thermal stability.

The challenge of wall slip, which commonly impacts rheometer readings across various mentioned geometries, can be mitigated by employing surfaces with grooves, characterized by a high level of roughness (Barnes, 1995).

Within these specific geometries, an applied force at the top or the bottom of the rheometer generates a torque, inducing movement in the geometry. This movement imparts velocity to the fluid confined in the gap between the upper and lower components of the geometry. The velocity is regulated by an internal resistance, representing viscosity (Macosko, 1994).

The rotational rheometer can operate under strain or stress control. In the case of strain control, a specified shear rate is applied, and the resulting stress is observed. On the other hand, in a stress-controlled rheometer, a predetermined stress is applied, and both the resulting stress and the deformation can be monitored (Macosko, 1994).

2.2. Characterization Techniques

Nanotechnology deals with structures on the nanometer scale, specifically at dimensions around 10^{-9} meters. These structures are exceedingly minute, rendering them invisible and untouchable to the human eye. Consequently, to gather information about these structures, it is imperative to employ equipment capable of interacting at the molecular and atomic levels. The characterization of these nanoparticles is crucial for analyzing the physical and chemical properties of a polymeric nanofluid (Kaufmann, 2003).

Material characterization involves acquiring information about a material's composition, structure, morphology, and general physical and chemical properties through the interaction of a signal—whether electrical, luminous, or thermal—with a portion of that material. Consequently, any material characterization entails subjecting the material to a disturbance. Examining the material's response to this disturbance enables the extraction of valuable information. Various characterization techniques exist, tailored to the specific interests associated with each material. Once the material's characteristics are identified, its nature and potential applications can be established (Cao, 2004).

A well-done characterization provides insights into the material under analysis, indicating whether it is a single crystal or polycrystalline, detailing its shape, size, particle distribution, the presence of defects within the crystal, the distribution of impurities, and whether the crystal surface is non-homogeneous or has absorbed layers (Kaufmann, 2003).

Several considerations should be taken into account when characterizing a material, including factors such as the sample's placement in the equipment, the quantity and concentration of the sample, and whether the sample is exposed to the atmosphere, among others. A comprehensive characterization of a sample cannot be achieved by applying a single technique. It is essential that the test responses align and complement each other, progressively providing more information about the sample with each conducted test.

The data obtained will undergo analysis using techniques such as X-Ray diffraction (XRD), Raman Spectroscopy, Thermogravimetric Analysis (TGA), Transmission Electron Microscopy (TEM), Fourier Transform Infrared (FTIR), X-Ray Photoelectron Spectroscopy (XPS), Dynamic Light Scattering (DLS), Potential Zeta, Scanning Electron Microscopy (SEM) and Modified Transient Plane Source (MTPS).

2.2.1. X-Ray Diffraction (XDR)

X-Ray Diffraction patterns have been widely used in nanoparticle research as a primary characterization technique to gather information about crystalline structure, crystal size, and interlayer distance (Cao, 2004).

Diffraction is a phenomenon inherent to wave motion, observed when a wave is "deformed" by an obstacle with dimensions comparable to its wavelength. In the case of X-rays, whose wavelength is on the order of Angstroms (10^{-10}m), they only undergo diffraction when interacting with atomic-level structures (Faraldos and Goberna, 2021).

X-Ray Diffraction is a non-destructive technique primarily used for characterizing crystalline materials. Essentially, it involves bombarding electromagnetic radiation onto a sample positioned between the source and the detector, resulting in the scattering of this beam. This enables the study of the effects caused by the material on the diffraction beam, characterizing the crystalline structure of the material. Atoms within the crystal act as X-ray scattering centers (Faraldos and Goberna, 2021).

2.2.2. Raman Spectroscopy

This non-destructive technique involves directing a monochromatic beam onto the surface of a material, leading to absorption and scattering. The laser produces the beam directed towards the sample. Mirrors and a focusing element improve the signal quality as it reaches the detector after dispersing within the sample. Upon reaching the sample, both elastic and Raman radiation scatter. It is crucial to eliminate elastic scattering, ensuring that only the Raman signal reaches the spectrometer (Faraldos and Goberna, 2021).

Raman scattering is a phenomenon observable when a small fraction of the scattered light exhibits energy distinct from that of the incident light, even though the scattered light may possess energy equal to that of the incident light (Cao, 2004). It is employed for characterizing materials, distinguishing between crystalline and amorphous structures. The objectives of this tool encompass investigating vibrational spectra, exploring electronic structure, and identifying the types of bonds occurring between the atoms within this structure (Kaufmann, 2003).

2.2.3. Thermogravimetric Analysis (TGA)

A technique is considered thermoanalytical when it necessarily meets three fundamental conditions. Firstly, it must measure a specific physical property.

Additionally, the resulting measurement needs to be expressed, either directly or indirectly, as a function of temperature. Lastly, the measurement must be carried out using a controlled temperature program. These conditions define the thermoanalytical nature of the technique, emphasizing the significance of the relationship between the measured physical property and the controlled temperature in the process (Faraldos and Goberna, 2021).

This is a thermoanalytical technique that assesses the thermal behavior of materials using a thermobalance where the sample is positioned for analysis. The sample undergoes heating, and throughout this process, the loss or gain of mass can be monitored relative to time or temperature under controlled atmospheric conditions (Ebnesajjad, 2013).

A curve depicting the variation of mass with temperature provides information regarding the thermal stability and composition of the original sample, as well as the thermal stability and composition of any intermediates that may form during the analysis. It also offers insights into the composition of the residue remaining at the end of the process (Faraldos and Goberna, 2021).

2.2.4. Transmission Electron Microscopy (TEM)

Utilizing images is a common practice for estimating the size of nanoparticles, whether in their pre-dispersion state or when already dispersed in a fluid. Additionally, some researchers leverage these techniques to assess the stability of nanofluids by examining the aggregation state of the particles (Barrett et al., 2013).

This method proves valuable in revealing details of materials at the nanoscale through high magnification. As electron microscopy has advanced, this approach has facilitated the extraction of properties from nanoscale materials, encompassing aspects like morphology, crystalline structure, composition, and topography. Insights into the morphology of nanomaterials are instrumental in discerning characteristics such as shape, size, strength, and ductility of particles (Zhou et al., 2023).

This method utilizes an electron beam as the radiation source directed onto a sample for observation, resulting in multiple interactions that can be captured. Despite their simplicity, these techniques offer a high degree of detail in image

acquisition. The electron beam interacts sufficiently with the sample as it traverses through it. The sample is positioned between the electron source and a screen, where the magnified image is formed through the impact of transmitted and diffracted electrons (Faraldos and Goberna, 2021).

2.2.5. Fourier Transform Infrared (FTIR)

In chemical analysis, infrared spectroscopy stands out as one of the most crucial techniques. This importance arises from the fact that the absorption bands observed in an infrared spectroscopy spectrum correspond to the vibration frequencies of the bonds between the atoms of a compound. Given that each molecule is a unique combination of atoms and bonds, the infrared spectrum serves as a distinct identification for each compound by investigating the composition of a sample or providing evidence for the presence of specific functional groups. Therefore, it proves to be a powerful tool in qualitative analysis (Ferraro and Basile, 2012).

The measurement process involves recording the amount of energy transmitted by a beam of infrared radiation as it passes through the sample. When a molecule absorbs radiation, it enters an excited energy state, a phenomenon occurring when the radiation frequency matches the vibration frequency of the bond, thereby amplifying the vibration's amplitude. The frequency or wavelength of absorption is contingent upon factors such as the relative masses of atoms, bond strengths, and the structural arrangement of atoms within the compound (Ismail et al., 1997).

2.2.6. X-Ray Photoelectron Spectroscopy (XPS)

X-Ray Photoelectron Spectroscopy stands as a non-destructive technique and a surface chemical characterization method that offers insights into surface activity, elemental composition, and the electronic state of elements within a material. The XPS spectrum is obtained by exposing the sample to an X-ray beam and assessing both the number of electrons and their kinetic energy. This powerful technique is employed to ascertain the surface composition of materials through elemental identification, analyze the relative abundances of these components on

surfaces semi-quantitatively, and determine the chemical state of polyvalent ions by measuring the binding energies of elements, providing crucial information related to the nature and strength of their chemical bonds (Baer et al., 2019).

XPS operates based on the photoelectric effect, leading to the emission of electrons from atoms in response to incident electromagnetic radiation. According to Einstein's prediction, photoelectrons would be produced from a material when the energy of the incident photons exceeded the binding energy of the electrons in that material. The energy involved in this process is directly proportional to frequency and remains independent of the intensity or duration of exposure to incident electromagnetic radiation. The kinetic energy of the emitted electron is connected to the binding energy of each electron. Considering that atoms possess multiple orbitals in distinct energy states, the result is a spectrum of emitted electrons with varying binding energies, ultimately forming an XPS spectrum (Stevie and Donley, 2020).

2.2.7. Dynamic Light Scattering (DLS)

Dynamic Light Scattering (DLS) quantifies Brownian motion and establishes its correlation with particle size. Brownian motion entails the unpredictable movement of particles resulting from the constant collisions with solvent molecules in their vicinity. The pace of Brownian motion is inversely proportional to the size of the particle or molecule; larger entities experience slower Brownian motion, while smaller particles are propelled further by solvent molecules, leading to quicker movements (Rajwar et al., 2022).

This technique is employed to determine the size of nanoparticles in colloidal suspensions or polymeric solutions, explore the stability of formulations, and identify the presence of aggregation or agglomeration. Measuring the hydrodynamic size of particles is done by observing the scattering of light from a laser as it passes through the colloidal solution. The analysis involves monitoring the modulation of the intensity of scattered light over time (Raval et al., 2019). The Brownian motion of particles is directly linked to their hydrodynamic diameter, with smaller particles exhibiting faster diffusion than larger ones. The DLS instrument produces a correlation function that is mathematically associated with the particle size and its time-dependent light-scattering capacity. DLS is applied in

measuring the particle size of dispersed colloidal samples, exploring the stability of formulations, and identifying the presence of agglomerates (Kermani et al., 2023).

2.2.8. Potential Zeta

Zeta potential, a scientific term denoting electrokinetic potential in colloidal dispersions, stands as a pivotal indicator of their stability. The magnitude of the zeta potential serves as a measure of the electrostatic repulsion strength between neighboring particles of similar charge within the dispersion. In the case of sufficiently small molecules and particles, a high zeta potential contributes to stability, preventing aggregation in the solution or dispersion. Conversely, when the potential is low, attractive forces might surpass repulsion, leading to dispersion breaking and flocculation. Zeta potential can be influenced by the dielectric constant of a particle and the ionic strength of the surrounding medium (Hunter, 2013).

This technique measures the electrical potential in the double interfacial layer of a particle immersed in a fluid located in the sliding plane in relation to a mass point in the fluid away from the interface, and shows the potential difference between the dispersion medium and the stationary layer of fluid attached to the dispersed particle (Yu and Xie, 2012). This serves as a valuable indicator of surface charge, offering the ability to predict and regulate the stability of colloidal suspensions based on the interplay between potential and pH.

In general, a value of ± 30 mV can be used as an arbitrary value to separate low-charged surfaces from highly charged ones. Thus, dispersions with a zeta potential of 30 to -30 mV are unstable and outside this range are considered stable (Joseph and Singhvi, 2019).

2.2.9. Scanning Electron Microscopy (SEM)

This method employs an electron beam as a radiation source directed onto the observed sample, enabling the capture of high-resolution spatial images. The electron beam scans the sample's surface, generating secondary electrons from the analyzed material, which are subsequently detected by a sensor. As the sample's

surface is irradiated, the resulting electrical signals are translated into image format (Faraldos and Goberna, 2021).

Characteristic X-rays collected during this process can be utilized to study the elemental composition through compositional and semi-quantitative mapping. The incidence of electrons initiates multiple interactions that can be recorded, providing a comprehensive level of detail in structural, spectroscopic, compositional, and crystallographic characterizations. Thus, high-resolution nanoscale images are achieved along with precise measurements. Scanning electron microscopy may detect backscattered electrons (to reveal morphology and topography and give insight as to composition), or secondary electrons (to reveal surface topography) (Rusiñol et al., 2023). It also makes it possible to combine structural analysis with chemical analysis, factors that have contributed to the wide use of this technique. The high depth of focus gives a three-dimensional appearance to the images obtained, which is very useful for understanding the surface structure of the sample.

2.2.9.1. Cryo-SEM

Cryo-SEM combines the high-resolution imaging of scanning SEM with cryogenic sample preparation techniques. The cryogenically frozen specimen is positioned within the specimen chamber on a cold stage, typically cooled by liquid nitrogen. The setup often includes a feature for fracturing the sample using a cold scalpel blade, revealing internal cell or tissue surfaces. Additionally, there is a sputter coater that enables coating the freshly fractured surface with metal while it is still inside the microscope's vacuum system so that the sample can then be sublimated for imaging (Wightman, 2022).

2.2.10. Modified Transient Plane Source (MTPS)

The conventional methods for analyzing the thermal conductivity of heat transfer fluids are both time-consuming and susceptible to errors, primarily due to the influence of convection. Convection tends to distort the effective measurement of thermal conductivity, acting as an additional factor in heat transfer. The Modified Transient Plane Source (MTPS) method offers a streamlined approach for precisely

measuring thermal conductivity and differentiating this mode of heat transfer. This method mitigates the impact of convection by utilizing the shortest test time, requiring minimal sample volume and employing a low-energy power flow to the sample under examination (Harris et al., 2014).

The system is comprised of a one-sided interfacial sensor that applies a constant current heat source to the sample. The sample is heated during the testing and absorbs some of the heat depending on its thermal conductivity, and the rest causes a temperature rise at the sensor interface. The rate of the increase in temperature at the sensor surface is inversely proportional to the ability of the sample to transfer heat. Thermal conductivity, calculated from the slope of the voltage data, and effusivity are measured directly, providing a detailed overview of the thermal nature of the sample material (Kuvandykova and Bateman, 2013). The MTPS is based on the transient plane source (TPS) method and has high accuracy, high sensitivity and a short test time.

2.2.11. Rheological Characterization

To assess the rheological properties of a fluid, various tests are conducted, including steady shear, flow curve, stress/strain sweep, and frequency sweep.

In the steady shear test, information about the time-dependent or time-independent nature of the fluid can be obtained, indicating the time it takes for the sample to reach a steady state (Mewis and Wagner, 2012).

The flow curve facilitates the rheological classification of a fluid and allows the evaluation of the impact of factors such as temperature, pressure and concentration of particles in the fluid through the analysis of the behavior of viscosity and shear stress with variation in the shear rate (Barnes, 1995).

According to Mezger (2020), in the stress/strain sweep, it is possible to identify the linear viscoelasticity region, characterized by a combination of viscous and elastic effects where the material properties remain unaffected by the test conditions. Material functions within this region are independent of the applied deformation. This test also helps determine the predominant modulus in a specific region, whether it is the storage modulus (G') or the loss modulus (G''), thereby indicating if there is a prevalence of viscous or elastic effects.

The frequency sweep is conducted to characterize the mechanical spectrum of the material. This involves examining the behavior of the storage modulus (G') and the loss modulus (G'') across different frequencies, along with determining the mean values of the phase angle ($\tan \delta = G'' / G'$). If $\delta = 0^\circ$ or $\tan \delta = 0$, the material exhibits 100% solid characteristics with ideal elastic behavior. Conversely, when $\delta = 90^\circ$ or $\tan \delta = \infty$, the material demonstrates ideal viscous behavior, representing a 100% viscous material. Lastly, if $\delta = 45^\circ$ or $\tan \delta = 1$, i.e., $G' = G''$, then the material is in a state of equilibrium between viscous and elastic properties (Mezger, 2020).

The rheological assessments outlined earlier can be conducted under three distinct types of shear flow: transient, steady and oscillatory. These shear flows differ in the manner in which deformation is applied to the sample.

In transient shear flow, this approach provides insights into how properties evolve over time under fixed deformation conditions. On the other hand, in steady shear flow, a rotation is employed allowing the measurement of shear stress and viscosity as functions of shear rate, as in the case of the flow curve. This regime yields crucial insight into shear-thinning and thixotropic behaviors, facilitates the determination of yield stress, and aids in understanding material behavior in practical scenarios like pumping, agitation, and extrusion.

Lastly, oscillatory shear flow involves tests that correlate angular velocity or imposed frequency with resulting oscillatory strain or stress. These tests mechanically disturb the samples without causing internal structural rupture. Stress and frequency sweeps are conducted within this category.

2.3. Drilling Fluid

A drilling fluid refers to any fluid employed in a drilling operation where the fluid is circulated or pumped from the surface, passing through the drill string, through the bit, and subsequently returning to the surface through the annulus, as illustrated in Figure 2.4 (Asme, 2005). The formulation of the fluid is designed to fulfill key functions essential for the success of the drilling operation. Typically, a drilling fluid comprises a base fluid, weight material, viscosifiers, and additional chemical components to impart the desired properties to the fluid (Kolle and Mesel, 1998).

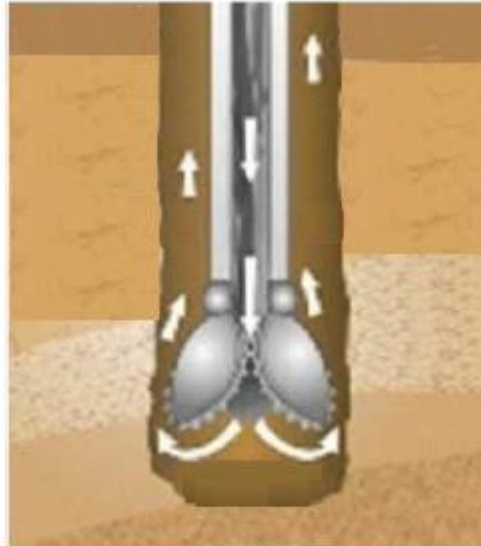


Figure 2.4 – Circulation of drilling fluid inside the well (Vryzas and Kelessidis, 2017)

2.3.1. Functions of drilling fluids

According to Caenn et al. (2011), the primary functions of a drilling fluid necessitate continuous monitoring and intervention as needed. Among the monitored functions, the following can be highlighted:

- Preventing Formation Fluid Influx (Kick): This involves monitoring fluid density (mud weight) and equivalent circulating density (ECD) to control the influx of formation fluids (water, oil, gas) into and out of the well. ECD is a combination of hydrostatic pressure and the additional pressure required to pump the fluid through the annular space of the well.

- Transporting Cuttings to the Surface: The viscosity profile must be managed to ensure efficient transportation of cuttings through the annular space.

- Forming a Mud Cake: A thin, low-permeability mud cake is formed to seal pores and other openings in permeable formations drilled by the drill. This is achieved by monitoring the particle size distribution of solids and maintaining appropriate materials.

- Well Wall Stabilization: The density of the drilling fluid and the chemical reactivity between the formation and the fluid are monitored to maintain the integrity of the well walls.

Drilling fluid also serves additional functions crucial for satisfactory drilling performance, including lubricating and cooling the bit, aiding in the separation of gravel on the surface, and facilitating geological interpretations of materials extracted from the well, among others (Asme, 2005).

2.3.2. Drilling fluids properties

In addition to these functions related to performance, it is desirable that the drilling fluid has certain characteristics, such as being chemically stable, being pumpable, accepting any chemical and physical treatment, presenting a low degree of corrosion in relation to the drilling string and other circulation equipment and not be harmful to the health of operators and the environment (Thomas et al., 2001).

Drilling fluid properties must be continuously monitored as they influence the performance of the drilling operation and help prevent difficulties encountered during drilling. The large number of functions performed by drilling fluid requires that some minimum properties be maintained, because when there are undesirable changes in the quality of the mud while it is subjected to well conditions, this makes its correct functioning difficult. Control properties can be physical, such as density, rheological parameters, gel strength, filtration parameters and solids content, or chemical, such as pH, chloride and bentonite content and alkalinity (Khodja et al., 2010).

Considering density as the first parameter to be evaluated, normally when there is a need to increase the density of the drilling fluid, barite is used or to reduce it, it is diluted with water or diesel oil, always keeping the density within the limits of variation allowed to drill a certain range of the reservoir which are established by the pore pressure (minimum limit) and fracture pressure (maximum limit) of the exposed formations (Thomas et al., 2001).

Rheological parameters such as the presence of yield stress and the degree of thixotropy influence the flow behavior, the calculation of pressure losses in the pipe and the speed at which the cuttings are transported to the surface and for this, it is desirable that a rheological model for the fluid is defined. The mud must possess adequate viscosity to effectively lift cuttings to the surface during drilling. However, it is crucial to strike a balance, ensuring that viscosity is not excessively high to minimize friction pressure loss (Khodja et al., 2010).

Gel strength is a parameter that indicates the degree of gelation due to the electrical interaction between dispersed particles. The difference between the initial gel force (initial resistance to put the fluid in motion) and the final gel force (resistance of the fluid to return flow after rest) measures the degree of thixotropy of the fluid (Parate, 2021).

The filtrate and the filter cake thickness are two measurements responsible for characterizing the behavior of the fluid in relation to the process known as filtration. This process is responsible for forming filter cake (a layer of solid and humid particles on the permeable rocks exposed by the drill) and occurs when there is an influx of the liquid phase of the drilling fluid into the formation. The fluid must have a fraction of particles smaller than the size of the pores of the exposed rocks (Thomas et al., 2001). The filtration of drilling mud during drilling operations can lead to various impacts, including formation damage, increased torque and drag during tripping operations. It is crucial to manage fluid loss properties effectively to prevent these issues from occurring (Davoodi et al., 2019).

The solids content is a parameter that must be controlled, as its increase impacts the wear of circulation equipment, increases the probability of formation fracture occurring due to the increase in hydrostatic pressure, can lead to column entrapment and a reduction in drill penetration rate, in addition to influencing the value of several properties such as viscosity and density (Parate, 2021).

All of these properties of the drilling fluid are important to be measured and controlled during the drilling process, however the focus of this work will only be on rheological and thermal conductivity parameters.

2.3.3. Operational challenges

Drilled solids, if not correctly removed, in addition to causing damage to reservoirs, contribute to increased expenses at the drilling stage. Some of the operational challenges associated with drilling fluid design in deepwater fields are clay swelling, gas hydrate formation, narrow pore/fracture pressure gradient margins, drilling through salt formations, potential for formation damage, loss circulation, well stability concerns, pipe entrapment, efficient cuttings transportation, and considerations related to environmental and safety aspects (Alcázar-Vara and Cortés-Monroy, 2018).

The issue of fracture/pore pressure gradient margins can be resolved by analyzing the operational window as shown in Figure 2.5. The operational window is responsible for defining the specific weight of the drilling fluid to be pumped at a given drilling stage. The weight is limited at the top by the fracture pressure and the lower limit is represented by the greatest value of the curve between the pore pressure and the collapse pressure. The safe operational window is different for each well. In HPHT conditions and extreme water depths, the safe operational window tends to be very narrow compared to onshore wells.

Inadequate pressure control during drilling can lead to phenomena like kicks, where fluid from the formation enters the well. If kicks are not properly managed, they may escalate into blowouts, an uncontrolled influx from the formation to the wellbore surface. Blowouts pose severe risks, including loss of life, extensive environmental damage, and financial losses for the oil company (Carlsen et al., 2013).

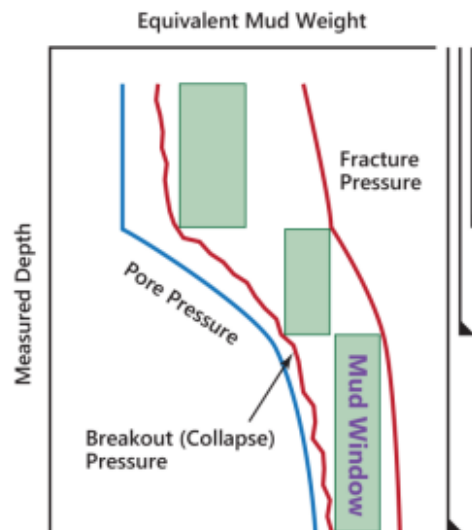


Figure 2.5 – Safer operating mud window (Naganawa, 2015)

Loss of circulation is an undesirable event where part of the drilling fluid escapes into the formation, usually in fractures or in highly permeable sections and thus a smaller amount of fluid returns from the interior of the well in relation to the amount of fluid that was pumped into. This event is the main cause of unproductive time in drilling, which can result in a significant increase in operational costs (Alcázar-Vara and Cortés-Monroy, 2018).

The loss circulation, as shown in Figure 2.6, is caused by two basic mechanisms: invasion and fracture. Invasion refers to the loss of fluid to formations that are cavernous, natural or induced, while the fracturing mechanism refers to the loss of fluid due to hydraulic fracturing from excessive induced pressures (Asme, 2005). For deepwater formations, water depth can cause lower fracture pressure, resulting in a narrow mud weight window, making it very challenging to maintain the required pressure within the wellbore and increasing the propensity for loss of circulation (Feng and Gray, 2017). Therefore, minimizing and controlling this problem is another important challenge for deepwater drilling fluid technology through evaluating the relationship between rheology and mud components using polymeric gels (Magzoub et al., 2021).

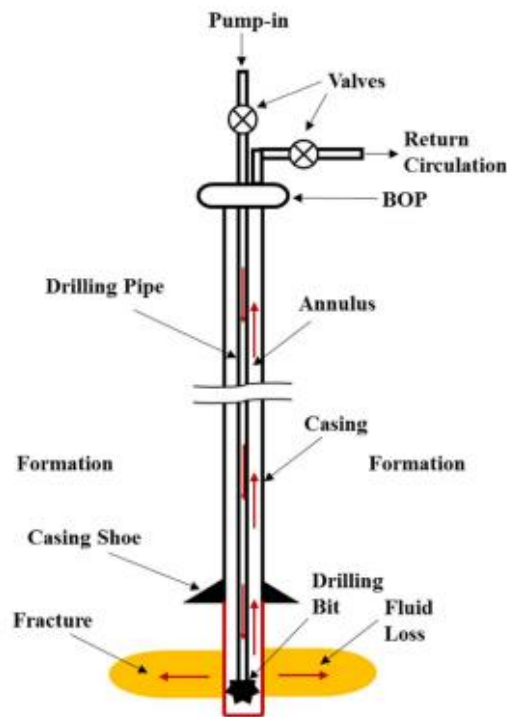


Figure 2.6 – Representation of lost circulation of drilling fluid in regions where there is fracture (Feng and Gray, 2017).

Formation damage is an economic and unwanted problem that can occur during various operations related to oil exploration, such as drilling, completion, stimulation and workover (Civan, 2023). Damaging the formation implies a drop in productivity and/or injectivity. In some cases, it is irreversible and its effects can negatively affect oil and gas recovery.

The formation damage is a reduction in the well-reservoir interface permeability that causes an additional pressure drop when the well fluid enters the reservoir rock (Bourdet, 2002). Part of the damage may be caused by the drilling fluid, through the filtrate, the liquid part that invades the formation, altering the permeability relative to the oil, or the mud cake, which works as a mechanical barrier (Civan, 2023). This type of problem can be solved with acid or solvent, through acid or hydraulic fracturing or through high penetration perforation (Thomas et al, 2001).

It is necessary that the well walls are stabilized for the safety and success of operations during drilling and some problems such as clay swelling have a negative impact and can result in well instability problems. The rock-fluid interaction is directly influenced by the physical-chemical properties of the clay-water system, as clays have characteristics that make them reactive when in contact with water-based drilling fluids, such as the high specific area and high expansibility of these minerals. In order to inhibit this clay swelling, some inorganic additives are used such as KCl, NaCl and CaCl₂. These inhibitors prevent the drilled solids from being incorporated into the fluid and prevent the well walls from swelling and collapsing (Halim et al., 2021).

Rock-fluid and fluid-fluid interactions around the wellbore region can lead to formation damage. As shown in Figure 2.7, an example of rock-fluid interaction capable of reducing well productivity is the interaction between clay minerals and drilling fluids.

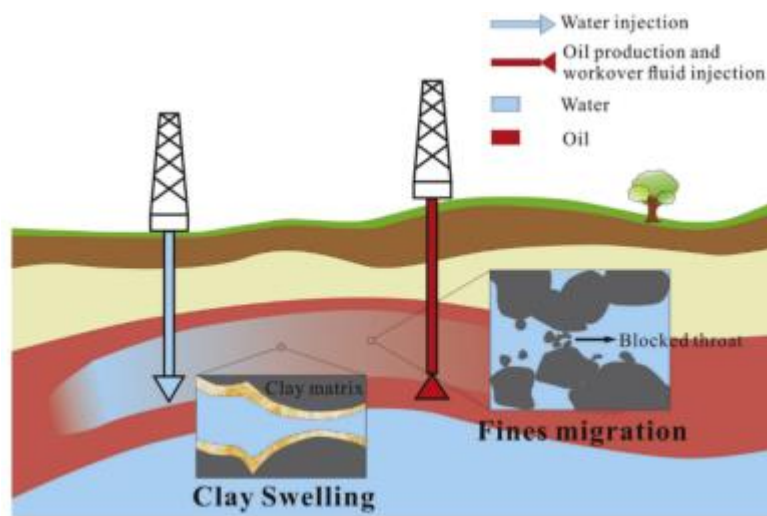


Figure 2.7 - Representation of permeability changes caused by clay swelling and migration of fines (Yang et al., 2019).

2.3.4. Types of drilling fluid

A drilling fluid is composed of a liquid phase (it can be water or oil), solid particles and sometimes gases, which, taking into account its chemical composition and the physical state of its components, allow the fluid to assume aspects of colloidal dispersion, emulsion or suspension. (Mitchell and Miska, 2011).

The main criterion for classifying drilling fluids is according to their composition, more specifically in relation to the main constituent of the continuous phase, which is more relevant than the components of the dispersing phase. As illustrated in Figure 2.8, they can be classified into three types: water-based drilling fluids (WBM), oil-based drilling fluids (OBM), and pneumatic fluid. Fluids with a continuous liquid phase are the most used, which can be emulsions, as in the case of OBM, or suspensions, when the continuous phase is water (Caenn et al., 2011).

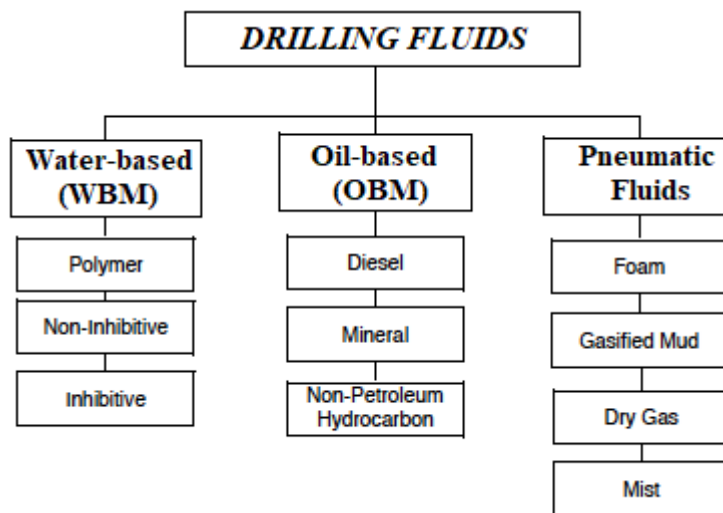


Figure 2.8 – Classification of drilling fluids

Decisions regarding the choice of drilling fluid for a particular well are guided by three primary factors: cost, technical performance, and environmental impact. Choosing the appropriate fluid for specific conditions is a crucial aspect of ensuring the success of drilling operations.

2.3.4.1. Water-Based Muds (WBM)

Water-based fluids are the most used in drilling. A definition of this fluid mainly considers the nature of water and chemical additives. Three types of water can be used (Thomas et al., 2001):

- Fresh water – Does not require chemical pre-treatment. It has a salinity of less than 1000 ppm NaCl (sodium chloride), and this basically does not affect the performance of the additives used;
- Hard water – Basically composed of dissolved calcium and magnesium that alter the performance of chemical additives.
- Salt water – It has a salinity greater than 1000 ppm NaCl, which can be sea water, or fresh water with added salts such as NaCl, KCl or CaCl₂.

Some factors must be taken into account when selecting the water to prepare the fluid, such as the cost of transportation and treatment, type of lithological formation and interval to be drilled, the chemicals that will be added to the fluid and the conditions of the well (Apaleke et al., 2012). For example, seawater-based fluid is often used to drill surface intervals that contain fewer additives. In deeper stretches, due to the high temperature and pressure conditions of the reservoirs, WBMs are usually replaced by OBM (Dowell et al., 2006).

In addition to water, WBM are a composition of minerals, salts and organic compounds. The main function of water is to serve as a dispersion medium for colloidal materials, such as clays and polymers that control the rheological properties of the fluid or other chemical products such as caustic soda, which controls the pH and serves as a flocculant or surfactants that reduce the interfacial tension of the emulsion. This type of fluid also contains biopolymers, such as xanthan gum, which are not toxic to the environment. Each of these additives are added in small quantities and are still capable of changing the properties of the mud and solving specific problems presented in each well interval (Neff, 2005). Figure 2.9 shows an example of the composition of a water-based fluid.

WBFs is divided into broad categories: non dispersed and dispersed. The lack of dispersant is the main characteristic that differentiates the two classifications. In dispersed systems, chemical dispersants, such as, lignite and lignosulfonate, are introduced to deflocculate clay particles, enhancing the rheology

of high-density muds. In non-dispersed muds, dispersants are excluded from the formulation. Bentonite serves as a viscosifier and fluid loss agent in water-based muds (WBM). Examples of non-dispersed systems include polymer systems with minimal or no bentonite and simple gel-water systems employed for drilling surface intervals (Parate, 2021).

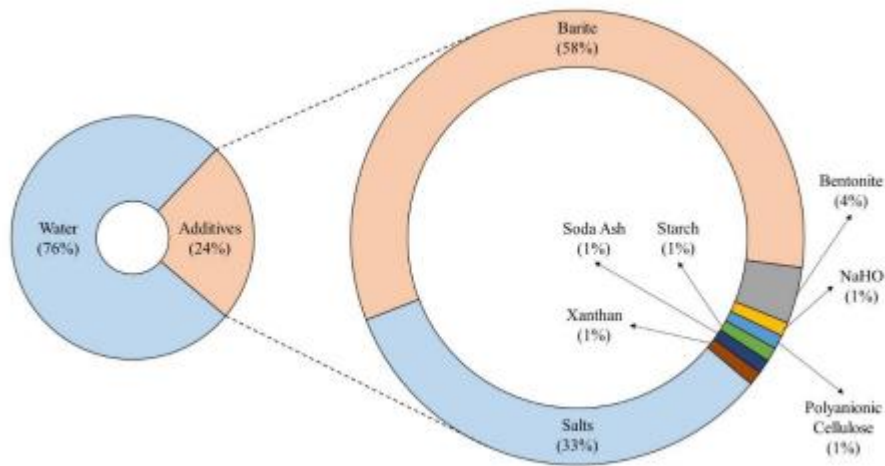


Figure 2.9 – Composition of a typical water-based drilling mud (WBM) and of the additives (Martin, 2022).

WBFs is divided into broad categories: non dispersed and dispersed. The lack of dispersant is the main characteristic that differentiates the two classifications. In dispersed systems, chemical dispersants, such as, lignite and lignosulfonate, are introduced to deflocculate clay particles, enhancing the rheology of high-density muds. In non-dispersed muds, dispersants are excluded from the formulation. Bentonite serves as a viscosifier and fluid loss agent in water-based muds (WBM). Examples of non-dispersed systems include polymer systems with minimal or no bentonite and simple gel-water systems employed for drilling surface intervals (Parate, 2021).

The main advantages of using this type of fluid are that it is environmentally friendly, has low toxicity, is easy to handle and prepare, is more economical and has a high penetration rate. However, it has disadvantages such as causing clay swelling in formations, causing corrosion to circulation equipment and suffering degradation more easily in HPHT environments (Apaleke et al., 2012).

Due to the advancements in high-performance and environmentally friendly fluids, there is a preference for water-based fluids, besides are considerably less expensive than oil-based fluids (OBFs) (Caenn and Chillingar, 1996).

2.3.4.2. Oil-Based Muds (OBM)

These fluid types consist of an oil phase, which can either be the continuous or dispersing phase, typically composed of hydrocarbons in the liquid state. They are categorized as water/oil emulsions when the water content is below 10% or inverse emulsions when the water content ranges from 10 to 45%. (Thomas et al., 2001). Developed to mitigate various drilling challenges like clay swelling, high bottom hole temperature, torque, drag, and stuck pipe issues, Oil-Based Mud (OBMs) primarily composed of diesel, mineral oil, or low toxicity linear paraffin. Similar to Water-Based Mud (WBM), OBMs use chemicals to control filtrate loss, alter pH, density, and rheological properties. A notable advantage of the oil-based system is its ability to inhibit shale swelling, achieved through a high-salinity water phase, primarily using calcium chloride for inhibitory properties. However, a significant drawback of petroleum-based systems is their environmental impact. In offshore drilling, discharging all drilling mud or cutting without processing is not permitted, necessitating the processing and shipping of waste fluids and cuttings, incurring additional costs (Dowell et al., 2006).

OBMs have some disadvantages in relation to water-based fluids, such as lower penetration rates, higher levels of pollution, high initial cost and difficulty in combating the loss of drilling fluid to the formation. Although WBMs are preferably chosen because they are more environmentally friendly, OBMs have several benefits that make them essential for use in some particularly long and difficult sections of a well. These fluids have a low corrosion rate, a high degree of inhibition in relation to active rocks, optimal control of properties at high temperatures, a high degree of lubricity and low solubility of organic salts. Due to these excellent characteristics, these fluids have shown excellent results when used in clay shale formations, saline formations, formations with low pore or fracture pressure, in directional wells or HPHT wells (Thomas et al., 2001).

2.3.4.3. Pneumatic Fluids

Pneumatic fluids use air, gas, mist (water dispersed in air) or foam (dispersion of gas in liquid) as the main constituent to promote the removal of cuttings from the bottom of the well to the surface. Areas with severe loss of circulation and formations that produce very low pressure or are susceptible to damage are some of the situations where these types of fluids are recommended as they have low density (Dowell et al., 2006).

Air drilling is recommended for formations where there is no large production of water or oil, where the objective of this drilling is to increase the penetration rate. Foam drilling is used when a fluid with high cuttings loading efficiency is desired, as it has a high viscosity. In regions where there are large circulation losses, aerated fluid is used, that is, a technique is applied that consists of injecting air into the continuous flow of drilling fluid (Thomas et al., 2001).

2.3.5. Drilling mud additives

One of the most important aspects of studying drilling fluids is to investigate the effect of a certain type of additive and its concentration on the properties of the mud. Additives are defined as a material that is added to the base fluid to perform certain specific functions and are classified according to their function, such as thinners agents, flocculants, surfactants, dispersants, viscosifiers, emulsifiers, filtration preventers, pH control additives, polymers, clays, nanoparticles, among others (Neff, 2005).

Clays, due to their high surface area, make them play an important role in drilling fluids, acting as catalysts and adsorbents of toxic substances. In addition to providing density, gel strength, viscosity, and yield stress to the fluid, they also provide excellent fluid loss control. Conventional WBM fluids use bentonite as viscosifiers because it is a cheap product that provides a good removal rate of drilled solids and helps with stabilization on the wellbore (Hall, 1987).

Polymers are macromolecules formed by small molecules (monomers) that bond together through a reaction called polymerization. In general, polymers can be classified as: natural, modified natural and synthetic. An example of natural polymers is xanthan gum, modified natural polymers have carboxymethylcellulose

(CMC) and synthetic polymers have polyacrylamide (Caenn and Chillingar, 1996). Polymers are very present constituents in almost all WBMs and their use helps control filtrate loss, viscosity, shale inhibition and prevent clay dispersion (Galindo et al., 2015).

WBMs do not present good thermal stability when used in wells with HPHT conditions and the use of nanomaterials, even in small amounts added, helps to provide greater thermal stability in more severe conditions, reducing the degradation of fluids at high temperatures and also provides mechanics properties more efficient simply because they are on the nano scale. Therefore, nanomaterial-based drilling fluids can help meet the special requirements needed to drill these wells (Salehnezhad et al., 2019).

2.3.5.1. Nanomaterials based drilling fluid

The use of nanoscale additives potentially helps solve drilling-related problems that are not easy to solve using conventional methods. Nanoparticles (NP) present in drilling fluid help to improve well stability by protecting the reservoir, reduce environmental impact, increase operational safety, improve rheological properties, among others (Vryzas and Kelessidis, 2017).

Drilling fluids incorporating nanoparticles possess the ability to mitigate wellbore instability (Singh et al., 2010). The size of nanoparticles is smaller than the pore throat sizes of rocks, enabling them to plug the pore throats. As per Suri and Sharma (2004), the particle size should not exceed one-third of the pore throat size to effectively build a bridge and plug the pores.

Several companies have already invested considerable time and effort in managing loss circulation through the introduction of additives or alternative muds. The incorporation of micro and macro particles has demonstrated restricted success (Zakaria et al., 2011). The application of nanoparticles has proven effective in minimizing loss circulation by significantly enhancing the carrying capacity to efficiently transport cuttings, while also maintaining drilling fluid density and pressure across a broad spectrum of operational conditions (Bicerano, 2009).

Nanofluids can contribute to resolving issues related to stuck pipes. Drilling muds incorporating nanomaterials have the capability to reduce the tendency of mud cakes to stick by forming a thin film on the drill pipe, addressing

the problem of pipe sticking (Amanullah and Ashraf, 2009). Furthermore, nanofluids exhibit excellent carrying capacity, effectively minimizing pipe sticking by clearing the wellbore of cuttings (Nabhani and Emami, 2012).

Drilling muds containing micro and macro materials have shown limited efficacy in addressing torque and drag issues (Wasan and Nikolove, 2003). Conversely, the use of nanoparticles results in a notable decrease in friction between the pipe and the borehole. Nanofluids hold the potential to create a slightly lubricating film at the wall-pipe interface, contributing to the reduction of torque and drag problems.

Nanoparticles can be utilized in drilling fluids to eliminate toxic and corrosive gases, such as hydrogen sulfide. The removal of this gas from drilling fluids is essential to mitigate environmental contamination, safeguard the health of drilling staff, and prevent corrosion of drilling equipment (Singh et al., 2010).

In addition to improving the performance of the drilling fluid, other benefits are obtained using nanomaterials, such as: the amount of material required is much smaller than if a specific additive was used for a given function, due to the fact that they have a superior ratio between surface area and mass which increases the reactivity of nanomaterials (Shah et al., 2010) and this reduces drilling costs (Nabhani and Emami, 2012), oil recovery in deeper formations has been improved (Abdo and Haneef, 2013) and non-productive time was reduced due to elimination of problems (Abdo and Haneef, 2012).

There are two ways to prepare a nanofluid: the nanoparticles are produced and dispersed simultaneously in the base fluid (one step) or they are first produced and then added to the base fluid (two steps) (Taha-Tijerina, 2013). The first method avoids several processes such as drying, storage, handling and particle dispersion, thus obtaining a more stable nanofluid, but there is preference for the second form of preparation. This preference is due to the ease of commercialization of these nanoparticles in powder form and because this process is an economical method for large-scale production, since nanostructure synthesis techniques are scaled to mass production levels (Das et al., 2007).

Nevertheless, the two-step technique presents certain limitations concerning dispersion and solubility. These nanoparticles tend to agglomerate rapidly and subsequently settle after being dispersed in the base fluid due to their inability to disrupt the interactions between the molecules in the base fluid (Cao,

2004). Figure 2.10 illustrates some common challenges in the development of nanofluids.

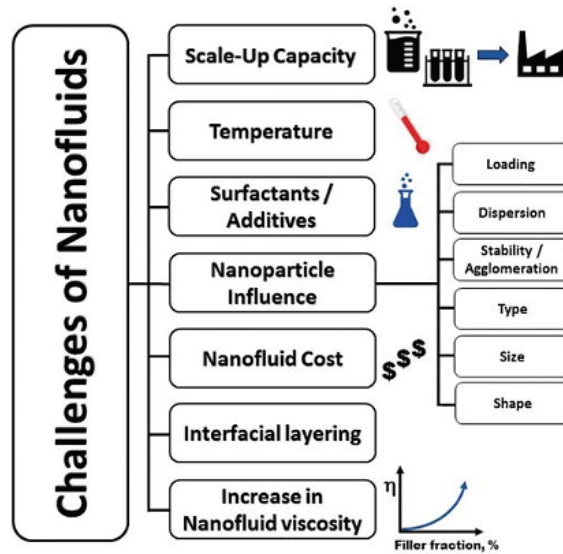


Figure 2.10 – Common challenges of nanofluid development (Taha-Tijerina, 2018)

Despite the unique properties of nanoparticles, such as a large surface area relative to volume and size-dependent physical properties that can enhance conventional fluid properties, achieving a stable dispersion has been a significant challenge for researchers in the absence of chemical agents such as pH change or surfactant addition. Addressing this challenge involves homogenizing the dispersion through stirring techniques, including the use of ultrasonic baths, magnetic stirrers, and high-pressure homogenizers. Factors such as stirring intensity and duration can also influence the dispersion effect (Fuskele and Sarviya, 2017).

Nevertheless, despite agitation, Van der Waals forces can cause the nanoparticles to agglomerate again, leading to settling, as depicted in Figure 2.11. To mitigate this issue and maintain stable suspensions for an extended period, surfactants are introduced (Hwang et al., 2008).

In addition to impacting stability, particle agglomeration leads to a reduction in the effective surface area/volume, thereby influencing the thermal conductivity performance of nanofluids. In light of these considerations, investigations into factors that can alter the thermo-physical properties should be conducted through various evaluation methods, including zeta potential (indicating the degree of repulsion between particles and the stationary liquid layer surrounding them), sedimentation rate, and pH control (Mackay et al., 2006).

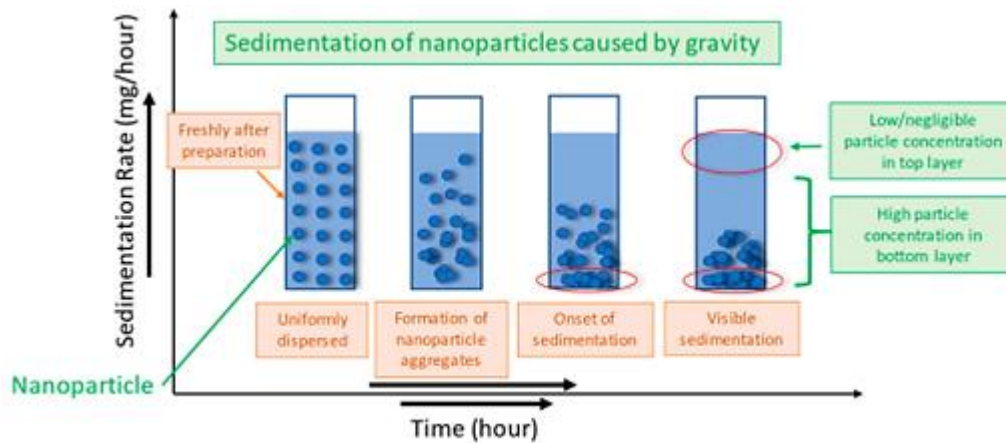


Figure 2.11 – Scheme of nanoparticles sedimentation (Ponticorvo et al., 2022)

Due to the intricate surface chemistry of nanofluids, variations in results exist across studies concerning their characteristics. Nevertheless, the drive to enhance these features and explore potential applications has intensified.

While standards and criteria for stability measurements have not yet been established, the investigation of other properties such as thermal conductivity and viscosity remains essential for determining future applications.

The characteristic that has garnered the greatest interest within the nanofluid research community is thermal conductivity. Presently, there is no universally accepted theory to predict the anomalous behavior of nanofluid thermal conductivity. Based on the experimental findings of numerous researchers, it is evident that the thermal conductivity of nanofluids is influenced by various physical parameters, including the thermal conductivities of the base fluid and nanoparticles, the temperature, the shape and size of nanoparticles, the concentration of particle loading and the surface area of nanoparticles within the nanofluid (Pryazhnikov et al., 2017).

The addition of nanoparticles to a base fluid, in addition to generally tending to increase thermal conductivity (as will be seen in the next section), is capable of altering the rheological and mechanical properties of the fluid (Behi and Mirmohammadi, 2012). The viscosity of nanofluids depends not only on the shape of the inserted nanoparticles, but also on the size and quantity. These nanoparticles form clusters which leads to increased viscosity. Some parameters are capable of affecting the viscosity of the nanofluid, such as preparation method, type of base

fluid, operating temperature, acidity (pH value), shear rate, use of additives or surfactants, particle aggregation, brownian motion and hydrodynamic diffusion (Taha-Tijerina, 2018).

Brownian motion, illustrated as the random movement of particles in Figure 2.12, naturally propels particles from regions of higher concentration to those of lower concentration. The Brownian forces exert a more substantial influence on nanoparticle charge fraction distribution and velocity field in comparison to other forces. The impact of Brownian motion is significant when dealing with nanoparticles in the fluid and are reduced as the particle size increases (Aminfar and Motallebzadeh, 2012).

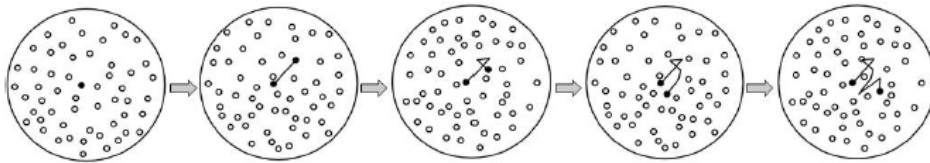


Figure 2.12 – Brownian motion of the particle (Taha-Tijerina, 2013)

2.4. Thermal Conductivity of Nanofluids

In recent years, nanofluids (NFs) have become leading candidates to improve or even replace traditional heat transfer fluids in diverse applications, from renewable energy to nanomedicine. Therefore, this topic presents the different techniques used to measure thermal conductivity and the fundamental parameters that affect the thermal conductivity of NFs.

2.4.1. Thermal Conductivity measurements methods

Static methods are currently used for thermal conductivity measurements, categorized into transient and steady state methods. Among the transient state methods encompass the transient hot wire, transient plane source theory, temperature oscillation method, laser flash method, 3ω method and modified transient plane source (MTPS), while the steady state methods are the parallel plane and coaxial cylinders methods (Xu et al., 2019). A concise overview of these

techniques will be provided in the subsequent subsections. Figure 2.13 illustrates the steady and transient state methods commonly employed for measuring the thermal conductivity of the NFs.

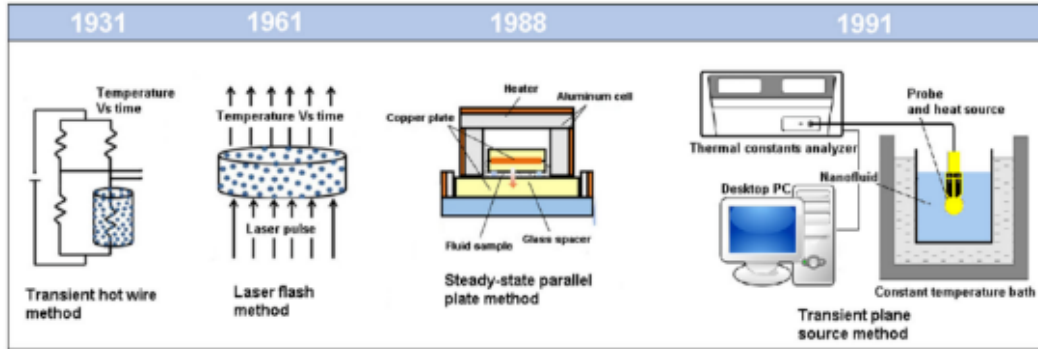


Figure 2.13 – Schematic diagram of methods for measuring the thermal conductivity of nanofluids (Gonçalves et al., 2021).

In steady-state methods, thermal conductivity measurement is performed when the temperature of the material remains constant over time, which is known as steady state. Thermal conductivity is calculated by considering the measured temperature difference and the heat flux applied across the surface. The simplicity of this method is attributed to its temporal independence, however, achieving ideal conditions for its use in practical testing settings can be challenging, which can be considered a disadvantage. On the other hand, in transient methods, the variation in temperature at a specific point over time is measured to estimate thermal conductivity. Unlike steady-state methods, it is not necessary to wait for the system to reach equilibrium, which results in shorter measurement times and therefore the analysis of this data becomes more complex (Kurt, 2014). In this study, thermal conductivity measurements were carried out using the MTPS technique.

2.4.2. Parameters that affect Thermal Conductivity

The structural and morphological characteristics of nanomaterials, the stability of these nanoparticles in the base fluid, as well as the way the suspensions are prepared, among several other factors, can affect, directly or indirectly, the thermal conductivity of nanofluids, as shown in Figure 2.14.

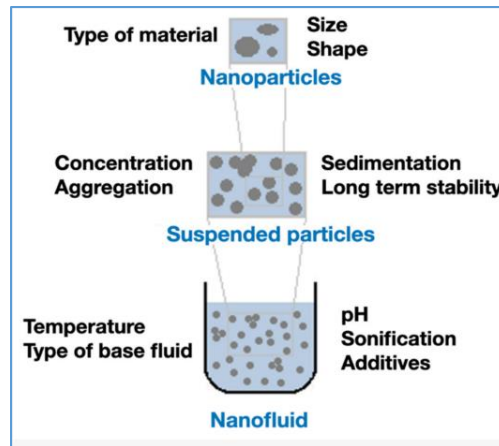


Figure 2.14 – Parameters that affect the thermal conductivity of nanofluids
(Gonçalves et al., 2021)

In addition to the type (such as metals, metal oxides, ceramics and carbon nanotubes) of the nanoparticle influencing thermal conductivity, most results presented in the literature state that reducing the diameter/size of nanoparticles increases their thermal conductivity, since their effective surface area is increased, thickening the interfacial layer and increasing Brownian motion (Xu et al., 2006; Anoop et al., 2009; Ambreen and Kim, 2020). Brownian motion is not present in micro-sized particles and thus thermal conductivity remains unchanged.

Several studies have already been carried out with nanoparticles of different shapes, such as spherical, cylindrical, rod-shaped, rectangular, among others (Murshed et al., 2005; Glory et al., 2008; Timofeeva et al., 2009; Jeong et al., 2013). The findings suggest that particles with higher aspect ratios play a significant role in boosting thermal conductivity. This is attributed to increased thermal penetration and a reduction in the adverse effects of interfacial thermal resistance on heat transfer.

The type of base fluid also influences the thermal conductivity of suspensions, since some results have shown that the base fluid with higher thermal conductivity presents a smaller increase in thermal conductivity when nanoparticles are inserted (Hwang et al, 2006; Chen et al, 2008; Gowda et al., 2010).

Most studies report an increase in thermal conductivity with increasing nanoparticle concentration due to a larger interfacial area between the base fluid and NPs (Esfe et al., 2018). However, some reports have observed opposite

behavior for high concentration values. The effect of nanofluid stability probably plays an important role in determining the ideal concentration (Philip and Shima, 2012; Qiu et al., 2020).

Particle agglomeration significantly contributes to increased thermal conductivity by introducing additional conduction pathways within nanofluids (NFs). Smaller particle sizes tend to promote aggregation more easily. The manner in which aggregation manifests itself in NFs with higher particle volume fractions depends on particle morphology. In investigations conducted by Hong and Kim (2012), a correlation was observed between increased particle aggregation and increased thermal conductivity in a water-based alumina NF. On the other hand, extensive particle agglomerations can precipitate particle sedimentation, resulting in decreased thermal conductivity (Jana et al., 2007; Nasiri et al., 2011).

In addition to the choice of preparation method (one step or two steps) of nanofluids, the type and concentration of surfactants used, temperature is also an impacting factor (Gonçalves et al., 2021). Some studies suggest that the escalation in thermal conductivity as temperature rises stems from the enhancement of Brownian motion and the decline in particle surface energy. Conversely, other research indicates a decrement in conductivity with increasing temperature for nanofluids featuring non-spherical particles, hinting at the significant influence of particle aspect ratio (Philip and Shima, 2012; Qiu et al., 2020).

The thermal conductivity of Nanofluids is impacted by the pH level, which influences the extent of nanoparticle aggregation. Additionally, research conducted by Wamkam et al. (2011) demonstrated that pH levels influence zeta potential, particle size distribution, rheology, viscosity, and stability, all of which play a role in altering thermal conductivity.

Sonication treatment is a prevalent practice in the formulation of nanofluids. In many instances, prolonging sonication duration leads to heightened thermal conductivity by minimizing sedimentation and enhancing Brownian motion, along with ensuring particle uniformity. Nonetheless, an excessive increase in sonication duration can diminish aggregation and subsequently lower thermal conductivity (Philip and Shima, 2012; Qiu et al., 2020). Moreover, prolonged sonication may cause the breakdown of nanoparticles with a high aspect ratio, such as nanotubes (Garg et al., 2009), and interfere with the effectiveness of dispersant incorporation in nanofluids (Asadi et al., 2017).

2.5. Hexagonal Boron Nitride (hBN)

The classification of nanofluids can be influenced by the specific type of nanoparticles suspended in the mixture. Various materials, including ceramic oxides, metallic oxides (CuO, ZnO, TiO₂, SiO₂), metals (Cu, Ag, Au, Fe), carbon nanotubes (single and multi-walled), and graphene, are utilized in the production of nanofluids, representing different categories of nanoparticles. (Taha-Tijerina, 2018).

The success in obtaining graphene has encouraged researchers to look for other nanomaterials capable of substantially improving the properties of other materials when used together (Vahedi and Lahidjani, 2017). Hexagonal Boron Nitride (hBN) has been a candidate because it is an inorganic material that has a hexagonal structural shape similar to that of graphite and that, when it goes through the liquid exfoliation process, reaches its full potential by becoming a nanomaterial, as in the case of graphene (Coleman et al., 2011). Figure 2.15 shows the crystal structures of hexagonal boron nitride and graphite.

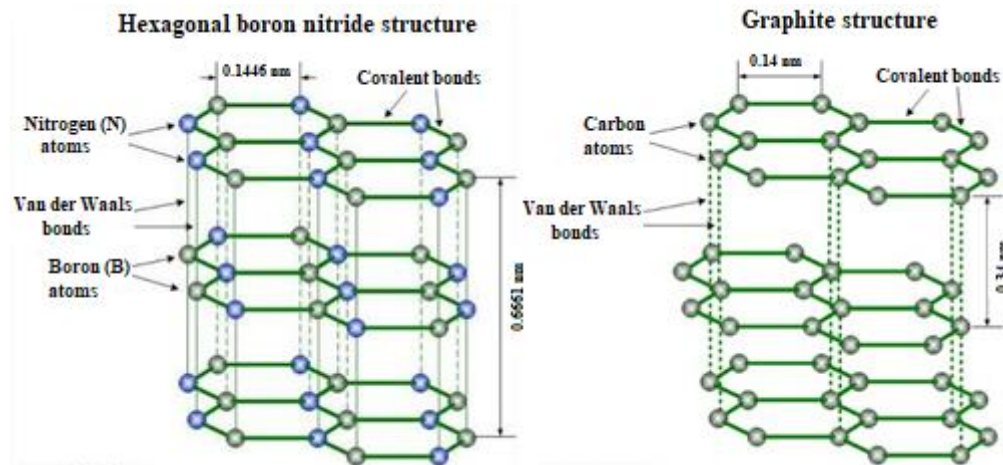


Figure 2.15 – Crystalline structures of hBN and graphite (Hod, 2012).

Boron and nitrogen, positioned as neighbors to carbon on the periodic table, share a similarity in their outer shell electron count and atomic radii with carbon. Consequently, boron nitride (BN) adopts a crystalline structure reminiscent of carbon, making BN compounds particularly intriguing (Lipp et al., 1989).

This binary chemical compound, composed solely of boron and nitrogen atoms, takes the molecular form BN. Unlike carbon, BN is not naturally occurring and must be synthesized. The process involves initially obtaining amorphous boron powder, which is then transformed into crystalline BN through heat treatment in a nitrogen atmosphere (Kim et al., 2011).

Boron Nitride was initially synthesized by English chemist W. H. Balmain in the 1840s through a method involving molten boric acid and potassium cyanide (Ertuğ, 2013; Eichler and Lesniak, 2008). However, this early formulation failed to produce a stable compound. For nearly a decade, Boron Nitride was only synthesized on a laboratory scale. It wasn't until the 1950s that Union Carbide initiated large-scale industrial production of BN composites, employing hot pressing techniques (Ertuğ, 2013).

Boron nitride (BN) stands out as a versatile material widely applied in various engineering and scientific domains. Its intriguing property of "polymorphism" allows it to crystallize into multiple structures, primarily influenced by variations in temperature, pressure, or both. These distinct structures, referred to as "polymorphs," exhibit significant differences in their physical properties despite sharing the same chemical formula. Consequently, understanding how to selectively promote the formation of a specific polymorph becomes crucial for effective material design (Nikaido et al., 2022).

Boron nitride can be synthesized in both amorphous and crystalline forms. The crystalline structures include four distinct forms, as illustrated in Figure 2.16. The first is Cubic, or c-BN, is a high-pressure diamond-like modification utilized as a superabrasive (Eichler and Lesniak, 2008; Engler et al., 2007). HBN, representing the most stable form, featuring a hexagonal layer structure. The wurtzite structure of boron nitride, w-BN, can be seen as a distortion of the cubic phase. BN also presents another less common phase, the rhombohedral (r-BN), which derives from different alignments of the hexagonal rings in the planes. Hexagonal and rhombohedral are composed of sp^2 type bonds and the cubic and wurtzite phases are composed of sp^3 type bonds. Each of these crystalline forms exhibits unique properties, rendering them suitable for diverse applications (Nikaido et al., 2022).

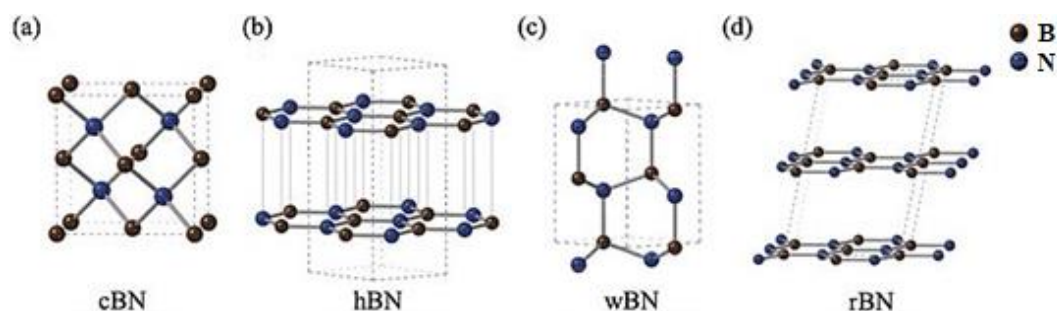


Figure 2.16 – Boron nitride crystal structures: (a) cubic, c-BN; (b) hexagonal, hBN; (c) wurtzite, wBN and (d) rhombohedral, rBN (Nikaido et al., 2022).

Preliminary investigations have empirically validated that nanostructures composed of boron nitride (BN) exhibit thermal and chemical stability comparable to, or even surpassing, that of nanostructures composed solely of carbon. Consequently, the utilization of boron nitride materials is favored for applications involving devices frequently exposed to elevated temperatures and chemically active environments (Kim et al., 2018).

HBN is the most stable crystalline form of Boron Nitride and presents some versatile properties such as high electrical resistance and thermal conductivity, lubricating action, excellent mechanical stability, notable chemical inertness, among others (Eichler and Lesniak, 2008; Golberg et al., 2010; Lin and Connell, 2012). Due to its chemical inertness, it has low toxicity and good environmental compatibility in relation to other ceramic materials.

In its crystalline structure, its molecules are arranged in layers that slide over each other, which gives its lubricity. Its lubricating effect combined with high thermal stability and oxidation resistance make hBN better than graphite for some applications such as thermal management systems, lubricants, ceramic composites and protective coatings (Aranganathan et al., 2016). The choice of lubricant depends on the specific requirements of the application, covering factors such as temperature, pressure and chemical compatibility. In summary, BN lubricants excel in high-temperature and chemically challenging environments, while graphite lubricants prove effective in mitigating friction and wear in low- to medium-temperature environments.

It appears as a white, fine and soft powder. Its two-dimensional (2D) layers are composed of boron atoms linked to three other nitrogen atoms by strong sp^2

covalent bonds in a honeycomb-type arrangement (Alem et al., 2009; Wang et al., 2011). Within each layer of this compound, each boron atom is covalently bonded to a nitrogen atom, which is one reason for the compound's strong thermal properties. While the overlapping layers are attracted to each other by weak van der Waals forces, which allows them to be easily exfoliated with mechanical work, such as in mixing and compounding methods or by other methods such as liquid exfoliation (Engler et al., 2007; Lipp et al., 1989).

Exposing lamellar material in solvent by ultrasonic waves is considered the most recent strategy for exfoliation. These waves are responsible for the formation of cavitation bubbles that collapse into jets of energy, fragmenting the crystals into exfoliated layers (Coleman et al., 2011; Niu et al., 2016). In addition to the exfoliative method with organic solvents, there are other methods that use surfactants, ionic liquids, electrochemical exfoliation or even exfoliate through shear.

This technique has been the most used because it does not involve chemical reactions and is a process that is not sensitive to air, thus maintaining the processability and intrinsic properties of the materials. It also presents the advantages of compatibility with any substrate, simplicity, versatility, reducing process costs and making these easily functionalized and high-quality nanoparticles obtained can be easily transformed into thin films, nanocomposites, nanohybrids, among other diverse applications (Coleman et al., 2011; Bao et al., 2016; Xie et al., 2015). Although this process presents difficulty in controlling the number and lateral size of nanolamellas, it presents a larger scale production than mechanical exfoliation (Coleman et al., 2011; Niu et al., 2016).

Liquid exfoliation involves using a small amount of material in powder form and mixing it with a solvent to form a low concentration dispersion. The solvent molecules are arranged between the lamellae of the material. Then, this solution is sonicated for a certain period of time capable of destroying the van der Waals force that exists between the atomic layers of the material, thus creating dispersions of isolated mono-layers as shown in Figure 2.17. In order to separate the material with few layers from the others, a centrifuge is used, resulting in a precipitate composed of poorly exfoliated material and a supernatant formed by the suspension of mono and few layers (Nicolosi et al., 2013; Zhou et al., 2011).

Some variables of the liquid exfoliation process, such as the type of solvent used, the initial particle size, the concentration of the dispersions, the sonication time and the centrifugation time and speed vary greatly from author to author and the efficiency of this process is directly linked the optimization of these mentioned parameters.

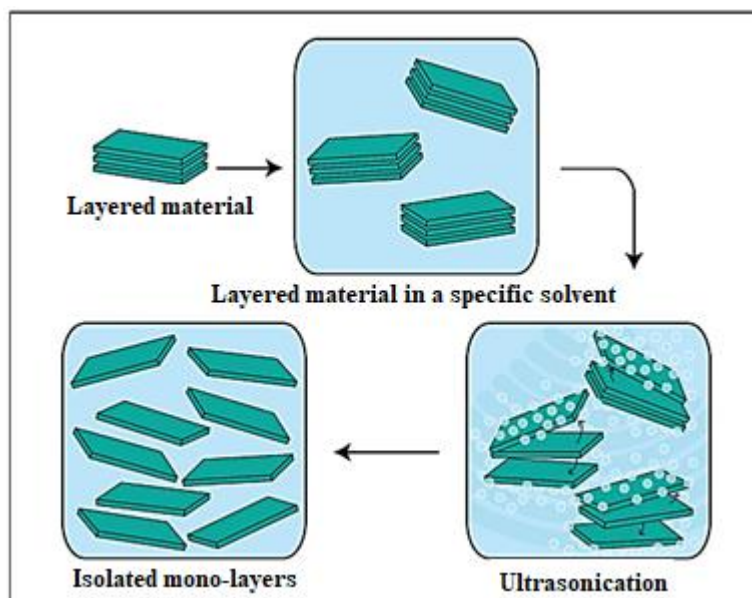


Figure 2.17 – Schematic of the liquid exfoliation process (Nguyen et al., 2016).

It is very important to know the corresponding value of the surface energy of the solvent and the material in question, because if these values are very close, the difference in energy between the exfoliated and reaggregated states becomes negligible, meaning that there is no reaggregation force stabilizing the two-dimensional layers of the material. When this occurs, the solvent is considered a good solvent. When aggregation and sedimentation of the lamellae occurs, the solvent is considered weak (Nicolosi et al., 2013). In Figure 2.18, it is possible to schematically observe what happens to the lamellae depending on the type of solvent used. Munaro et al. (2017) determined that the solvent composed of 20 % isopropyl alcohol (IPA) in water obtained the best liquid exfoliation performance of boron nitride.

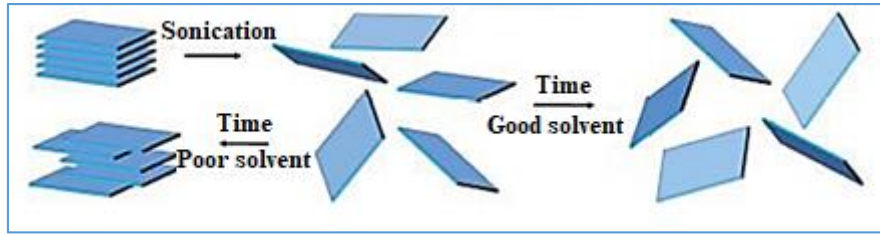


Figure 2.18 - Liquid exfoliation with ultrasound in “good” and “poor” solventes (Lin et al., 2017)

The ultrasonic bath is considered the most important step in this process. The sound waves propagated in the solution cause alternation of high and low pressure cycles, shaking the material in the dispersion and the vibration of these waves is responsible for causing the separation of the layers of the 3D material through the interactions between the solvent molecules and the surface of the particles (Niu et al., 2015; Cao et al., 2014).

As previously discussed, hexagonal boron nitride has a stacked sheet structure and the slip between these layers means that hBN can be used as an effective dry lubricant over a wide range of process temperatures due to its high thermal stability. (Ertuğ, 2013; Engler et al., 2007). It also has the ability to retain its low coefficient of friction even at extremely high temperatures, while similar materials such as molybdenum disulfide and graphite burn at lower temperatures (Ertuğ, 2013).

HBN also has good dielectric properties, that is, low relative permittivity. This low dielectric constant characteristic is the basis for its use in electrical insulation that can be fundamental for various applications. The dielectric constant of hBN is equivalent to half that of $\alpha\text{-Al}_2\text{O}_3$, a ceramic material widely used as thermal interface material (TIM), making it a viable substitute with better performance (Ertuğ, 2013; Armin, 2013).

There are other characteristics that make this material so desired for various applications. One of them is its low density of 2.27 g/cm^3 (theoretical) and high thermal stability with a melting point of approximately $2600 \text{ }^\circ\text{C}$. hBN is chemically inert and has strong resistance to acids and molten metals. Furthermore, it shows good stability in air up to $1000 \text{ }^\circ\text{C}$, argon gas up to $2200 \text{ }^\circ\text{C}$ and nitrogen up to $2400 \text{ }^\circ\text{C}$ (Lipp et al., 1989; Engler et al., 2007). Some other key properties are

its low thermal expansion, good thermal shock resistance, microwave transparency and non-toxicity (Ertuğ, 2013).

HBN initially was used in cosmetics and was later revitalized for various industrial uses, including metal plating, automotive, high-temperature furnaces, thermal management, and numerous other applications (Eichler and Lesniak, 2008; Engler et al., 2007). It can be employed in powder, coating, and sintered forms, showcasing its versatility and extending its range of applications (Eichler and Lesniak, 2008).

In the last decade, the use of ceramics as functional fillers has become increasingly common and their application is essential to maintain high performance and extend the useful life of products in general. Materials such as aluminum oxide, silicon nitride, silicon carbide and magnesium oxide are relatively inexpensive and provide an increase in thermal conductivity and electrical insulation. However, these ceramic fillers are abrasive, which can cause wear on equipment and tools during processing. The addition of hexagonal boron nitride compared to conventional materials shows significantly higher thermal conductivity in composites with the additional characteristic of being lubricants. These properties can be used not only to increase product performance, but also have the potential to increase the efficiency of the manufacturing process (Ng et al., 2005).

2.6. Previous experimental work studies on water-based drilling fluids under high pressure and high temperature conditions

The subsequent section provides a concise overview of pertinent research on the rheology of water-based drilling fluids under high pressure and high temperature conditions, showing the impact of xanthan gum on the rheological properties of these fluids.

Hamed and Belhadri (2009) delved into two distinct drilling fluid formulations featuring diverse biopolymers: one incorporating scleroglucan and the other employing xanthan gum, both dissolved in distilled water. Additionally, consistent concentrations of starch and a bactericide were integrated, while materials such as clay, calcium carbonate, and potassium chloride varied across different concentrations. All assessments were conducted at 25 °C utilizing the

Rheostress 600 by ThermoHaake. Through this study, an array of effects stemming from additives in water-based drilling fluids was discerned, revealing a consistent trend of shear-thinning behavior characterized by low yield stress and high permeability across all fluids

Amani, Al-jubouri et al. (2012) investigated in their work the rheological behavior of drilling fluids with different densities with the intention of discovering the temperature at which these fluids would degrade when subjected to high shear rates and high pressure. They were able to reach the conclusion that high temperatures lead to thermal degradation of the polymer and solid components, causing the expansion of the molecules and reducing the fluid's resistance to flow.

The utilization of water-based drilling fluids has experienced a significant surge, prompting investigations into improving their rheological and thermal characteristics under high-pressure and high-temperature (HPHT) conditions. Given their improved thermo-physical properties and stability, the incorporation of nanoparticle suspensions alongside drilling fluids has been advocated for such scenarios (Elkatatny et al., 2018; Echt and Plank, 2019).

William et al. (2014) analyzed the electrical, thermal and rheological properties of water-based drilling fluids under HPHT conditions using CuO and ZnO nanofluids (size <50 nm) in an aqueous suspension of xanthan gum. Tests were carried out at temperatures of 25, 70, 90 and 110 °C and pressures of 1 bar and 100 bar. They concluded that, even at low concentrations, the nanoparticles led to an increase in the thermal and electrical conductivity of the suspensions in which they were inserted. At higher concentrations, the effects of pressure and temperature on the rheology of the suspensions were suppressed and the Herschel-Bulkley model was the best fit model for the rheological behavior of the analyzed suspensions.

Jain et al. (2015) discussed the viability of polyethylene glycol/SiO₂ nanocomposite grafted with polyacrylamide as a potential additive for water-based drilling fluids and observed that the nanocomposite improved the rheological properties of the fluid as well as increased plastic viscosity (17 -26 mPa.s), apparent viscosity (25-41 mPa.s), gel strength (0.66-3.83 Pa) and yield stress (8-15 Pa). The developed fluid also showed a relatively high return permeability value (74%), indicating less formation damage effect due to the formation of less permeable filter cake.

Anoop et al. (2019) studied the rheology of a water-based drilling fluid suspended with CNT (carbon nanotubes) particles and observed that with a concentration of just 0.22 wt.% of CNT the viscosity values were increased by five times when compared to those of the fluid base. Both the base fluid and the nanofluid with low concentration had an increase in viscosity with increasing pressure, while suspensions with higher concentrations of CNT, a decrease in viscosity was observed with increasing pressure. Regarding the effect of temperature, it was observed that for higher concentrations of CNT filler, the viscosity values decreased with an increase in temperature similar to that of water. They explained that this decrease was due to the fact that the addition of these nanoparticles in high concentration led to the agglomeration of mud particles in the CNT chain, separating the water from the drilling fluid mixture and thus reducing its viscosity.

Mansoor et al. (2021) investigated the application of natural aloe vera nanofluids (base fluid) and CuO (in concentrations of 0.2, 0.4 and 0.6 wt.%) combined as additives in water-based drilling fluids (WDF) under HPHT conditions. The results revealed that aloe vera-based CuO nanofluids improve the thermal stability and rheological properties of drilling fluid and significantly decrease American Petroleum Institute (API) filtrate. There was a drop in WDF viscosity of 61.7% upon heating to 90°C. The rheological data were adjusted to the Herschel-Bulkley model and suggested improvements in the rheological and filtration properties of the suspensions with the implementation of these additives.

Kalhuri et al. (2023) used in their research the $CeVO_4/Al_2O_3/rGO$ nanocomposite synthesized by the hydrothermal method to evaluate the impact on the rheological and thermal properties of a drilling fluid with its application. It was observed that after adding 0.5 wt.% of the nanofiller, there was only 6 ml of circulation loss and that the plastic viscosity (PV) of the suspension was tripled by increasing the concentration from 0.01 to 0.5 wt.%. Thermal conductivity and gel strength in all samples were significantly improved, especially in the presence of Al_2O_3 nanoparticles.

Many studies have already been carried out in the area of water-based drilling fluids using nanoparticles according to the works mentioned above, however, there is still a lack of rheological studies of drilling fluids using hBN nanoparticles, as was the focus of this work. Although there are still few data in the

literature on hBN nanofluids, there are recent works reporting some of their properties such as rheological behavior, thermal conductivity and stability.

Ilhan et. al (2016) experimentally investigated the increase in thermal conductivity and viscosity of nanofluids based on DI water, ethylene glycol (EG) and DI-EG water (50 % each), with hBN particle volume concentration varying between 0.03 % and 3 %. Observed that hBN nanofluids have notably higher thermal conductivity values than their corresponding base fluids, depending on the volume concentration of the dispersed nanoparticles, and furthermore, that water-based hBN nanofluids with relatively dilute particle suspensions exhibited a significant increase in thermal conductivity and viscosity.

Navaneethakrishnan et al. (2019) studied BN/epoxy nanocomposites produced by the liquid casting method. The SEM images showed the uniform dispersion of BN particles in epoxy matrix and the agglomeration of BN particles was absorbed into 2 % of the BN/epoxy nanocomposites and that the mechanical properties of the nanocomposites increased with the increase of BN particles by up to 1 %. They also found that the wear rate and friction coefficient of the nanocomposites were decreased due to the load-bearing characteristics of the BN particles.

Liu et al. (2019) assessed the thermal transfer performance of three hBN size geometries: microscale hBN powder, hBN nanosheets, and a combination of micro- and nanoscale hBN. The findings indicate that hBN nanosheets demonstrate the highest in-plane thermal conductivity with loadings ranging from 0 to 5 wt%. For through-plane thermal conductivity, all three geometries exhibit similar thermal properties when the filler loading is below 5 wt%. However, through-plane thermal conductivity experiences a sudden increase to $5.69 \text{ W.m}^{-1} .\text{K}^{-1}$ at a loading of 5 wt%.

Cheng et al. (2020) demonstrated the use of silicone composites / few-layer hexagonal boron nitride (FL-hBN) for heat dissipation applications by introducing pure hBN and FL-hBN into the silicone with different ratios to study their properties thermal. They concluded that the silicone/FL-hBN composite exhibited higher thermal conductivity than the silicone/hBN composite. They also observed that with the ideal filler content of 30 wt% FL-hBN, the thermal conductivity of the composite can be increased to 230 %, which is higher than that of silicone/hBN (189 %), thus indicating that jet cavitation was an effective and

rapid way to obtain few-layer hexagonal boron nitride and that it effectively increased the thermal conductivity of silicone composites.

Ysiwata-Rivera et al. (2020), studied the effect of incorporating pure and modified hexagonal boron nitride (hBN) nanosheets on the stability, viscosity and electrochemical behavior of a waterborne emulsion acrylic coating. The results prove an effective deposition of PAA films on the hBN surfaces, which increased the stability and the acrylic viscosity of the nanostructured coatings. Electrochemical analysis demonstrated an increase in corrosion resistance in nanostructured acrylic coatings with 1 wt.% of unmodified and modified hBN nanoplatelets compared to pure acrylic paint.

The study by Urbaniak et al. (2022) was made with a PAO₄-based lubricating oil, which contained hexagonal boron nitride nanoparticles and a succinic acid imide-based dispersant. The results demonstrate that hBN improves the tribological properties of lubricating oils, however, oil preparation and quantitative selection of components strongly influence the results.

Although there are some studies exploring the properties of hBN and showing its excellent results, there are no studies in the literature focused on the petroleum industry that reinforce drilling fluids with hBN nanoparticles, which is the focus of this work, aiming to improve their rheological and thermal properties.

2.7. Xanthan Gum

Microbial biopolymers are macromolecules normally formed by monosaccharides and uronic acid derivatives, which, due to their ability to form viscous solutions and gels in an aqueous medium, are also known as gums (Sutherland, 2005). This class of polymer can exhibit suspending agent, thickening, stabilizing and gelling properties. Furthermore, they have some advantages over synthetic polymers, obtained from vegetables and seaweed, such as production independent of climatic conditions, possibility of using renewable raw materials, faster production, as well as the possibility of modifying rheological properties through the control of process parameters (Gowthaman et al., 2021).

Xanthan gum is a natural polymer produced by bacteria of the genus *Xanthomonas*, with *Xanthomonas campestris* being the most used species. It is generally obtained by aerobic submerged cultivation, at around 28°C and depends

not only on the composition of the medium, but also on the cultivation conditions and feeding techniques. Thus, it is possible to obtain a variation in the yields and quality of the polymer, as these variables such as the composition of the culture medium, carbon source, nitrogen source, mineral salts, fermentation conditions, time, pH, temperature, agitation speed and oxygen concentration rate influence the composition, rheological properties and the molecular structure of the biopolymer (Casas et al., 2000; García-Ochoa et al., 2000; Rosalam and England, 2006).

The molecular mass of xanthan gum can vary from 15 to 30,000,000 g.mol⁻¹, but is generally 2,000,000 g.mol⁻¹, depending on the fermentative process and the *Xanthomonas* strain used. The primary structure of this exopolysaccharide, in general, consists of repeating pentasaccharide units composed of two glucose units, one glucuronic acid unit and two mannose units in addition to variable proportions of pyruvate and acetyl substituent groups, as shown in Figure 2.19. (Jansson et al., 1975; Moreno et al., 1998; Rosalam and England, 2006).

The main chain contains β-D-glucose units linked at positions 1 and 4. The trisaccharide that constitutes the side chain contains two D-mannose units linked at the O-3 position of glucose residues in the main chain and one unit of D-glucuronic acid between these two units. Around 50% of the terminal D-mannose residues contain pyruvic acid residues, with an indeterminate distribution. There is an acetyl group at the O-6 position on the D-mannose unit that is attached to the main chain. The acetyl and pyruvate groups are related to the viscosity of aqueous solutions of these polymers and make the polysaccharide an anionic type (García-Ochoa et al., 2000; Sutherland, 2005).

The ionic character, due to the presence of acetyl and pyruvate groups, and the side chain, are related to the molecular conformation in addition to increasing its hydration and conferring tonicity to xanthan.

The way in which a polysaccharide dissolves depends on the primary structure (chemical composition) and secondary structure (conformation of the polymer chain). The secondary structure of xanthan gum is contingent upon the conditions under which the molecule is characterized, exhibiting either an ordered or disordered conformation. The ordered conformation may be native or renatured, and there is no consensus regarding the relationship between conformational activity and the verified structure type. The native form prevails at temperatures below the molecule's conformational transition point, influenced by the ionic

strength of the medium in which xanthan is dissolved. The "order-disorder" conformational transition, as shown in Figure 2.20, is prompted by temperatures surpassing the transition point and/or a reduction in ionic strength. Both native and renatured configurations hinge on the same factors (Born et al., 2002).

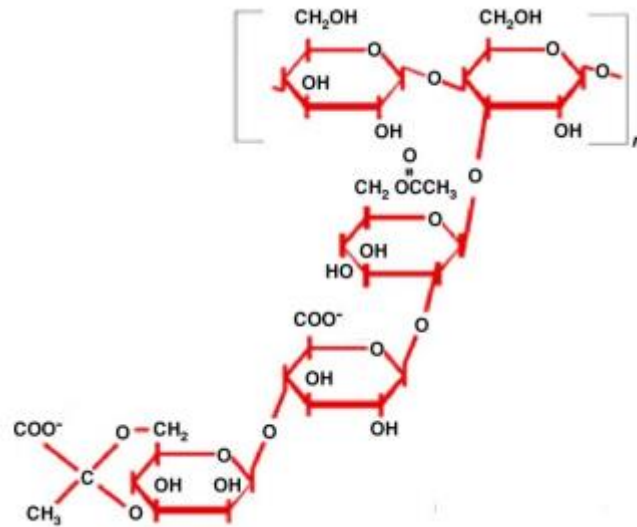


Figure 2.19 – Structure unit of xanthan gum (Rosalam and England, 2006)

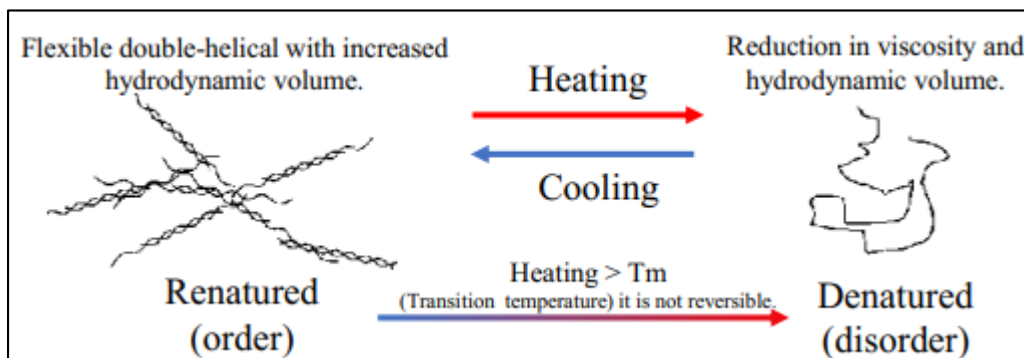


Figure 2.20 – Schematic representation of the order-disorder conformation of xanthan gum (Adapted from Ardila, 2021)

If xanthan gum is heated, or is in a saline solution or in a medium with weak ionic strength, it goes through a process of changing the conformation from order to disorder. This process generally starts at 70 °C and ends at 90 °C and results in a decrease in shear-thinning behavior (Morris, 1996; Ardila, 2021). Order-disorder conformation can be considered a partial double helix joining process. Due

to high temperatures, a complete unwinding of this double helix is possible (Liu and Norisuye, 1988). The difference between the ordered and disordered conformations is that in the ordered one, the side chain is folded in association with the main chain, whereas in the disordered one the side chain is not associated but rather distant from the main chain (Pelletier et al., 2001).

There is contradiction regarding the effect of adding salts to xanthan solutions. In some studies, the viscosity of diluted xanthan solutions increases in the presence of sodium chloride (NaCl), while in other cases, the viscosity decreases subtly. (Higiro et al., 2007). Generally, XG solutions are stable in the presence of most salts. The polymer may precipitate due to divalent ions if subjected to specific pressure and temperature conditions, that is, if the cation interacts with the negatively charged part of the carboline this may lead to precipitation. The way in which the salt concentration can affect the viscosity of this solution depends on the concentration of the polymer. Monovalent salts such as NaCl reduce the viscosity of the suspension when there is a gum mass concentration lower than 0.5%. (Mi Swaco, 2001.)

Gums are polymers capable of forming aqueous solutions with very high viscosity even at low concentrations. Aqueous solutions of these biopolymers have excellent rheological properties, due to their pseudoplastic character, and because they maintain stable viscosity over a wide range of salt concentrations, temperatures and pH (Kennedy and Bradshaw, 1984; Rosalam and England, 2006). This polysaccharide has numerous applications as an emulsion stabilizer, suspending agent and thickener in the agricultural, pharmaceutical and food products sector (García-Ochoa et al., 2000). In the oil industry it is usually used as viscosifiers in WBMs together with other polymer additives such as carboxymethylcellulose, depending on their molecular structure and chemical configuration (Caenn and Chillingar, 1996; Benyounes et al., 2010; Jang et al., 2015). The addition of these viscosifiers results in a shear-thinning and thixotropic behavior of the mud that improves the filtrate control and facilitates the cleaning of the well and the suspension, and removal cuttings in absence of fluid flow (Ezell et al., 2010).

To determine its functionality and applications, it is important to know the chemical composition of xanthan gum. Gums of commercial interest must be capable of forming secondary, tertiary and, sometimes, quaternary structures in an aqueous medium, once the primary structure has a configuration that favors these

arrangements. Through genetic manipulations, it is possible to modify the degree of acetylation and the degree of pyruvation to obtain polymers with better yields. Its chemical composition can also be changed through deacetylation reactions by heat treatment or alkaline hydrolysis with the aim of improving its properties (Riaz et al., 2021). The Table 2.1 shows the value of concentrations used for each type of industrial applications of xanthan gum.

Table 2.1 – Main industrial applications of xanthan gum (adapted by García-Ochoa et al., 2000)

Application	Concentration (% w/w)	Functionality
Salad dressings	0.1 – 0.5	Emulsion stabilizer, dispersant
Dry mixes	0.05 – 0.2	Eases dispersion in hot or cold water
Syrups toppings, relishes	0.05 – 0.2	Thickener, heat stability
Beverages (fruit and non-fat dry milk)	0.05 – 0.2	Stabilizer
Dairy products	0.05 – 0.2	Stabilizer viscosity control of mix
Baked goods	0.1 – 0.4	Stabilizer, facilitates pumping
Frozen foods	0.05 – 0.2	Improves freeze-thaw stability
Pharmaceutical (cream and suspensions)	0.1 - 1	Emulsion stabilizer, uniformity in dosage formulations
Cosmetic	0.2 - 1	Thickener and stabilizer
Agriculture (additive in animal feed and pesticide formulations)	0.03 – 0.4	Suspension stabilizer, improved sprayability, reduced drift, increased cling and permanence
Textile printing and dyeing	0.2 – 0.5	Control of rheological properties of paste, preventing dye migration
Ceramic glazes	0.3 – 0.5	Prevents agglomeration during grinding
Slurry explosives	0.3 - 1	Thickens formulations
Petroleum production	0.1 – 0.4	Lubricant of friction reduction
Enhanced oil recovery	0.05 – 0.2	Reduces water mobility by increasing viscosity

3. MATERIALS AND METHODS

3.1 Materials

The reagents used for the production of oxidized boron nitride (hBN-oxi) were boron nitride <1 μ m> 98 %, sulfuric acid (H₂SO₄) 99 %, nitric acid (HNO₃, ACS reagent, 70 %) (all provided by Sigma -Aldrich) and isopropyl alcohol (IPA) (delivered by Synth). For the preparation of nanofluids, xanthan gum (provided by Plury Química Ltda), sodium benzoate, and potassium sorbate (obtained from Vetec) were employed. The deionized water was supplied by PUC-Rio through the water purification system using the reverse osmosis method.

3.2 HBN oxidation and exfoliation process

The oxidized nanomaterial was obtained by liquid exfoliation in a mixture of 20 % by volume of IPA in DI water, a proportion that, according to a study carried out by Munaro (2017), obtained the most promising exfoliative process. For the boron nitride oxidation procedure, 5.0 g of hBN were placed in a volumetric flask in an ice bath, slowly adding firstly 12.5 mL of HNO₃ and then 37.5 mL of H₂SO₄ under constant stirring for 3 hours of oxidation. This procedure was adapted from Silva et al. (2018). This process took place with a condenser coupled to the balloon and the circulation bath, as it generates toxic gases. After this process, the acid suspension was diluted with deionized water until reaching a pH of around 5.5-6.5. This step also took place under an ice bath, as it is an exothermic reaction. Once the ideal pH was reached, the suspension was placed at rest for 24 hours for the decantation of the hBN-oxi, and then filtered with a vacuum pump and heated in an oven at 100 °C in order to remove the aqueous residues that still existed in the material. Exfoliation was performed by exposing the material to ultrasonic waves in a tabletop 416 DA ultrasonic washer. The lamellar crystals were exfoliated through cavitation, generating the nanolamellae. The efficiency of this process strongly depends on the choice of solvent, time, and power of the ultrasound. For that reason, it was performed in a mixture of 20 % IPA/H₂O in an ultrasound bath for 4 hours at a frequency of 40 kHz. This process can be observed in Figure 3.1.

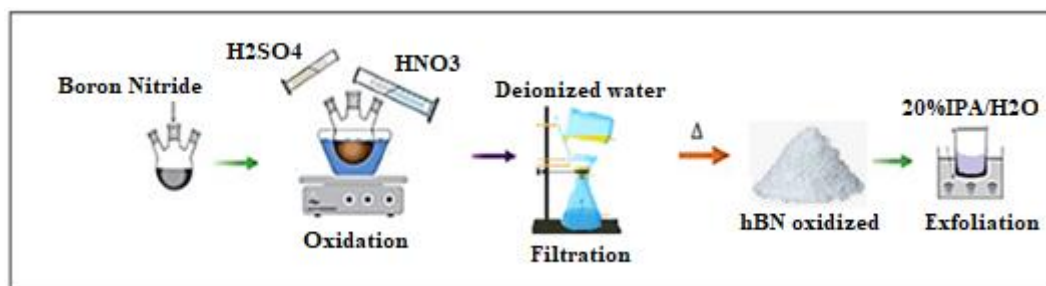


Figure 3.1 – HBN-oxi preparation method

Samples for rheological and thermal studies were prepared with concentrations ranging from pure solvent to a concentration of 60 mg mL^{-1} of hBN-oxi, as shown in Table 3.1.

Table 3.1. The concentration of the hBN-oxi suspensions used for rheological and thermal studies.

Concentration (mg mL^{-1})	Concentration (wt.%)
0	0
5	0.5
10	1.0
15	1.5
30	3.0
60	6.0

3.3 Nanofluid Preparation

In the present study, nanofluids were prepared by the two-step method to homogeneously disperse the hBN-oxi 2D nanostructures within the base fluid. Then, the xanthan gum (XG) was added to the nanofluid as can be seen in the Figure 3.2. The xanthan gum used was the F200 with an average molecular weight of $2 \times 10^6 \text{ g mol}^{-1}$. This biopolymer is a natural polysaccharide that presents a complex molecular structure and, due to the fact of presenting excellent rheological properties and stability in a wide range of pH and temperature, it is widely used as an additive in the petrochemical industry (Garcia-Ochoa et al., 2000). To prepare a suspension with 0.86 wt.% XG (Vargas et al., 2020), 0.688 g of the polymer powder was slowly dispersed in a mixture of 20 % by volume of IPA and 80 % of DI water

under constant mechanical agitation under 300 rpm rotation for 15 min. Then, 0.4 g of each weighed bactericide (sodium benzoate and potassium sorbate) was added, and the suspension was stirred for another 1 hour. The suspensions were left to rest for 24 h, which is the time required to completely hydrate the molecules (Vargas et al., 2020). The structure characterization and the thermal and rheological tests were carried out after 3 days of sample preparation, as this is the time required, on average, to obtain stable homogeneous nanofluids (Taha-Tijerina et al., 2020).

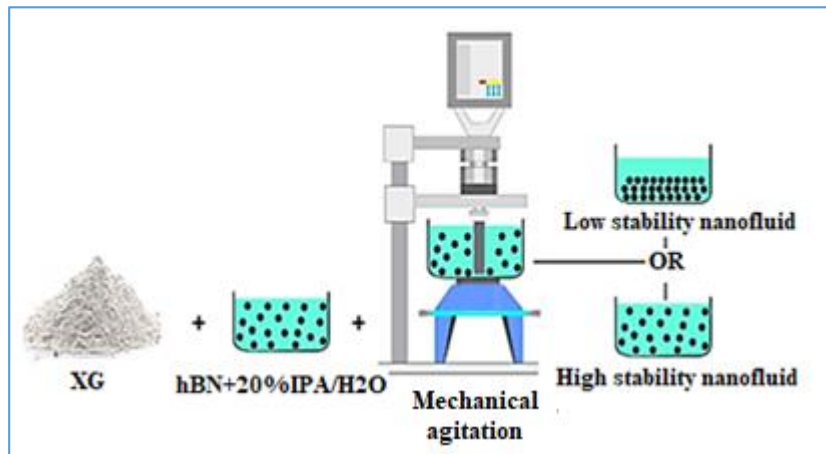


Figure 3.2 – Nanofluid preparation

The nanofluid systems (C.0 to C.5) prepared for the study to analyze the effect of nanoparticle concentration, temperature and pressure are shown in Table 3.2.

Table 3.2. Nanofluid formulations to analyze effect of nanoparticle concentration, temperature and pressure

Concentration of hBN-oxi (mg mL ⁻¹)	Base fluid	Nomenclature used
0	0.86 wt.% XG in 20% IPA/H ₂ O	C.0
5	0.86 wt.% XG in 20% IPA/H ₂ O	C.1
10	0.86 wt.% XG in 20% IPA/H ₂ O	C.2
15	0.86 wt.% XG in 20% IPA/H ₂ O	C.3
30	0.86 wt.% XG in 20% IPA/H ₂ O	C.4
60	0.86 wt.% XG in 20% IPA/H ₂ O	C.5

3.4 Morphological and structural characterizations

Several tests were performed to obtain the characterization of hBN-oxi nanoparticles by researchers at Mackenzie-SP. Scanning electron microscopy (SEM) images were obtained using a Quanta 200 equipment, model FEG-FEI 2006, operating under vacuum with an electron beam under acceleration voltage between 5 and 30 kV. The samples were covered with gold via sputtering. Later, transmission electron microscopy (TEM) images were obtained on an FEI TECNAI G2 equipment, operating in vacuum with an electron beam (tungsten filament) of 200 kV. The Fourier transform infrared spectroscopy (FTIR) was used to analyze the hBN-oxi vibration modes between nitrogen and boron atoms with powdered samples, and the spectrum of 500 to 4000 cm^{-1} was recorded on Bruker Vertex 70 with a resolution of 4 cm^{-1} and 61 s of scan time. To perform the X-ray diffraction (XRD) analysis, the dried samples were placed in the sample holder of the equipment. The diffractograms were obtained in a Rigaku Miniflex II equipment operating with a copper filament tube ($\lambda = 1.5406 \text{ \AA}$), with steps of 0.02 $^\circ$ and a scan rate of 1 $^\circ \text{ min}^{-1}$. X-ray photoelectron spectroscopy (XPS) was obtained using monochromatic Al $K\alpha$ radiation (1486.6 eV) with an electron energy analyzer (Specs, Phoibos-150). The base pressure in the vacuum chamber was 2.0×10^{10} mbar. The detailed oxidation states of the elements were obtained from fitting the XPS peaks assuming their shape as a convolution of Lorentzian and Gaussian of the different contributions (Silva et al., 2018). Thermogravimetric analyses (TGA) were performed using a TA Instruments model SDT Q600 thermal analyzer. The sample was heated from 30 to 800 $^\circ\text{C}$ with a heating rate of 5 $^\circ\text{C}\cdot\text{min}^{-1}$ under a nitrogen atmosphere. Dynamic light scattering (DLS) was used to analyze agglomerations and particle size distributions in the nanofluid, and Potential Zeta was employed to determine the stability of the nanofluids, both measured on an Anton Paar DLS Litesizer 500 particle size analyzer. Two samples with a concentration of 1.0 mg mL^{-1} were used in the analysis, and the suspensions were taken before the nanofluid homogenization for 30 minutes in an ultrasound bath. Raman spectra have been obtained from Horiba xplora, $\lambda = 532 \text{ nm}$.

Images of the XG suspension with hBN-oxi were also obtained by Cryo-SEM, using the TESCLAN CLARA field-free Ultra-High Resolution (UHR) electron microscope and the Cryo system PP3010T (Quorum). The suspensions

were quickly frozen when immersed in liquid nitrogen ($T < -210$ °C) and then fractured using a cooled knife. Employing an accelerated voltage of 5kV and vacuum circumstances at -140 °C, several observations were carried out.

3.5 Thermal measurements

Thermal conductivity measurements were carried out on nanofluids at various nanostructure concentrations according to MTPS (Modified Transient Plane Source) technique employed by the C-Therm TCi™ Thermal Conductivity Analyzer. The method employs a reflectance heat sensor that momentarily applies heat to the sample, allowing the analysis to only need a flat surface to be used. After heat is applied, the sensor monitors the temperature variation at the interface and thus determines the thermal conductivity. The Liquids Cell accessory was utilized as a sample containment support during the assay, conducted using the Polymers method, with water considered as the contact agent. Part of the nanofluids were placed in a Becker and the sensor inserted into the fluid ensuring contact between it and the sample. With the intention of analyzing the influence of concentration on the thermal conductivity of suspensions, five different measurements were performed for each suspension at room temperature (approximately 23 °C).

Then, with the intention of analyzing the influence of temperature on the thermal conductivity of suspensions, the assay was performed at temperatures of 5, 20, 50, and 70 °C. The sensor was placed inside an environmental chamber that use a hot air forced-convection principle. After temperature stabilization, calibration was performed using standard material (Pyrex). Subsequently, the sample already placed in the Liquids Cell accessory was introduced into the heated chamber, and after the temperature of the sample stabilized, five different measurements were performed for each suspension.

3.6 Rheological measurements

The rotational physical rheometer MCR501 (Anton-Paar) and the rotational rheometer Haake Mars III (Thermo Fisher Scientific) measured the rheological properties of these nanofluids through cone-plate geometry (MCR501) and concentric cylinders (Haake Mars III). Both systems can be seen in Figure 3.3.

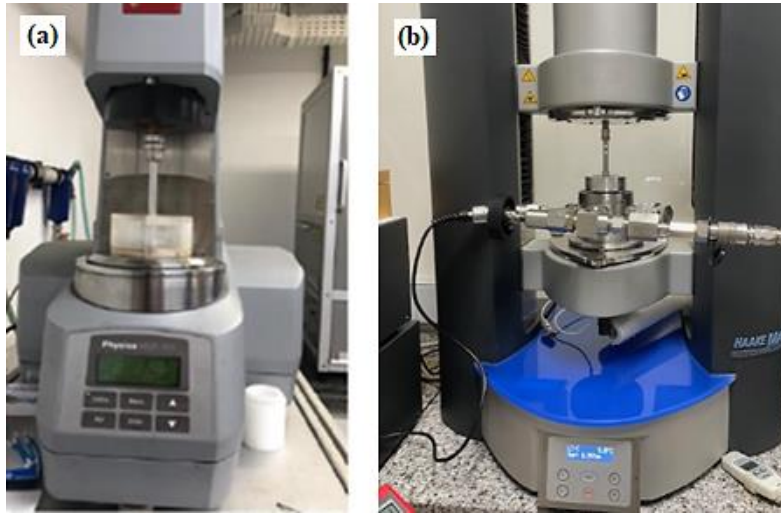


Figure 3.3 – (a) Physica rheometer MCR501 and (b) Haake Mars III

The rheological study was carried out in steady state, dynamic and transient conditions. Such procedures differ from each other through the way in which the deformation is applied to the sample. The follow parameters were analyzed: concentration, temperature, and pressure. The cone-plate specifications are the conical body angle, which is less than 0.01 rad ($\alpha = 6^\circ$), a planar circular plate with a diameter of 60 mm, and a gap of 0.057 mm between both parts, where the suspension is placed. The flow with this type of geometry is homogeneous because the shear rate is uniform. Then, it is not necessary to correct the data obtained. The dimensions of the concentric cylinders are shown in Table 3.3.

Table 3.3. The dimensions of concentric cylinders system

Specifications	Dimension
Radius internal	17.5 mm
Raius external	19.5 mm
Cup length, internal	80 mm
Approximate sample volume	46 mL

Before performing the tests, the samples were homogenized by reducing the maximum amount of sedimented particles in the suspension using a magnetic stirrer for 15 minutes at a constant frequency of 600 Hz. Each test was performed at least three times to guarantee good reliability and reproducibility of the results.

A protective cap was used above the cone-plate in order to contain solvent evaporation in each test performed on MCR501.

Rotational and oscillatory tests were performed for different temperature conditions (4, 20, 50 and 80 °C) controlled by a Peltier plate in and for two pressures (0.1 and 30 MPa). High pressure tests were carried out on the Haake Mars III where the sample was pressurized with nitrogen gas (N₂). Measurements were also made after the sample reached 80 °C and returned to room temperature of 20°C. These results were identified as AC 20 °C (after cooling) in this study. As the drilling fluid reaches high temperatures at high depths and after it returns to the surface, it returns to around 20°C, so this analysis was carried out with the aim of evaluating the degradation of the fluid after going through these stages of the drilling process. These temperature and pressure values were chosen to simulate HPHT environments where reservoirs reach high temperatures such as 150 °C and 70 MPa (Amani and Shadravan, 2012). However, due to the limitations of the rheometer, we were able to carry out tests up to 80 °C and 30 MPa (maximum 40 MPa).

With the pre-shear results it was possible to conclude that the samples reached the steady state quickly, taking around 100 seconds. Therefore, flow curves were obtained ranging from the highest shear rate of 1,000 s⁻¹ to the lowest 0.1 s⁻¹ (Vargas et al., 2019) and the results were plotted on a logarithmic scale. The choice to sweep these shear rate values, considering the limitations of the rheometer, is due to the range of shear rates in a drilling circulating system as shown in Table 3.4.

Table 3.4. Range of Shear Rates in a Drilling Circulating System (Guo and Liu, 2011).

Location	Approximate Shear rate (s ⁻¹)
Mud pumps	< 1 - 5
Annulus	5 - 200
Pipe/Collars	100 – 10,000
Bit Nozzles	> 10,000

As for the oscillatory tests, tests such as deformation, time and frequency sweep were performed and thus the responses of the storage (G') and loss (G'') modules were obtained as a function of each of those parameters. To determine the linear viscoelastic region (LVR) of nanofluids, the deformation sweep was performed at a fixed frequency of 1 Hz varying the strain from 10 % to 10,000 %.

And in the dynamic frequency sweep, a fixed strain value obtained from the region of linear viscoelasticity is applied and the frequency was varied from 0.1 to 100 Hz, to investigate the structure of the suspensions and obtain the characterization of the mechanical behavior of the material. Points where the torque value was less than 3 $\mu\text{N}\cdot\text{m}$ were discarded due to the rheometer torque transducer limitation.

4. RESULTS AND DISCUSSIONS

This chapter outlines the findings derived from characterizations aiming to enhance comprehension of the morphological and structural traits arising from processing methods. The analyses conducted based on these results shed light on the impact of nanostructures on thermal and rheological properties of these suspensions.

4.1 hBN-oxi nanoparticles characterization

Morphological and structural characterization of the nanomaterials is extremely important to understand the rheological and thermal responses of the suspensions. Some characteristics of hBN-oxi such as crystal structure, chemical composition, and morphological properties must be analyzed in order to understand the thermal and rheological behavior. Figure 4.1a shows the XRD diffractogram obtained for samples of hBN bulk, hBN-oxi, and the hBN diffraction pattern of the Powder Diffraction File™ (PDF®) card 34-0421 (Gates-Rector and Blanton, 2019). The sharp and intense peak at 26.8° could be assigned to the (002) crystallographic plane of the hBN structure, revealing an interlayer spacing of 0.332 nm (Kostoglou, 2015). Applying Bragg's Law to the plane (002) the d-spacing obtained for hBN-oxi was 0.334 nm, similar to the interlayer distance of graphite (0.335 nm) (Kostoglou et al., 2015). Other peaks, yet much weaker, can also be observed at 41.51, 44.26, 50.37, and 55.11, related to the (100), (101), (102), and (004) planes, respectively. The XRD pattern of the hBN samples revealed a highly ordered crystalline structure. As can be seen in the hBN-oxi diffractogram, no significant changes were observed in the peaks' diffraction angles, but the diffraction peaks suffered a considerable intensity decrease upon the exfoliation/oxidation process. Moreover, by applying the Debye-Scherrer equation to the (002) peak of the hBN-oxi, the average crystalline thickness of the nanomaterial was found to be equal to 15.2 nm.

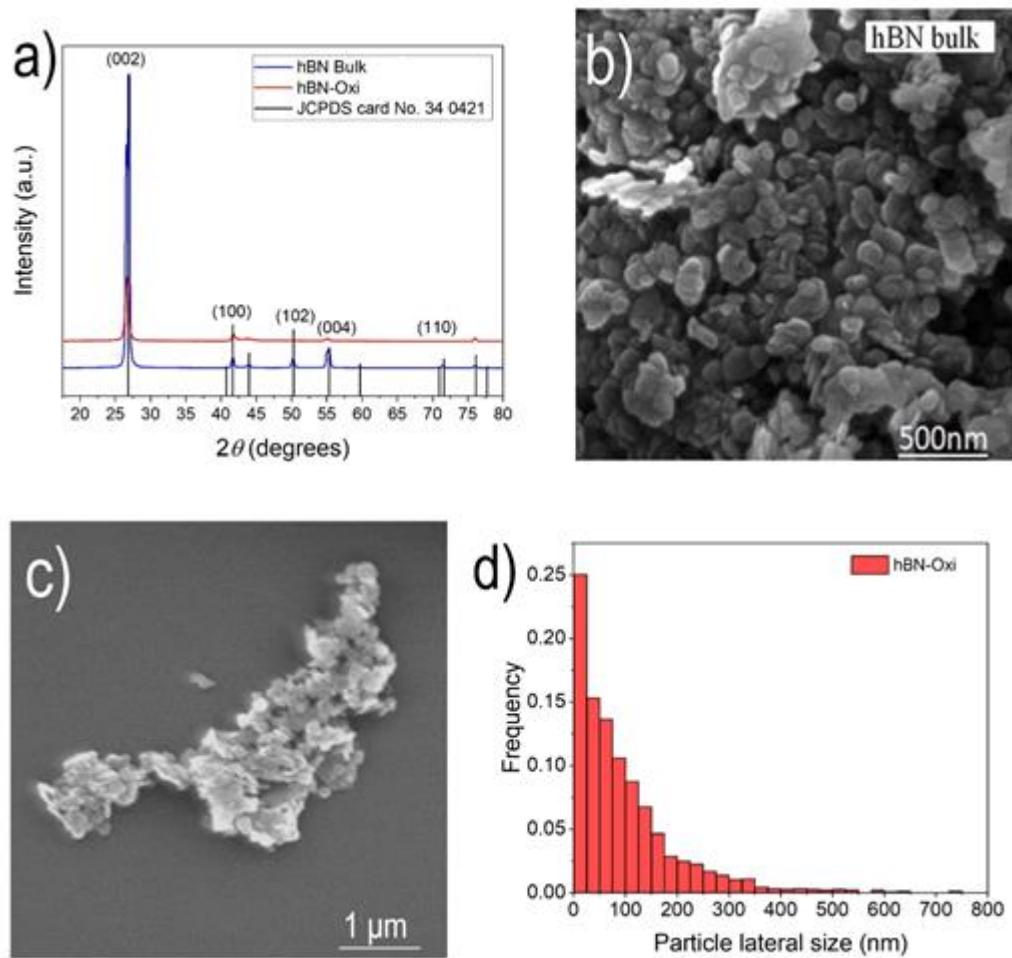


Figure 4.1 – (a) X-ray diffractograms of the as-received and oxidized hBN compared to the diffraction pattern of the PDF card n. 34-0421; SEM images of (b) as-received and (c) oxidized hBN; and (d) hBN-oxi particle size histogram.

Figure 4.1b shows a representative SEM image of the bulk of the pristine hBN, where rounded grains and aggregates of varied sizes can be observed. Although the granulated aspect was also exhibited by the hBN-oxi particles, as shown in Figure 4.1c, the material had much smaller particles. The lateral size of more than 500 and 1500 particles of the bulk and oxidized hBN, respectively, was measured from the SEM images, being determined as the average of their maximum and minimum Feret diameters (ISO/TS 21356-1:2021, 2021). While the bulk hBN particles presented a mean lateral size of 7200 nm, the hBN-oxi nanoparticles had a maximum lateral size of 730 nm, varying according to the histogram shown in Figure 4.1d, with a mean of 100 nm. Thus, considering the particles' dimensions, i.e., the mean lateral size measured by SEM and average thickness found through

XRD, the aspect ratio of the nanoparticles could be determined as lower than 10. Figure 4.2 shows TEM images with different magnitudes for the hBN bulk (Fig. 4.2a), and the hBN-oxi dispersion (Fig. 4.2b-c) sample obtained from a 10 mg mL^{-1} suspension. It was possible to observe that hBN-oxi sample was efficiently exfoliated in nanostructures containing few layers and lateral sizes between 35 and 100 nm upon the liquid exfoliation process, agreeing with the previously found by XRD and SEM.

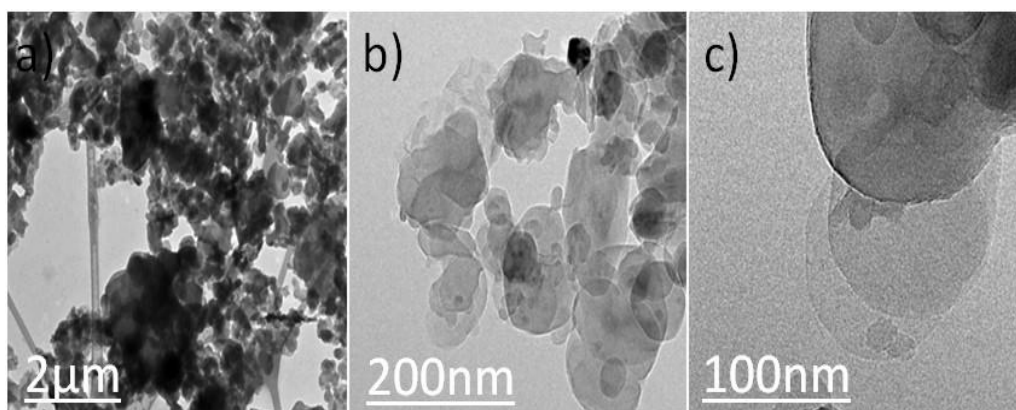


Figure 4.2 – TEM images of hBN bulk (a), and hBN-oxi from a 10 mg mL^{-1} dispersion (b-c).

Raman spectroscopy is also utilized for the purpose of identify a particular substance by analyzing the frequency at which its lattice vibrates (Tay, 2018). HBN displays two main vibrational modes: an in-plane mode at high frequency and an interlayer mode at low frequency. The high-frequency mode is associated with in-plane vibrations where boron and nitrogen atoms oscillate in opposite directions, producing a signal about 50 times stronger than that of the lower frequency mode (Reich et al., 2005; Stenger et al., 2017). The obtained Raman spectrum depicted in Figure 4.3 exhibits a prominent peak at 1373 cm^{-1} , this can clearly identify the E_{2g} vibrational mode of hBN. The E_{2g} lattice vibration peak corresponds the B and N atom in-plane stretching vibrations. Two factors influence this peak position: (a) the number of layers and (b) strain (a built-in stretching of bonds) (McLean and J. Paga, 2023; Shi et al., 2010).

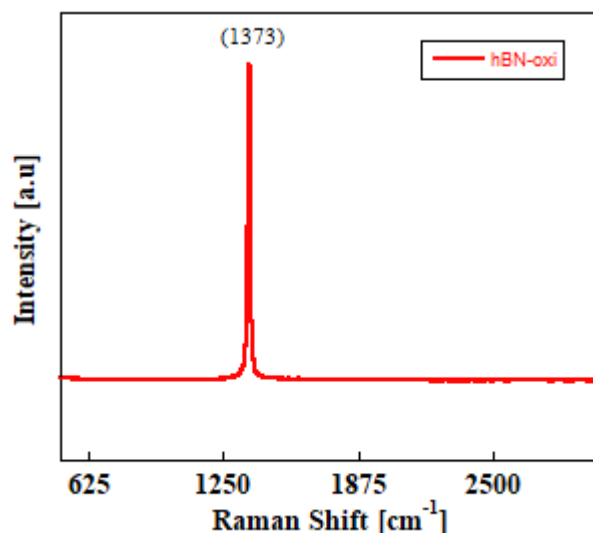


Figure 4.3 – Raman spectra of exfoliated hBN-oxi samples

XPS is an exceptional spectroscopic technique for the characterization of nanomaterials surface. Therefore, XPS spectra were used to obtain more information about the hBN-oxi chemical composition. Figure 4.4a shows the XPS survey of B1s, N1s, and O1s scans of the hBN-oxi sample. All the XPS data were corrected using the binding energy of C–C at 285.31 eV. The presence of B1s (~191.12 eV), C1s (285.31 eV), N1s (398.5 eV), and O1s (533.89 eV) were observed in the spectrum. The small C signal identified in the hBN-oxi may be related to some type of contamination (Silva et al., 2018). The B1s, N1s, and O1s photoemission spectra scan energy for all samples are shown in Figs. 4.4b-d. The B1s peak (Fig. 4.4b) at 190.20 eV and 187.34 eV correspond to the B–N and B–N bonds respectively (Silva et al., 2018). The N1s peak (Fig. 4.4c) at 398.45 eV and 396,50 eV correspond to the O–B–N (or N–O), and N–B bonds respectively, which confirmed the efficiency of the oxidative process used (Silva et al., 2014). The O1s spectrum is shown in Figure 4.4d. For hBN-oxi, there were three peaks, at 532.90, 535.33, and 530.61 eV, related to B–O (B₂O₃), O–H, and Fe–O (Fe₂O₃), respectively, related to the oxidation process (Silva et al., 2018).

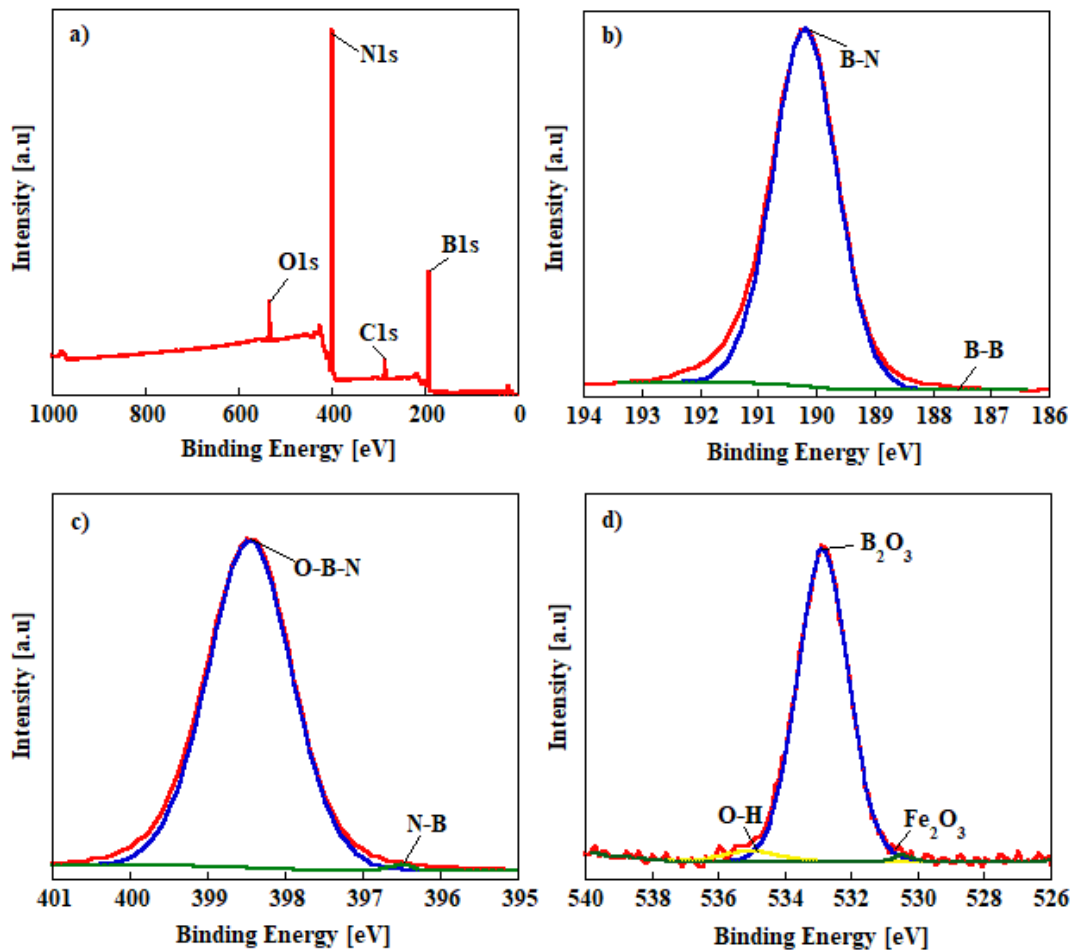


Figure 4.4 – XPS extended spectra (a) and the high-resolution spectrum obtained in the region of the binding energy of B1s, N1s, and O1s respectively for hBN-oxi (b-d).

Figure 4.5(a-d) shows the results obtained for the analysis of DLS and Zeta potential for the dispersions obtained for the as-received hBN and hBN-oxi samples. The hBN suspension showed an average particle size of about 52 nm and zeta potential of -15 mV, which represents an unstable dispersion. However, when the material was chemically modified with hydroxyl groups to form hBN-oxi, a distribution with a mean size centered at 35 nm was observed. Such a particle size is comparable to those observed in the SEM and TEM images. The zeta potential value of -32 mV for the hBN-oxi sample showed that the chemical modification process favored the stability of this dispersion. This result is in agreement with the work by Joni et al. (2011) that stabilized an aqueous phase dispersion of hBN by functionalizing its surface with silane-based coupling agents. (Joni et al., 2011).

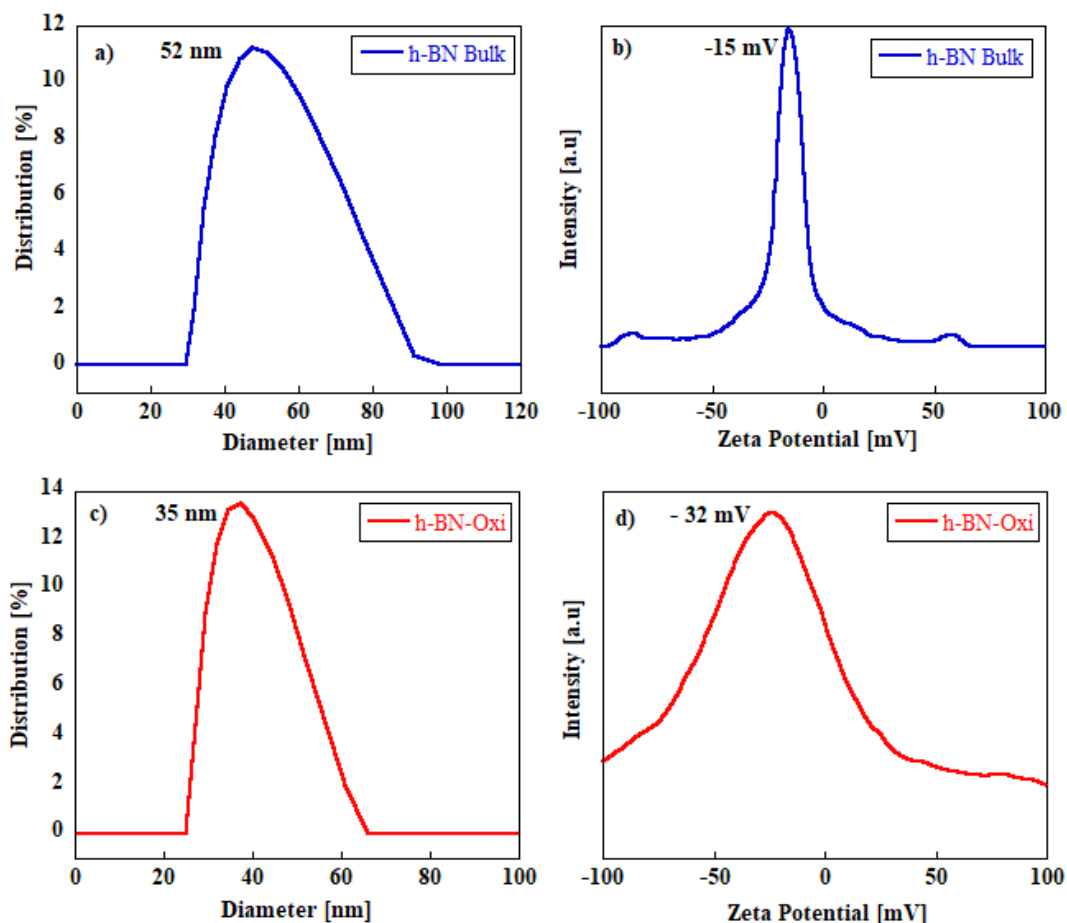


Figure 4.5 – Average size and zeta potential of hBN (a,b) and hBN-oxi (c,d) suspensions 1 mg mL^{-1} in a mixture of 20 % by volume of IPA and 80 % DI water.

In the work reported by Sainsbury (2012), a series of low-intensity bands is shown only in the case of hBN-oxi and suggests that these bands are associated with the functional group B–OH, however, these peaks do not appear in this analysis. As seen in Gorbachev (2011), the intensity of the peak can be related to the number of layers of hBN. The only and very significant difference is in the intensity of the peaks of the analyzed samples since the hBN-oxi sample recorded the value of 4415 a.u. and the hBN Bulk was 3415 a.u. Figure 4.6 shows the FTIR spectra of unmodified and oxidized hBN samples. The absorption band with a peak at $\sim 1402 \text{ cm}^{-1}$ is assigned to in-plane stretching or in-plane ring vibration of the B–N bonds, while the band with a vibration peak at $\sim 798 \text{ cm}^{-1}$ show the out-of-plane bending of the B–N–B bonds for the commercial sample. In exfoliated hBN-oxi the band with the same peaks is shifted to $1,346 \text{ cm}^{-1}$ with a sharper peak and 779 cm^{-1} , for stretching and bending respectively (Shi et al., 2010; Krečmarová et al., 2019).

These observed band shifts are related to the surface modification of hBN-oxi in relation to hBN (Joni et al., 2011). The very weak band of surface OH groups at 3,000–3,600 cm^{-1} appears in the hBN-oxi sample; however, the presence of this group was only detected by XPS analysis.

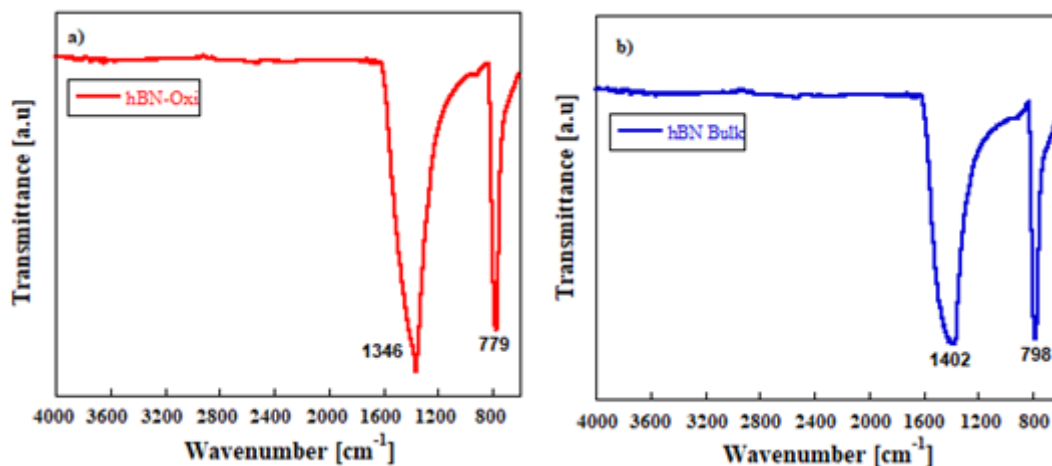


Figure 4.6 – FTIR spectra of (a) hBN bulk and (b) exfoliated hBN-oxi samples.

Figure 4.7 shows the thermogravimetric analysis of hBN-oxi sample where it can be observed a mass loss of approximately 0.6 %. The first mass loss, between 100 and 200 °C, is related to the evaporation of some solvent adsorbed on the sample (Kostoglou et al., 2015). The second loss of mass between 300–450 °C may be related to the burning of the oxidized groups present on the surface of the sample, as verified by Silva et al. (2018), for the boron nitride nanotubes oxidized sample by a method similar to this work, which confirms the results obtained by the XPS analysis (Silva et al., 2018).

The images provided by cryo-SEM (Fig. 4.8) allowed us to observe the morphological difference in the structure of the suspensions of pure XG and XG with hBN-oxi 60 $\text{mg}\cdot\text{mL}^{-1}$. Both presented a honeycomb network however, the suspension with nanoparticles is thicker and denser than pure xanthan gum. As the hBN concentration increased, a well-structured gel with a interconnected network was formed, indicating strengthening of the microstructure and the presence of tangles (Xue et al., 2021). As these nanoparticles have an extremely large specific surface, they can allow greater interaction with the polymer in the suspension,

helping in the formation of polymer bridges (Soares et al., 2023). The images obtained from pure XG are like those found in research by Xue et al. (2021).

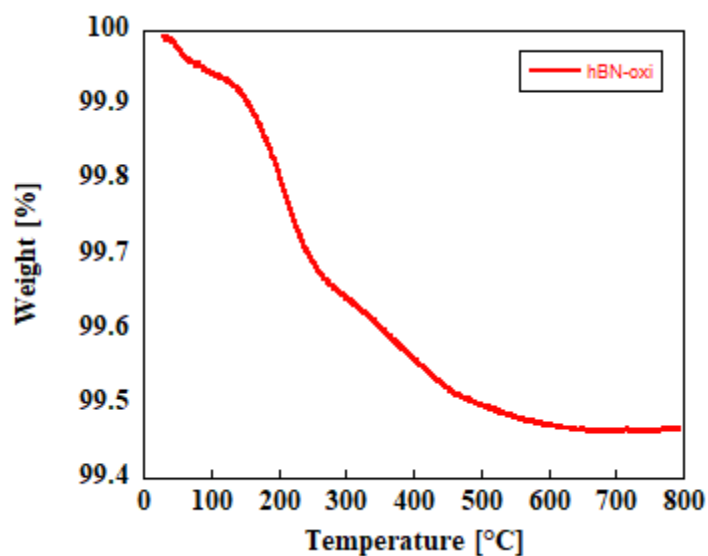


Figure 4.7 – Representative TGA analysis of hBN-oxi sample.

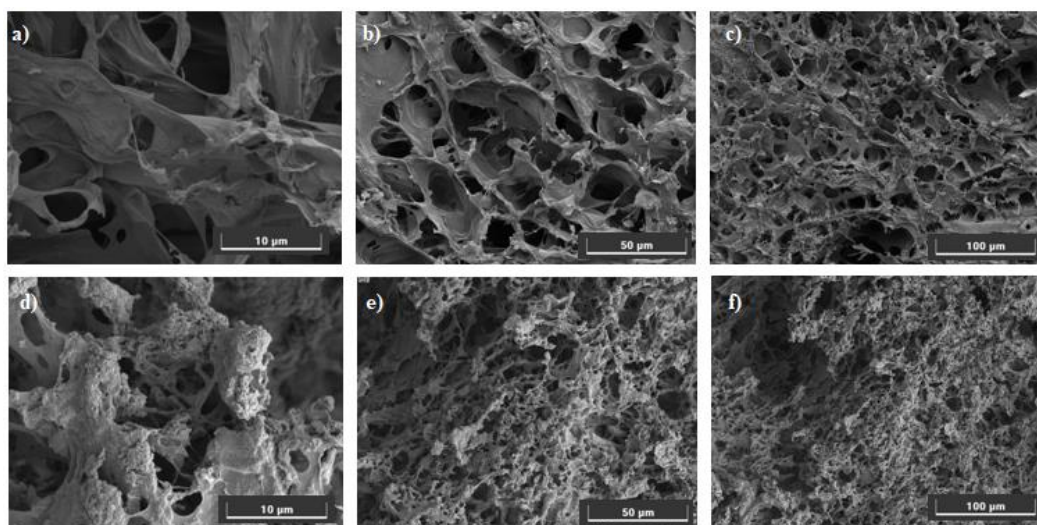


Figure 4.8 – SEM observations at different scales of pure XG (a,b,c) and XG with hBN-oxi 60mg.mL (d,e,f).

After the results of all these characterizations, it was possible to conclude that the nanoparticle obtained was well oxidized and exfoliated, and that by inserting it into the base fluid it was possible to obtain a stable suspension and a well-structured gel with a interconnected network formed between the nanoparticle and the polymer molecules of the suspension.

4.2 Thermal conductivity of hBN-oxi Suspensions

Recent research has been conducted to understand how the aggregation, morphology, and size of nanoparticles affect the thermal conductivity mechanism of nanofluids (Prasher et al., 2006; Karthikeyan et al., 2008; Jang and Choi et al., 2004 and 2007). Although most studies demonstrate an anomalous increase in the value of thermal conductivity with the addition of nanoparticles, some studies have shown that this increase was not significant and that it can be predicted by effective medium theories (Keblinski et al., 2008; Kim et al., 2009).

4.2.1 Effect of concentration on thermal conductivity

Figure 4.9 shows the change in the thermal conductivity for different concentrations of hBN-oxi nanoparticles in aqueous suspensions of xanthan gum. Even with a decrease in the conductivity value of the suspension with 5 to 15 mg mL⁻¹, all samples showed a conductivity value superior to that of the sample containing the pure polymer. The highest percentage increase observed was for the suspension containing 60 mg mL⁻¹ (6.0 wt.%) in relation to the pure polymeric solution, whose increase reached around 7 %. This increase in thermal conductivity observed in the suspensions, within the scope of the oil industry, indicates that there is an increase in the cooling rate of the drilling fluid as it moves to the surface. Rheological studies show that this increase helps prevent degradation and maintain fluid viscosity (William et al., 2014).

According to William et. Al (2014), the thermal conductivity value for an aqueous suspension of xanthan gum with a concentration of 0.4 wt.% was 0.372 W.(mK)⁻¹. However, in this work, the xanthan gum suspension was prepared with solvent in the proportion of 20 % IPA and 80 % deionized water and with a concentration of 0.86 wt.% and its measured thermal conductivity was 1.163 W.(mK)⁻¹. Comparing the results obtained for the xanthan gum solution of this study with that of William's work, it was possible to conclude that the increase in the concentration of xanthan gum led to an increase in thermal conductivity.

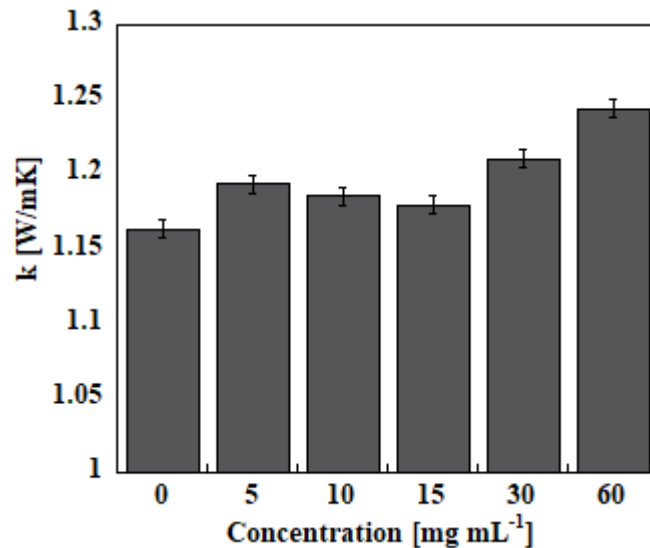


Figure 4.9 – Thermal conductivity of samples for different hBN-oxi concentrations

4.2.2 Effect of temperature on thermal conductivity

Various factors have the potential to affect the thermal conductivity of nanofluids, encompassing phenomena like the molecular-level layering of the liquid at the liquid/particle interface (nanolayer), the Brownian motion of nanoparticles, clustering, nanoparticle size, pH, temperature, and the inherent heat transport characteristics within the nanoparticles (thermal resistance of nanoparticles) (Ahmadi et al., 2018). It appears that none of these factors alone can be solely accountable for the improvements in thermal conductivity; instead, a comprehensive hybrid model should consider the interplay of all these parameters (Aybar et al., 2015).

Figure 4.10 shows how the temperature and concentration of hBN-oxi nanoparticles can influence the thermal conductivity of aqueous xanthan gum suspensions. It was possible to observe that for all concentrations, compared to the sample containing the pure polymer, the thermal conductivity was higher and as the concentration increased, the conductivity increased along with it. The greatest percentage increase observed was for the suspension containing 60 mg.mL⁻¹ (6.0 wt.%) in relation to the pure polymeric solution, whose increase reached approximately 12% at 70°C. The percentage increase between these two samples reached a value of approximately 11 % at 5 °C, 7 % at 20 °C and 9 % at 50 °C. The

inclusion of nanoparticle sizes results in an increase of the surface area per unit volume of the particle. Given that heat transfer is influenced by the surface area, this enhances the nanoparticles' efficacy in transferring heat to the base fluid. (Fazelabdolabadi et al., 2015).

According to Williams et al. (1991), there is a temperature corresponding to an order-disorder conformational transition of xanthan gum. The transition temperature largely depends on the concentration of the polymer (Rinaudo, 2001). Ardila (2021) observed in his study that the transition from an ordered state to a disordered state of xanthan gum begins at 70 °C and ends at 90 °C. Therefore, it can be summarized that the ordered molecule of xanthan gum in the drilling fluid undergoes a dissociation of the double helix into simple filaments (a disordered flexible spiral) in the referenced temperature range. (Callet et al., 1989; Kawakami and Norisuye, 1991). Therefore, the results observed in Figure 4.10 of thermal conductivity for pure polymer and for suspension with 15 mg.mL⁻¹ showed a drop in their values, because upon reaching this critical temperature of 70 °C, the mobility of the system increased, causing a disturbance in the jelly-like structures of the xanthan gum, leading to destructuring of this percolated network, thus reducing the heat conduction capacity within the system of these samples. And when reaching higher concentrations, the presence of the nanoparticle prevented this phenomenon.

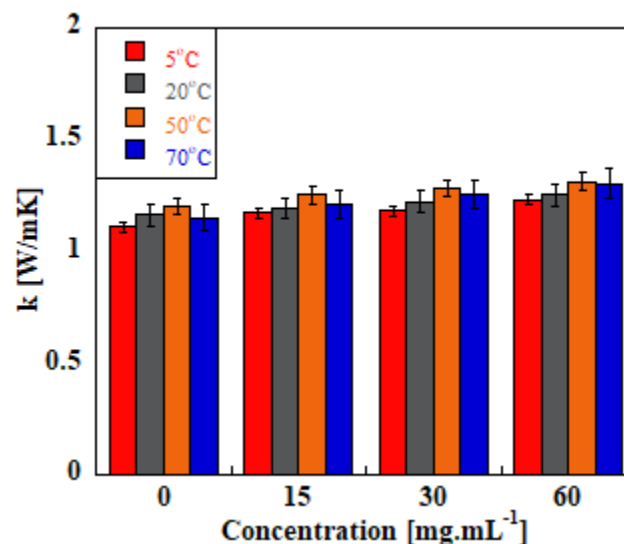


Figure 4.10 - Influence of temperature on thermal conductivity of samples for different concentrations of hBN-oxi

4.3 Shear Rheology of hBN-oxi Suspensions

The existence of a complex network in the solution formed from rigid rod-like polymer chains gives XG distinctive rheological features, such as high low-shear viscosity and significant shear-thinning character (William et al., 2014). The addition of nanoparticles to a base fluid, besides usually increasing the thermal conductivity, can change the rheological properties of the nanofluid (Behi et al., 2012).

Figure 4.11 shows the flow curves in the range from 0.01 to 1,000 s^{-1} , obtained for aqueous suspension of xanthan gum for a concentration of 0.86 wt.%, where it can be observed the shear thinning behavior and no yield stress. This result is in agreement with the XG rheology data reported by Vargas (2019), which validates the preparation method used for obtaining the aqueous solution of xanthan gum.

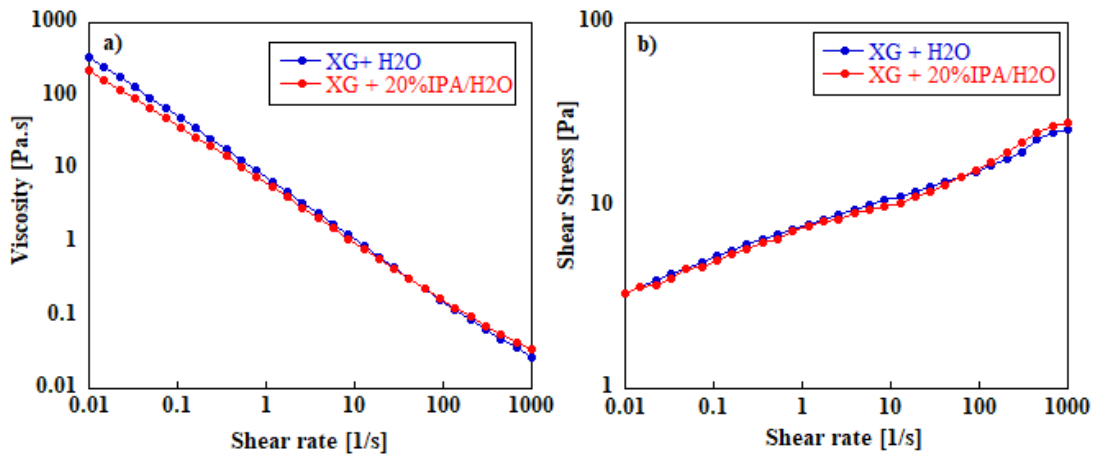


Figure 4.11 – Flow curves of XG + H₂O and XG + 20 % IPA/H₂O (a) viscosity and (b) shear stress as a function of the shear rate

As the concentration of 20 % of IPA in water was established as the solvent that obtains the best yield of liquid exfoliation of boron nitride (Munaro et al., 2017), the first step was to verify if the rheological results obtained with the choice of this solvent would be different from those obtained only with the aqueous solution. As a result, both the aqueous suspension of XG and the suspension of XG

with 20 % IPA/H₂O presented remarkably comparable results, and, for these reasons, future tests were carried out adopting the mixture of 20% IPA in water as base fluid, as shown in Figure 4.11.

In order to analyze the polymer solution degradation with time and to guarantee the reliability of the results within a specific period for carrying out the experiments, several tests were performed from 24 h after the preparation of the suspension to 30 days later. This type of study is of great importance, as drilling fluids that contain polymers can degrade in the long term.

Figure 4.12 shows that within 1 month, the shear viscosity does not change significantly. Therefore, it is possible to guarantee that the rheological properties of these suspensions are maintained, and the results suggest there is no polymer degradation.

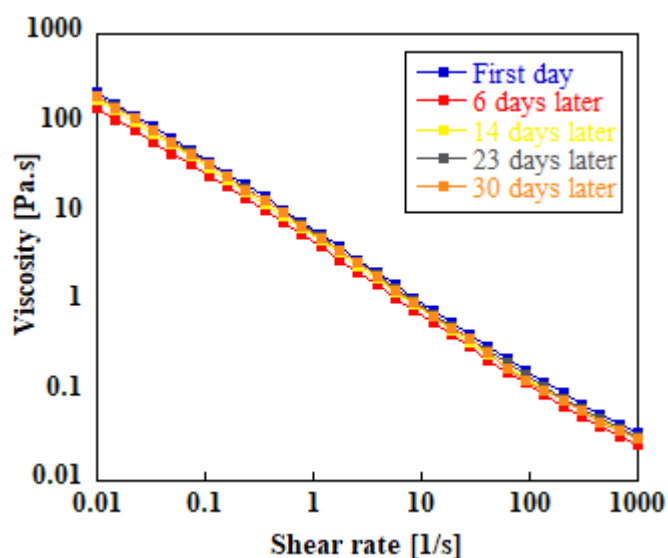


Figure 4.12 – Flow curve of XG solution with 20%IPA/H₂O performed at 1, 6, 14, 23, and 30 days after sample preparation

4.3.1 Effect of concentration on rheological properties

With the aim to investigate the influence of the concentration of hexagonal boron nitride nanoparticles on the rheological properties of the xanthan gum solution, flow curves were performed for suspensions with 0, 5, 10, 15, 30, and 60 mg mL⁻¹ of the hBN-oxi. The results of the measurements performed are shown in Figures 4.13 and 4.14.

Figure 4.13 shows the study of the rheological behavior for suspensions with different concentrations using shear rates ranging from 0.001 to $1,000\text{s}^{-1}$ to cover a large variety of applications. It was possible to observe in figure 4.13a that for high shear rates, the samples from the pure polymer to the concentration of 15 mg mL^{-1} of hBN-oxi present practically the same behavior, differing only as the shear rate decreases. As the concentration of hBN-oxi nanoparticles increased, there was an increase in the value of the suspensions' viscosity. This increase was even more easily highlighted for suspensions prepared with 30 and 60 mg mL^{-1} . The covalent functionalization of hBN with inorganic molecules as in the case of H_2SO_4 and HNO_3 , as observed in the XPS and TGA results, significantly altered the surface energy of hBN-oxi, therefore, its solubility (Sainsbury et al., 2012). These nanoparticles start to present an extremely large specific surface that allows better interaction with the polymer in the solution. Wang et al. (2004) experimentally proved that the addition of nanoparticles leads to an increase in the shear viscosity of the polymeric solution since the flow resistance increases as the polymer bridges between particles are extended. The Bridging effect (Kamibayashi et al., 2008) is the essential mechanism behind this intriguing rheological behavior, which states that many particles are connected by a polymer's intra-chain bridge due to the size effect.

It was also possible to observe in figure 4.13a that all samples present the same shear-thinning non-Newtonian behavior, as the decrease in viscosity with increasing shear rate occurs at almost the same shear rate. The networks generated between hBN-oxi nanoparticles and the polymer can explain the rheological nature of these observed suspensions. At rest, these networks are kept structured. The network structure is broken as a shear rate is applied and the particles are orientated along the flow direction. The reduction in viscosity is owing to this action, together with the slip/orientation of the shear hBN-oxi layers (Giannelis, 1998).

In figure 4.13b it is possible to observe that, at the highest concentrations, as in the case of samples with 30 and 60 mg mL^{-1} , the suspensions began to show dynamic yield stress. This behavior is due to the networks generated between hBN-oxi nanoparticles and the polymer as mentioned before. Moreover, this rheological characteristic is critical for drilling fluids, as it is directly related to several issues in the oil industry such as hole cleaning, barite sag, equivalent circulating density, and surge/swab pressures, among others (Power and Zamora, 2003).

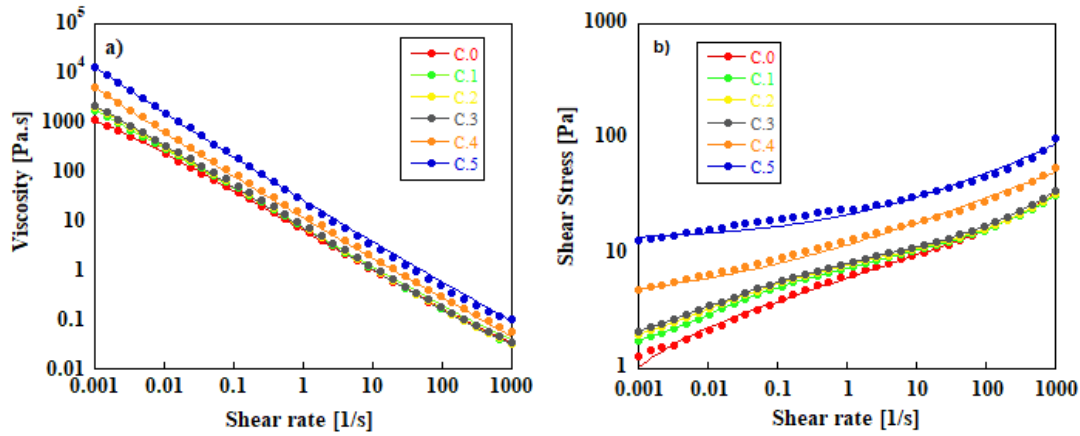


Figure 4.13 – Flow curves of various concentrations of hBN-oxi nanoparticles (a) viscosity x shear rate and (b) shear stress x shear rate. Lines from C.0 to C.3 show the Carreau-Yasuda model and lines of C.4 and C.5 show the Herschel-Bulkley model (C.0 – pure, C.1 – 0.5 wt.%, C.2 – 1.0 wt.%, C.3 – 1.5 wt.%, C.4 – 3.0 wt.% and C.5 – 6.0 wt.%)

There are many models describing shear-thinning behavior that were used to fit data only from rotational tests and not oscillatory tests. The one that best fits the curves of pure polymer up to 15 mg.mL^{-1} is given by the Carreau-Yasuda and the fitting parameters for the Carreau model are summarized in Table 4.1.

Table 4.1. Fitting parameters for the Carreau-Yasuda Model of nanofluids with an hBN-oxi concentration of 0 up to 15 mg.mL^{-1}

Concentration hBN-oxi (mg mL^{-1})	η_o (Pa s)	η_∞ (Pa s)	λ (s)	n	a	R^2
0	3000	0.01	2130.2	0.19638	0.8	0.9965
5	3000	0.01	1885.2	0.20087	2.6	0.9996
10	3000	0.01	1520.9	0.1702	2.8	0.9990
15	3000	0.01	1389.8	0.16217	2.8	0.9988

The two suspensions with the highest concentrations represent a model with dynamic yield stress, which is often modeled using the Herschel-Bulkley equation (Herschel and Bulkley, 1926; Oppong et al., 2006) and the rheological parameters that describe this behavior are presented in Table 4.2.

Table 4.2. Fitting parameters for the Herschel-Bulkley Model of nanofluids with an hBN-oxi concentration of 30 and 60 mg.mL⁻¹

Concentration hBN-oxi (mg mL ⁻¹)	τ_y (Pa)	k	n	R^2
30	3.5	8.382	0.253	0.99
60	12.8	8.728	0.312	0.977

According to Kamibayashi et al. (2008), increasing particle concentration slowly generates an increase in suspension viscosity. In figure 6.14, the viscosity as a function of the concentration is plotted for the same shear rate of 0.01 s⁻¹, allowing better visualization of the influence that the concentration has on the viscosity of the suspension. Hence, figure 4.14 corroborates the work by Kamibayashi.

For the concentration of 15 mg mL⁻¹, there was a 52 % increase in the viscosity of the polymeric suspension with the addition of hBN-oxi nanoparticles and for the concentration of 60 mg mL⁻¹ such percentage increase was even greater reaching the value of approximately 642 %. This increase in viscosity is quite important for drilling fluids as it keeps the borehole from collapsing and helps to suspend the mud solids (Al-Khdheawi and Mahdi, 2019).

A polymeric material's viscoelastic behavior can be defined into the non-linear or linear viscoelastic regime. In the linear viscoelastic regime, the rheological behavior is modeled at slow and small deformations, so that the molecules do not leave their equilibrium state, thus allowing the characterization of this material at the structural level. However, in the non-linear viscoelasticity regime, larger deformations are applied, causing the molecules to leave their equilibrium condition, where the structural level changes as the fluid deforms and the viscoelastic properties become dependent on the shear rate and the kinematics of the deformation (Vinogradov and Malkin, 1980).

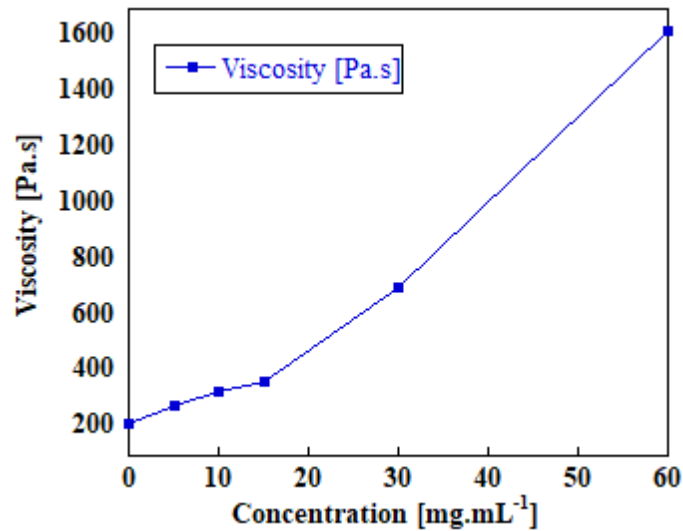


Figure 4.14 – Viscosity as a function of concentration at 0.01 s^{-1}

The oscillatory tests allow the determination of the viscoelastic properties of the samples, whether there is a linear viscoelastic region (LVR) or not. In the LVR, where the storage (G') and loss (G'') modulus are independent of strain, the strain applied in this region is insufficient to break the bonds that constitute the nanofluid's microstructure. Figures 4.15a,b show, respectively, the values of storage and loss modulus obtained from the suspensions for all concentrations.

The storage or elastic modulus measures the deformation energy which is stored in the sample during a shear process, and the loss or viscous modulus represents the deformation energy that is used during a shear process and lost for the sample (Mezger, 2020). It is possible to observe that there is an increase in the value of both moduli with increasing concentration (Figures 4.15a,b). From the suspension without the nanoparticle to a concentration of 30 mg mL^{-1} these values are very close at high strains and only begin to be distinguished more for deformations below 100 %. This is justified since the low strain measurements mainly give information about the nanomaterial network, whereas high strain responses are more influenced by polymer matrix contributions (Thomas et al., 2016).

After LVR, as the strain increases, a transition region begins to occur. G' begins to decrease, indicating decreased elasticity, breakage of the initial nanofluid microstructure (Kim et al., 2003) and a strain overshoot phenomenon becomes more remarkable. This phenomenon takes place at an intermediate strain range, close to

the crossover between G' and G'' in suspensions with higher concentrations that presented yield stress. Within this region the increase in G'' occurs due to the dissipation of mechanical energy resulting from the movement of a strong network structure between hBN-oxi nanoparticles and the polymer. Nevertheless, G' is still higher because the nanofluid microstructure is stiff enough to preserve a significant elastic response (Vargas et al., 2019). When the strain amplitude is increased further, the non-linear region appears before G' and G'' crossover point. The storage modulus drops quickly to levels below G'' and a severe breakdown of the nanofluid microstructure occurs at this strain level, resulting in viscous behavior.

In Figure 4.16 it was possible to notice that, in the LVR, the values of the storage modulus are greater than the values of the viscous modulus for all concentrations. These results lead to the conclusion that the responses of the modulus are corresponding to a gel and that they present a static yield stress, since the suspensions behave more like a solid than a liquid and that the suspensions have a preponderance of elastic behavior and low internal dissipation (Piau, 2007). This observation is another indication that the oxidation of hBN, as noted in the TGA and XPS, facilitated the exfoliation and dispersion of the hBN layers, allowing greater interaction with xanthan gum.

In addition, as the hBN-oxi concentration increases, it is possible to observe that the linear viscoelastic region of the material decreases and that the crossover points between G' e G'' occur for smaller strain amplitudes and, as a result, the breaking of the physical crosslinking occurs at lower strains.

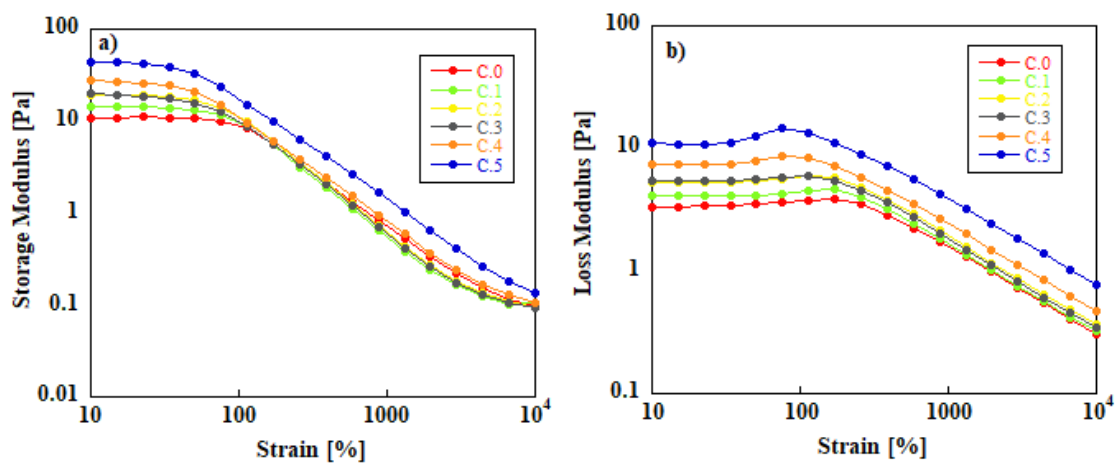


Figure 4.15 – (a) Storage (G') and (b) loss (G'') modulus as a function of strain for different concentrations

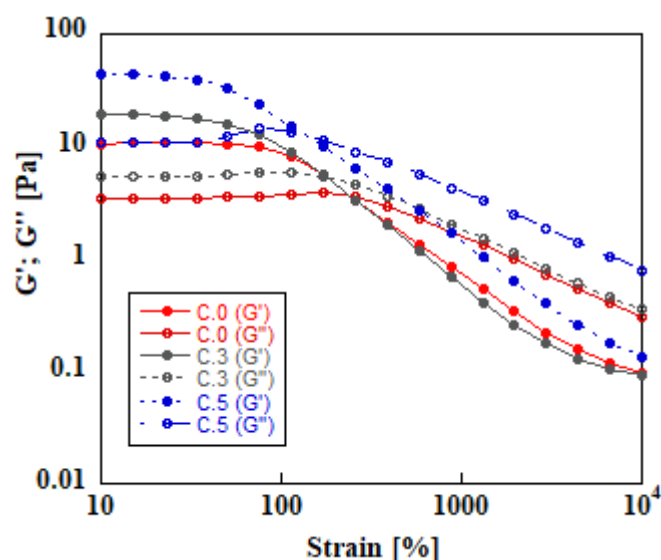


Figure 4.16 – Strain sweep of pure XG and XG+ hBN-oxi with 15 and 60 mg mL⁻¹

Figure 4.17 shows the storage (G') and loss (G'') modulus as a function of frequency. Values from 45 to 100 Hz that did not appear in the graph since they were discarded either because they presented a torque value below the minimum required or because the phase angle is not between 0 and 90 °, and the material structure could be at the beginning to break. A strain of 20.0 % corresponding to the linear viscoelastic domain was chosen to perform the dynamic measurement and a frequency sweep of 0.1 to 100 Hz was performed. Low frequencies allow the analysis of the response of nanoparticles dispersed in the nanofluids and high frequencies provide the response of the nanofluid polymer matrix. Some researchers observed that increasing the dispersion of nanoparticles with a high aspect ratio such as the hBN led to an increase in the elastic modulus value of the nanofluids (Kemp and Compton, 2020; Zyla et al., 2015; Decol et al., 2020), however, none of these works performed tests with oxidized hBN and in non-Newtonian fluids. Corroborating these studies, it is possible to observe in Figure 4.17 that, in addition to the increase in the values of the storage modulus with increasing concentration, there was also an increase in the values of the loss modulus. Moreover, all suspensions presented G' greater than G'' correspondent to a solid-like behavior and indicating the formation of a strong network with hBN-oxi. And, as in the strain sweep, this observation is another indication that the oxidation of hBN, as noted in the TGA and XPS, facilitated the exfoliation of the

hBN layers, promoting the dispersion of the 2D nanomaterials with high surface area, and consequently, higher interactions with the xanthan gum. It is also possible to conclude that suspensions with 5, 10, and 15 mg mL⁻¹ presented values remarkably close to these material functions and that, at high frequencies, all suspensions tended to present similar values of storage modulus.

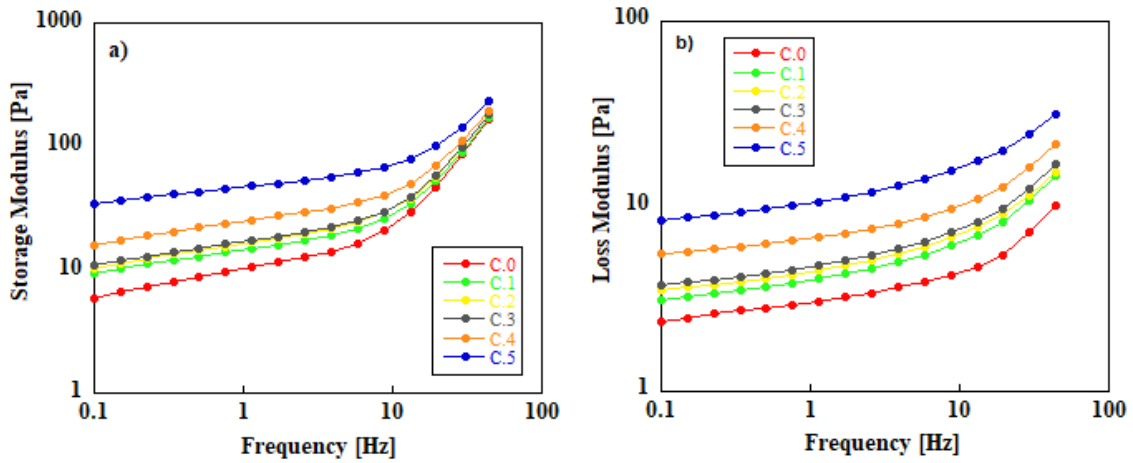


Figure 4.17 – (a) Storage (G') and (b) loss (G'') modulus as a function of frequency for different concentrations

4.3.2 Effect of temperature on rheological properties

Nanofluid rheology at high pressures and temperatures is a fascinating field of research that focuses on studying the viscoelastic behavior of fluids containing nanoparticles under extreme conditions. This field of study plays a fundamental role in several industrial applications, such as the oil and gas industry, where operating conditions can be extremely challenging with increasing depth. Therefore, this section will show the discussion about the improvement of the rheological properties of xanthan gum suspensions prepared with various concentrations of hBN-oxi nanoparticles subjected to pressures of 0.1 and 30 MPa at various temperature conditions. The effects caused by pressure variation will be discussed in the next section.

Figure 4.18(a-d) shows the flow curves in the range from 0.01 to 1,000 s⁻¹, from the pure polymer to a concentration of 60 mg.mL⁻¹ for a temperature range in which the first measurements were made at 4 °C gradually rising to 80 °C. After

heating the sample to 80 °C, we cooled the sample to 20 °C again, as it is shown as AC 20 °C, which means after cooling, to observe the degradation of the polymer with temperature.

It is evident that all the samples exhibit a consistent shear-thinning, non-Newtonian behavior, as observed in several studies such as Kalhor et al. (2023) and Oseh et al. (2023) who also investigated the rheological behavior of the influence of nanoparticles in a water-based drilling fluid. This is characterized by a decrease in viscosity as the shear rate increases, occurring across the entire measured range. This observed rheological behavior can be attributed to the formation of networks between hBN-oxi nanoparticles and the polymer. These networks maintain their structured form when the suspension is at rest but become disrupted when a shear rate is applied, causing the particles to align in the direction of flow. The decrease in viscosity is a result of this phenomenon, in conjunction with the slip and orientation of the shear hBN-oxi layers (Giannelis, 1998).

It was also possible to note that the increase in temperature had a significant effect on the viscosity of the xanthan gum suspensions, which can be explained by the fact that the fluid molecules gain kinetic energy and, consequently, greater thermal mobility (Jangir et al., 2021). This increase in molecular agitation promotes a decrease in viscosity, making the drilling fluid less viscous, as found in the work of Anoop et al. (2014) who worked with SiO₂ nanoparticles and Lai et al. (2023) with nano-silica. It is worth noting that during drilling operations temperature conditions can vary considerably as the well is drilled at increasingly greater depths.

Another observation can be made based on Figure 4.18 is that as we increase the concentrations of hBN-oxi in the samples, we observe that the flow curves become more stable in relation to the temperature variation, that is, the drop in viscosity with temperature was reduced with the addition of nanoparticles to the suspension. This means that the viscosity of the fluid becomes less sensitive to thermal fluctuations, providing a more stable response as the temperature varies. This phenomenon is related to the ability of hBN-oxi nanoparticles to strengthen the suspension structure, reducing the influence of temperature changes on the rheological properties of the fluid, which is a crucial aspect for several industrial and technological applications and corroborates the results found in the study carried out by William et al. (2014).

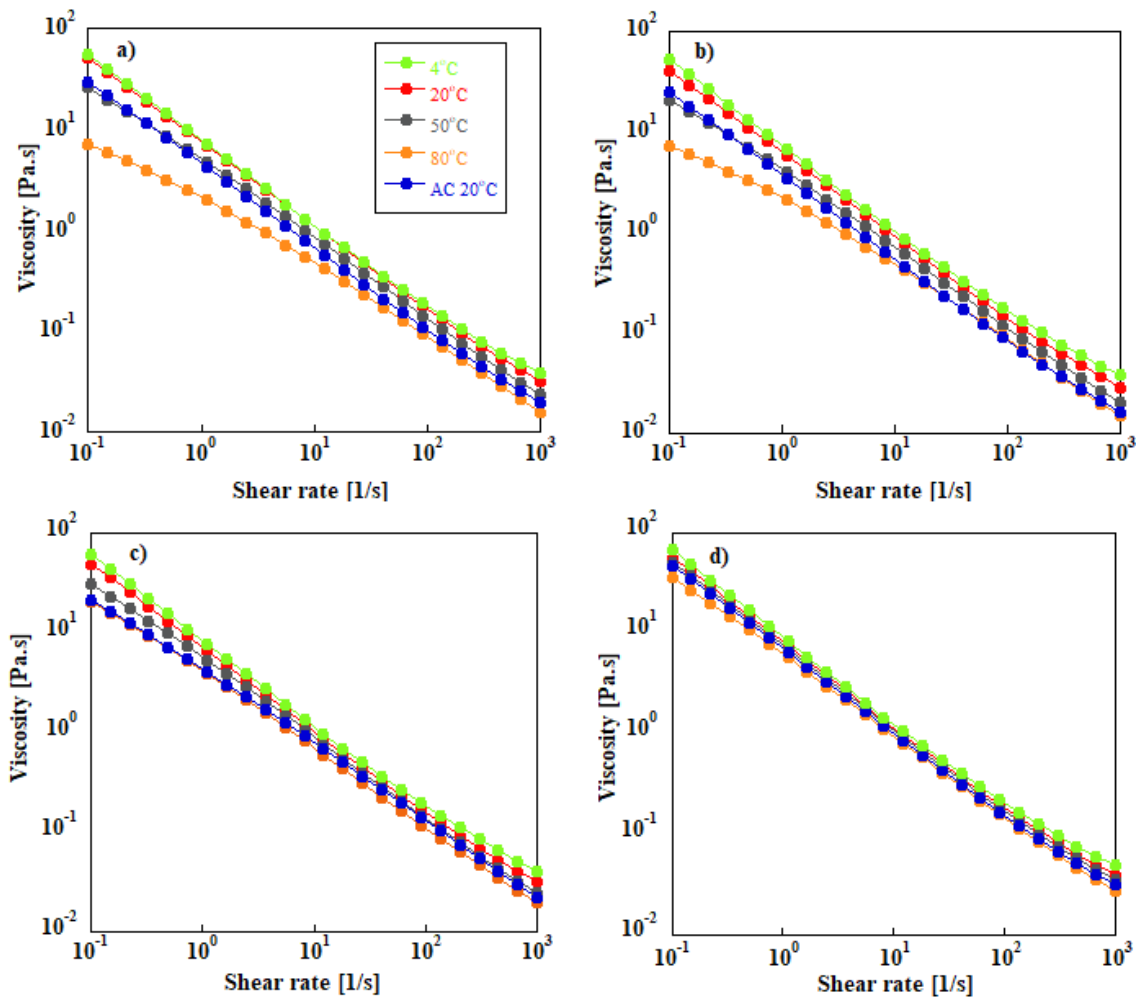


Figure 4.18 – Influence of temperature on flow curves for suspensions (a) pure XG, and with hBN-oxi concentration of (b) 15, (c) 30 and (d) 60mg.mL⁻¹

In Figure 4.19a, as the concentration of hBN-oxi nanoparticles increases, there is a rise in the viscosity of the suspensions, and this difference is more pronounced at higher temperatures. Notably, the covalent functionalization of hBN had a substantial impact on the surface energy and solubility of hBN-oxi (Sainsbury et al., 2012). Consequently, these nanoparticles start to present a large specific surface area, facilitating enhanced interaction with the polymer in the solution. This rheological behavior primarily arises from the Bridging effect where in numerous particles are interconnected by intra-chain bridges formed by the polymer, a phenomenon largely attributable to size effects. Therefore, due to this interaction, the drop in viscosity (due to the increase in temperature) in the sample with a concentration of 60 mg.mL⁻¹ is less pronounced than in the suspension with pure polymer.

It is also possible to observe in figure 4.19b that only the sample with 60 mg.mL⁻¹ measured at room temperature presents yield stress. This phenomenon arises from the networks formed between the hBN-oxi nanoparticles and the polymer, as previously discussed. The establishment of an adequate yield stress is of paramount importance in drilling operations. It serves the crucial function of allowing the fluid to efficiently carry the drilling cuttings to the surface while preventing unnecessary extra pressure on the drilling pump. In essence, a well-defined yield point ensures that the drilling fluid can effectively transport the cuttings, which is essential for maintaining the stability and integrity of the borehole. This not only enhances drilling efficiency but also minimizes the risk of equipment damage and costly downtime associated with excessive pressure on the drilling pump, underscoring the significance of maintaining an optimal yield point in drilling operations (Sajjadian et al., 2020).

The experimental data obtained through flow curves in Figure 4.19b were adjusted according to the Carreau-Yasuda model, for the curves of the pure xanthan gum suspension and Herschel-Bulkley, for the curves of the suspension with a concentration of 60 mg.mL⁻¹. The rheological models considered are given below and Table 4.3 and 4.4 presents the parameter values of each model.

Table 4.3. Fitting parameters for the Carreau-Yasuda Model of the pure XG suspension

Temperature (°C)	η_o (Pa s)	η_∞ (Pa s)	λ (s)	n	a	R^2
20	3000	0.01	2130.2	0.19638	0.8	0.9965
80	800	0.001	2595.2	0.26506	0.8	0.993

Table 4.4. Fitting parameters for the Herschel-Bulkley Model of suspensions with an hBN-oxi concentration of 60 mg mL⁻¹

Temperature (°C)	τ_y (Pa)	k	n	R^2
20	12.8	8.728	0.3120	0.977
80	8	5.146	0.3787	0.995

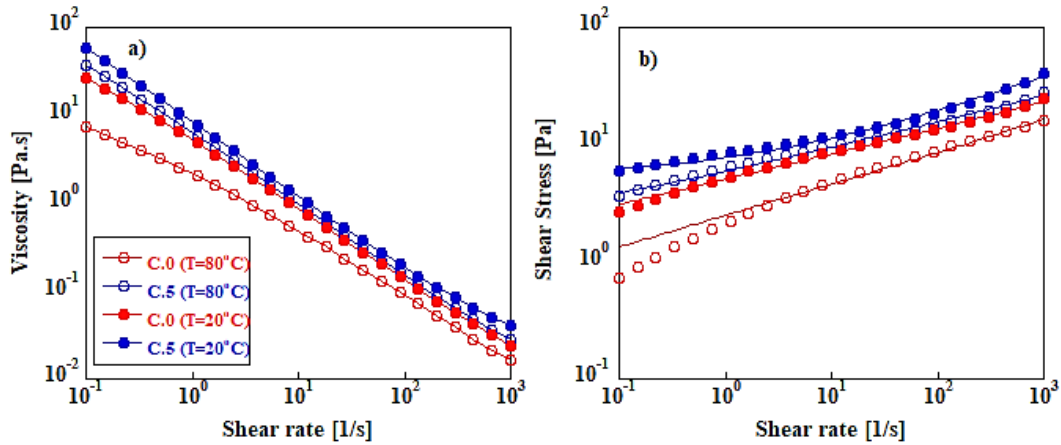


Figure 4.19 – Flow curves of pure XG (C.0) and XG with concentration of 60 mg.mL⁻¹ hBN-oxi (C.5) (a) shear stress x shear rate and (b) viscosity x shear rate.

Figure 4.20 shows that the percentage viscosity variation ($|\Delta\mu|/\mu$) for each temperature is more pronounced at the lower shear rate than at the higher shear rate. This indicates that changes in fluid viscosity are more sensitive to temperature variations when the fluid is subject to slower motion, while at higher shear rates, viscosity remains more stable with temperature changes.

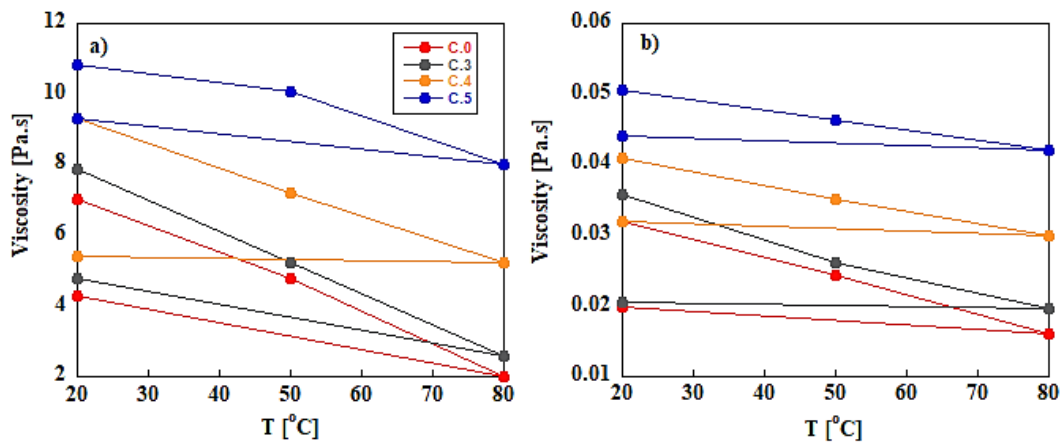


Figure 4.20 – Variation of viscosity with temperature for each concentration at rates of (a) 1 and (b) 1,000 s⁻¹

A drilling fluid should exhibit high viscosity at low shear rates and decrease as the flow rate increases. This entails high viscosity during static conditions (such as tripping time) and low viscosity during dynamic conditions (like

drilling operations), which are essential for effectively removing cuttings from the bottom hole (Ahmed et al., 2020). It is important for a drilling fluid to be rheologically stable when used at high drilling rates so that the fluid maintains its rheological properties in the way it was programmed to act in each region. Table 4.5 shows $|\Delta\mu|$ for each concentration, at rates of 1 and 1,000 s^{-1} varying the temperature from 20 to 80 °C and from 20 to AC 20 °C.

Table 4.5. $|\Delta\mu|$ % with respect to the viscosity at 20 °C

Sample	Shear rate (s^{-1})	80 °C (%)	AC 20 °C (%)
C.0	1	71.5	38.94
	1,000	49.73	37.68
C.3	1	66.98	39.23
	1,000	45.40	42.61
C.4	1	44.11	41.91
	1,000	26.63	21.74
C.5	1	26.32	14.00
	1,000	16.71	12.75

Figures 4.21a-d and 4.22a-d show the storage (G') and loss (G'') modulus as a function of deformation and frequency, respectively, as the temperature varies for a given concentration. Analyzing both figures, it can be concluded that elevating the temperature has a notable effect on the rheological properties of the suspensions, particularly concerning the storage and loss moduli. As the temperature rises, both the storage and loss moduli experience a reduction. In fact, like many polymers, the viscoelastic properties are significantly influenced by temperature levels. Heat induces the breaking of intermolecular bonds, facilitates molecular mobility, and thereby imparts greater flexibility to the macromolecular network, resulting in a lower capacity to retain and dissipate energy (Placet et al., 2008).

At 80 °C, a notable proximity is observed in the values of both moduli compared to the other temperatures at which the measurements were carried out, for all samples. This indicates that, at this higher thermal condition, the viscoelastic properties of the samples become more balanced. This convergence suggests greater stability in the structure of the samples, with a more effective interaction between the elastic and viscous components.

Another observation that can be made is that as the concentration of hBN-oxi increases, there is a reduction in the variation of the modulus values with temperature. Increasing the concentration of nanoparticles increases the density of the interconnected network, restricting molecular mobility. Consequently, suspensions become less susceptible to increasing temperature (Al-Muntasheri et al., 2007). This trend signifies a higher degree of stability in the material's viscoelastic response across different temperature ranges. In essence, the increased concentration of hBN-oxi nanoparticles contributes to a more consistent and temperature-resistant behavior, which is advantageous in applications where maintaining a stable viscoelastic profile is crucial.

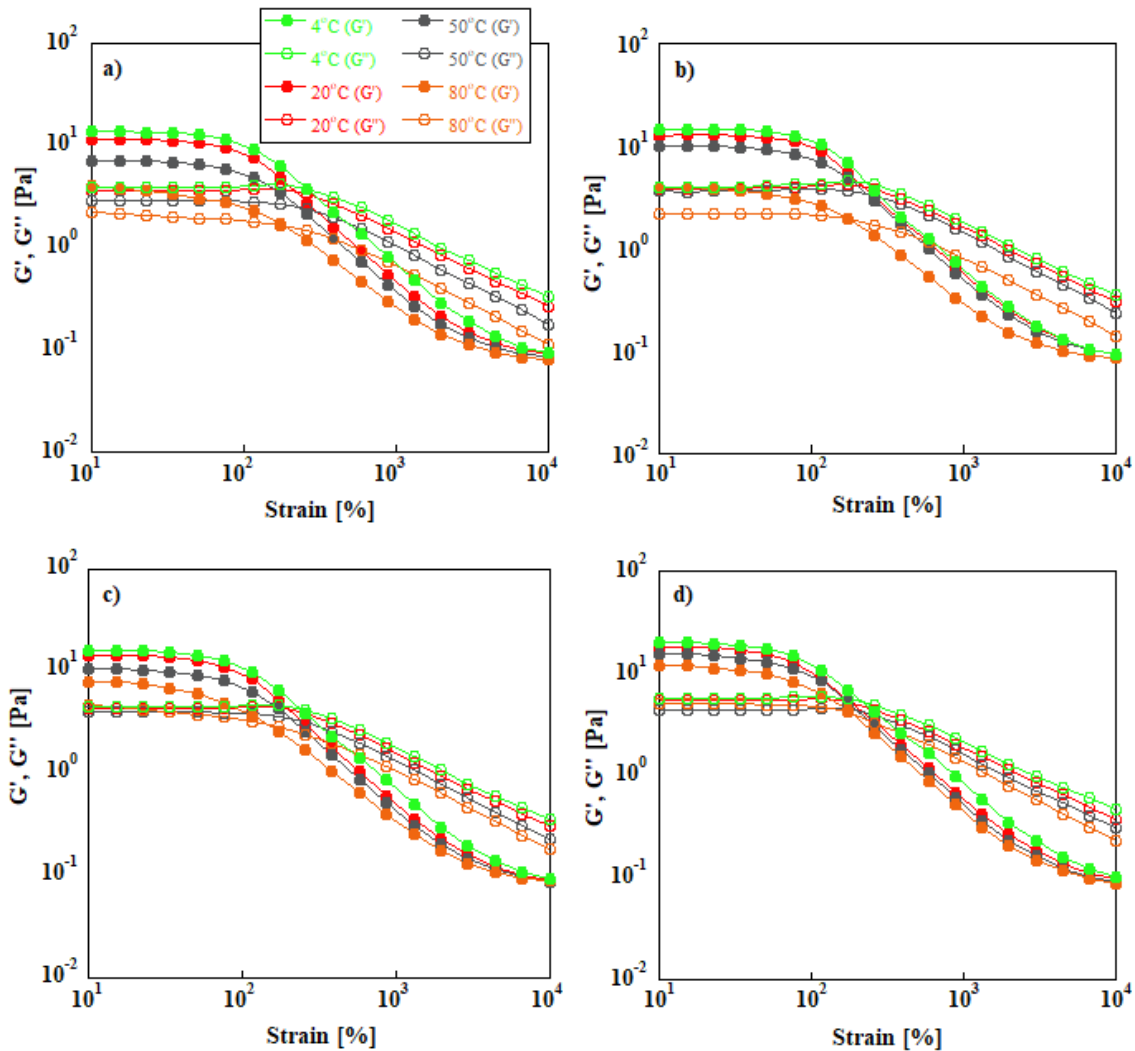


Figure 4.21 – Loss and storage modulus as a function of deformation at different temperatures of samples of (a) pure XG, and with hBN-oxi concentration of (b) 15, (c) 30 and (d) 60mg.mL⁻¹

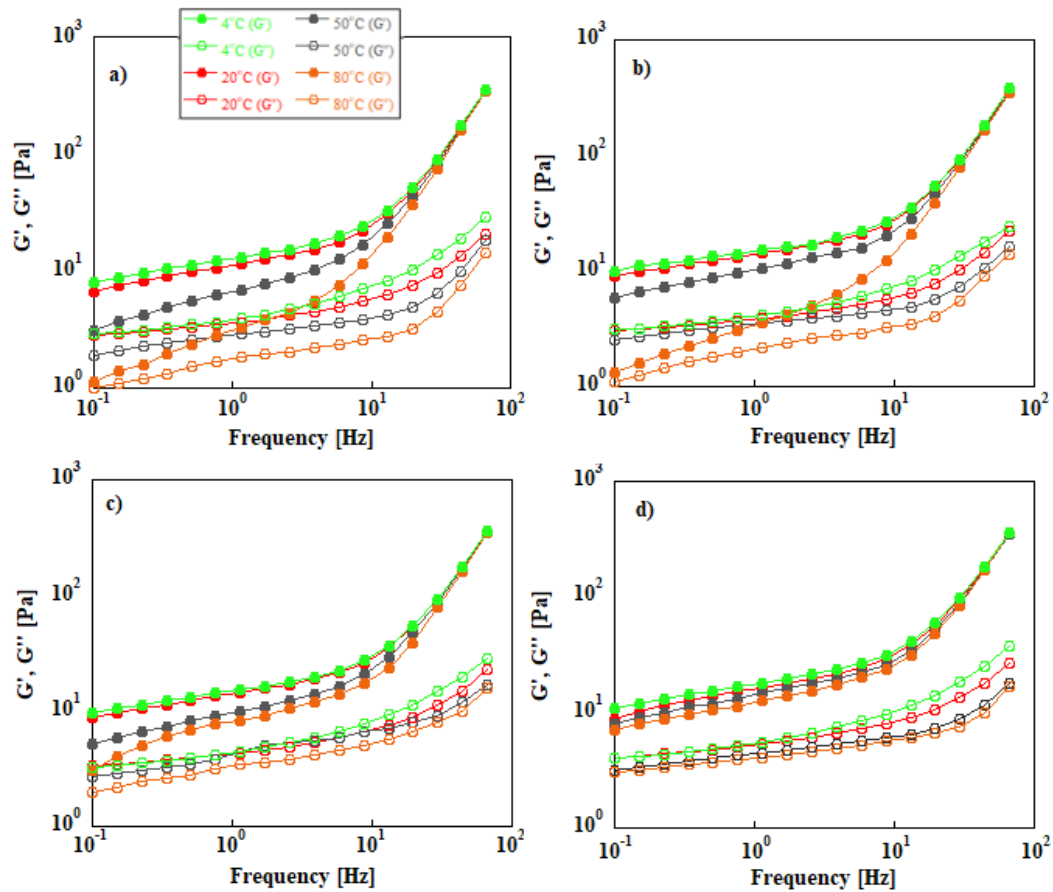


Figure 4.22 – Loss and storage modulus as a function of frequency at different temperatures of samples of (a) pure XG, and with hBN-oxi concentration of (b) 15, (c) 30 and (d) 60mg.mL⁻¹

4.3.3 Effect of pressure on rheological properties

The influence of pressure on the rheology of drilling fluids is a critical factor in drilling operations in challenging environments such as deep oil wells. Under high pressures, drilling fluids can exhibit significant changes in their rheological properties. Pressure affects the compressibility of fluids, influencing their density and viscosity. Additionally, high pressure can change the solubility of components in the drilling fluid, such as gases, and affect suspension stability. These rheological changes have a direct impact on the drilling fluid's ability to transport drill cuttings, maintain wellbore stability, and avoid problems such as loss of circulation. Therefore, the study of rheology under high pressures is essential for

the effectiveness and safety of drilling operations in challenging environments (Anoop et al., 2016; Agwu et al., 2021).

Figures 4.23, 4.24 and 4.25 show the flow curves of the suspension with pure polymer, and with hBN-oxi concentrations of 30 and 60 mg.mL⁻¹, respectively, first analyzing the effect of temperature at ambient pressure, then the effect of temperature at pressure of 30 MPa and finally comparing the effect of pressure for the temperatures of 20 °C and 80 °C. The drop in viscosity observed when comparing the suspension at 20 °C with that of the suspension after heating the sample and subsequently cooling it back to the same temperature, is less pronounced under a pressure of 30 MPa compared to 0.1 MPa. This difference in behavior can be attributed to the influence of high pressure, which acts as a compression factor, maintaining viscosity more consistently (William et al., 2014). Under high pressures, the molecules in the fluid are more densely packed, which limits their movement and, consequently, reduces the change in viscosity during the heating and cooling cycle. On the other hand, at low pressures, the molecules have greater mobility and, therefore, respond more sensitively to temperature variations. This phenomenon highlights the importance of considering the effects of pressure when analyzing the rheological properties of fluids, especially in high-pressure environments that demand precise control of fluid characteristics.

It is also possible to note that the influence of pressure on the rheology of the samples is mitigated by the addition of nanoparticles. The incorporation of nanomaterials maintained the shear thinning properties of the fluid, in which viscosity decreases as the shear rate increases, even under conditions of high pressure and temperature. Furthermore, at higher nanoparticle concentrations, rheological performance has improved, resulting in greater stability of the fluid's viscous properties, making nanofluids a promising choice for applications where rheological consistency needs to be maintained under a wide range of operating conditions. This observation further suggests that the oxidation of hBN aided in the exfoliation of the hBN layers, facilitating the dispersion of the hBN-oxi nanoparticles that had a large surface area. Consequently, this leads to stronger interactions with the xanthan gum.

Analyzing figures 4.23c ,4.24c and 4.25c it can be concluded that for the pure XG at lower temperatures, the pressure influenced the viscosity value, causing the suspension at the same temperature to have a lower viscosity at a pressure of 30

MPa compared to ambient pressure, while no change is observed for the nanofluid. At higher temperatures such as 80 °C, where a more significant decrease in viscosity can be anticipated, pressure did not significantly affect the viscosity, meaning that the flow curves for the pure XG and for all concentrations presented the same value at high temperatures for 0.1 and 30 MPa. Overall, the predominant effect of pressure is neglected, maintaining viscosity stability at higher temperatures, while at lower temperatures, the impact of pressure is significant. This is attributed to the high-pressure compressive nature of the base fluid, which is water, which sustains the viscosity. These results are in accordance with William et al. (2014).

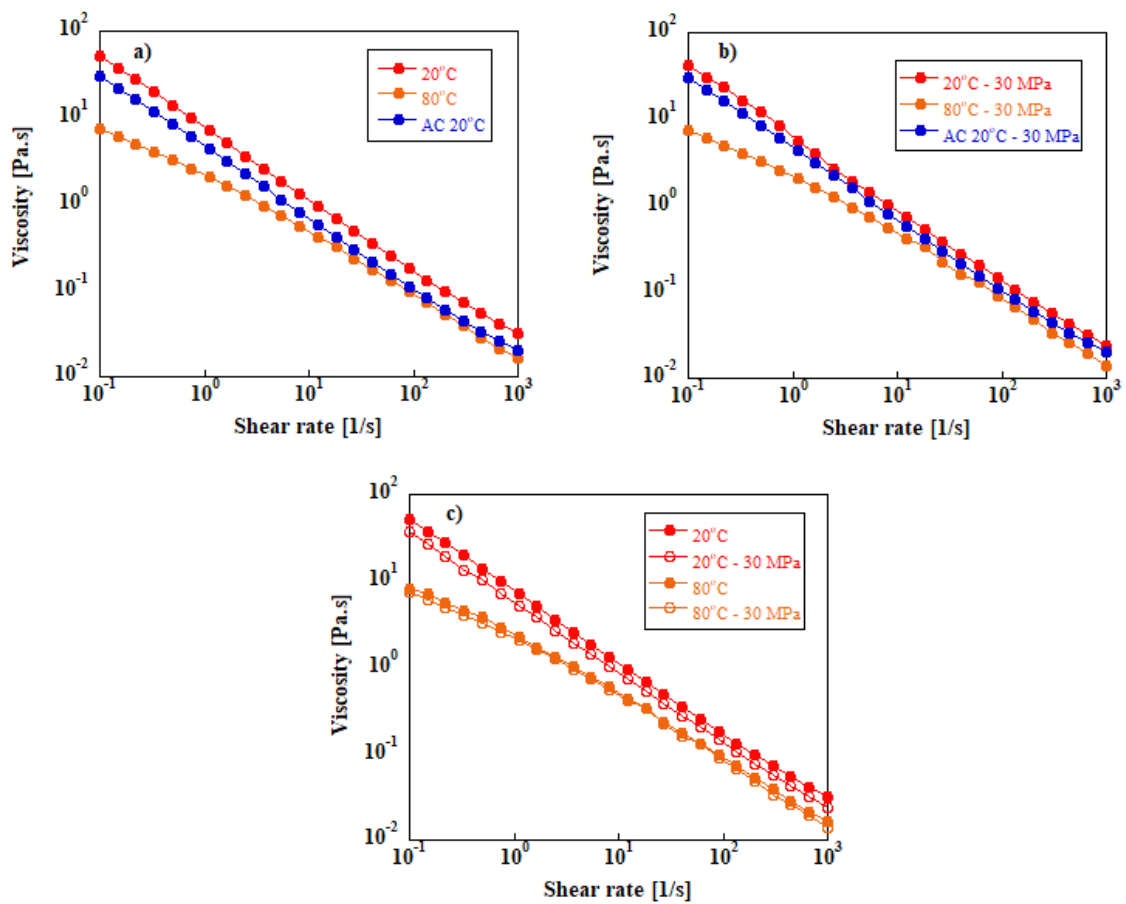


Figure 4.23 – Flow curve of pure XG analyzing (a) effect of temperature at 0.1 MPa (b) effect of temperature at 30 MPa (c) effect of pressure.

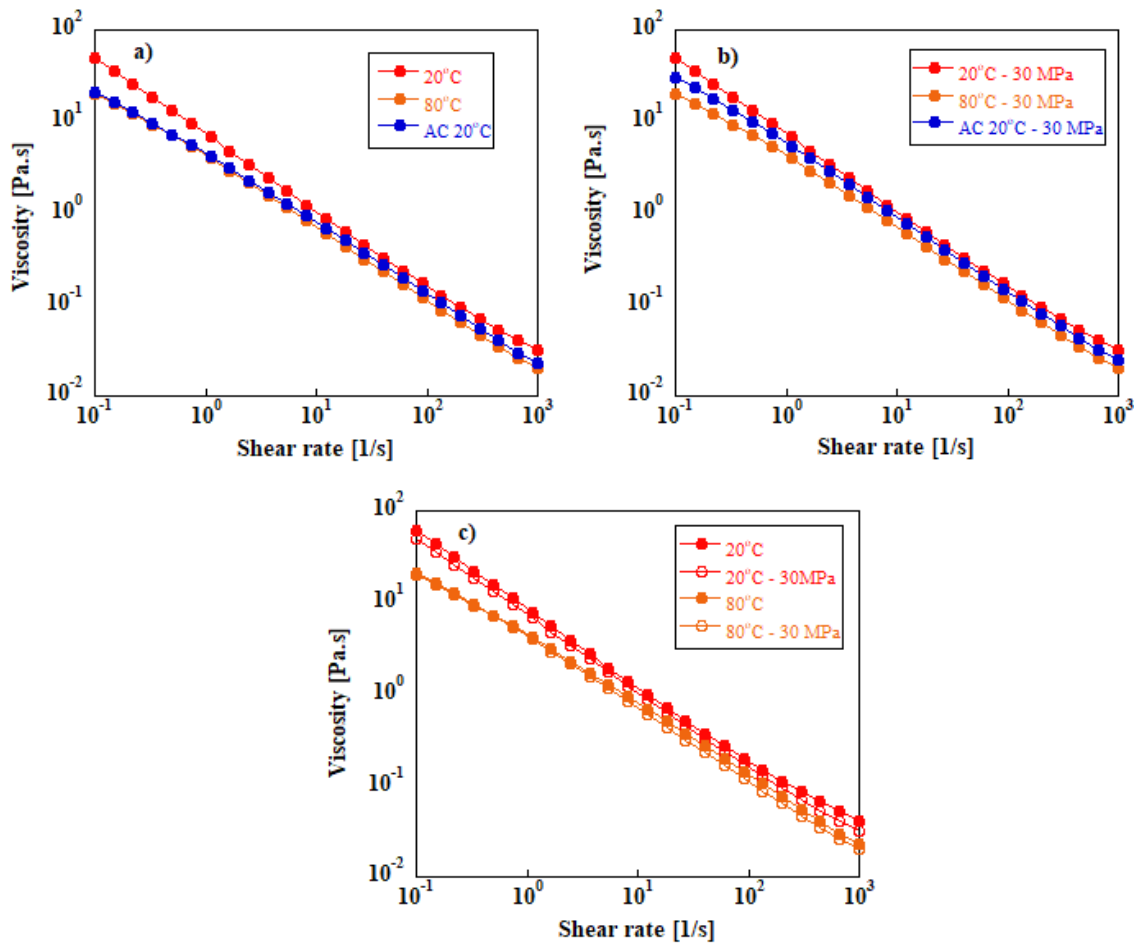


Figure 4.24 – Flow curve of XG with hBN-oxi concentration of 30 mg.mL^{-1} analyzing (a) effect of temperature at 0.1 MPa (b) effect of temperature at 30 MPa (c) effect of pressure.

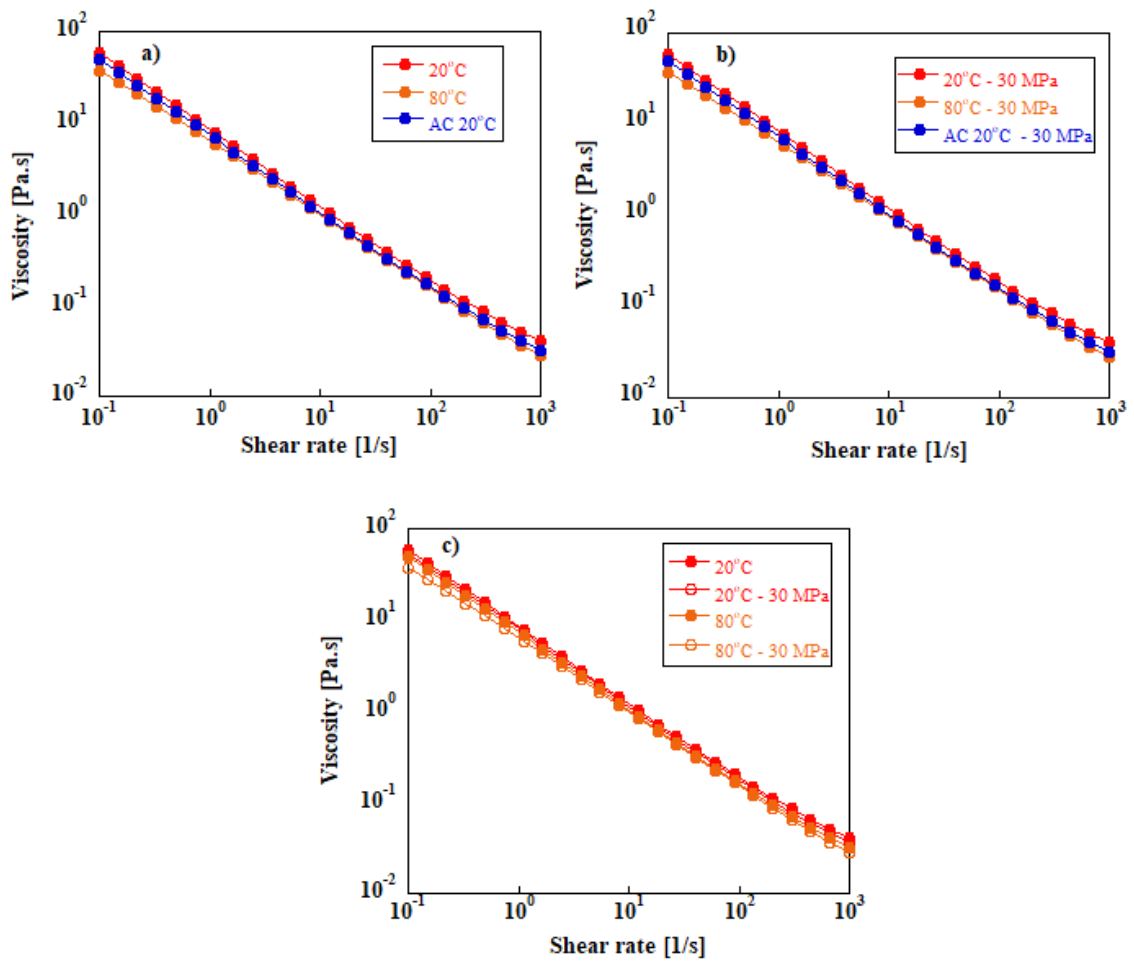


Figure 4.25 – Flow curve of XG with hBN-oxi concentration of 60 mg.mL^{-1} analyzing (a) effect of temperature at 0.1 MPa (b) effect of temperature at 30 MPa (c) effect of pressure.

5. FINAL REMARKS

In this work, the impact of hBN oxidation and exfoliation on the interaction with XG and the nanofluid stability was addressed. Moreover, the influence of concentration of oxidized hexagonal boron nitride (hBN-oxi) nanosheets, pressure and temperature on the thermal and rheological behavior of aqueous suspensions of xanthan gum was investigated. Experimental studies were conducted at different concentrations, ranging from 0 to 60 mg mL⁻¹, of hBN-oxi produced by the liquid exfoliation method.

Morphological and structural characterizations were conducted by different techniques, which showed the differences between commercial boron nitride (bulk) and exfoliated boron nitride, such as lateral size, level oxidation, and layer thickness. It was also observed that good oxidation occurred, in fact, facilitating the exfoliation process and generating nanoparticles with much smaller sizes compared to the hBN bulk.

Results from the thermal conductivity measurements showed that the conductivity of the suspension was influenced by the addition of nanoparticles since the values of conductivity increased as the concentration of hBN-oxi increased in the base fluid. The material prepared with the highest concentration studied in this work had a thermal conductivity value 7 % higher than the sample without the presence of nanoparticles.

The inclusion of different wt% of hBN-oxi nanoparticles in the base fluid, attributed to the efficient exfoliation and dispersion processes used, elevated the thermal conductivity up to 12 % at 70 °C of the produced suspensions. Additionally, at elevated temperatures, these nanostructures assisted xanthan gum suspensions in retaining their heightened thermal conductivity.

The rheological study of the nanofluids allowed the investigation of the dependence of the suspension viscosity on the shear rate. It was possible to observe that the viscosity values of all samples increased with the increasing concentration of hBN-oxi and that the suspensions with higher concentrations presented yield stress, although all suspensions presented a shear-thinning behavior. This pseudoplastic behavior can be described by the Carreau-Yasuda model for low concentration suspensions and the Herschel-Bulkley model fitted very well the suspensions with higher concentrations.

It was also observed a decrease in the viscosity of the suspension with increasing temperature, the flow curves became more stable as we increased the concentrations of hBN-oxi in the samples and finally, that the viscosity variation ($\Delta\mu$) obtained for each temperature was greater at the lowest shear rate than at the highest shear rate.

Regarding the oscillatory tests, it was possible to verify that all samples present elasticity at a low level of deformation. Moreover, it was observed that with the increase of the concentration, the modulus that characterizes the material's ability to store energy (G') is higher than the modulus that represents the ability of this material to dissipate this energy (G''). Also, it was observed that suspensions with higher concentrations of hBN-oxi presented a strain overshoot, which indicates a strong network formation.

It was also noted that both viscous and elastic moduli values decreased with increasing temperature because heat induces the breaking of intermolecular bonds, facilitates molecular mobility resulting in a lower capacity to retain and dissipate energy. An important result showed that as we increase the nanoparticle concentrations, the fluid showed higher thermal stability, since the viscosity was almost unaffected by the temperature change.

Regarding the influence of pressure on rheological properties, it was observed a slight decrease in viscosity for the pure XG and low temperature, but as the temperature increases and with the addition of the nanoparticles the pressure effect was suppressed.

The main difficulty in carrying out this research was in obtaining the hBN-oxi nanosheets. Each time this procedure was performed, only 10g of nanoparticle was obtained. The oxidation and exfoliation processes did not cause any difficulties, however the process of stabilizing the pH in the neutral range of 5.5-6.5 was a process that took a long time, around two weeks. Some other experimental limitations were in the preparation of hBN-oxi suspensions in xanthan gum. When the xanthan gum was added to the nanofluid and when the finished suspension was transferred from one bottle to another, these were delicate situations that required a lot of concentration and sometimes ended up with small losses of material, although not significant.

Thermal and rheological analyzes were also a difficult task. In thermal analyzes using the MTPS technique, we were having a problem with the

evaporation of the solvent at high temperatures and to solve this, a support was made to accommodate the gelled samples. And as for rheological analyses, the main difficulties were in the high pressure tests regarding the choice of geometry, as the geometries required a huge amount of sample, that is, a large amount of nanoparticles produced.

In this work, high concentrations of hBN-oxi were used, which are not economically viable for the industry, but very important objectives for the scientific community were achieved. Tests with lower concentrations were not having results where it was actually possible to see the impact that these nanosheets could provide in terms of changing the rheology of the suspensions and that is why tests were carried out with concentrations of 3.0 and 6.0 wt% of hBN-oxi.

The results achieved provided new perspectives on hBN-oxi nanofluids, revealing their potential to improve, in high pressure and temperature (HPHT) environments, both the rheological and thermal characteristics of base fluids composed of xanthan gum, as is the case of water-based drilling fluids. However, additional studies are needed to deepen the understanding of the fundamental chemical and physical interactions between hBN-oxi nanoparticles and any polymeric matrix.

Therefore, in addition to studies under high temperature and pressure conditions in a real drilling fluid that are already being carried out, as a suggestion for future work, studying hybrid systems would be interesting, such as hBN-oxi together with graphene oxide nanosheets, as these nanomaterials together could produce synergistic effects on the properties of nanofluids. It would also be interesting to examine the effect of hBN nanoparticles in xanthan gum suspensions on some drilling fluid properties such as pH, gel strength, filtrate loss and mud cake thickness in order to improve knowledge about hBN-oxi suspensions when exposed to high-pressure and high-temperature environments.

6. REFERENCES

Abdo, J., Haneef, M., 2012. Nano-Enhanced Drilling Fluids: Pioneering Approach to Overcome Uncompromising Drilling Problems. *J. Energy Resour. Technol.*, 134(1), p.014501.

Abdo, J., Haneef, M. D., 2013. Clay nanoparticles modified drilling fluids for drilling of deep hydrocarbon wells. *Applied Clay Science*, 86, pp. 76-82.

Agwu, O. E., Akpabio, J. U., Ekpenyong, M. E., Inyang, U. G., Asuquo, D. E., Eyoh, I. J., Adeoye, O. S., 2021. A critical review of drilling mud rheological models. *Journal of petroleum science and engineering*, 203, 108659.

Ahmadi, M. H., Mirlohi, A., Nazari, M. A., Ghasempour, R., 2018. A review of thermal conductivity of various nanofluids. *Journal of Molecular Liquids*, 265, 181-188.

Ahmed, N., Alam, M. S., Salam, M. A., 2020. Experimental analysis of drilling fluid prepared by mixing iron (III) oxide nanoparticles with a KCl–Glycol–PHPA polymer-based mud used in drilling operation. *Journal of Petroleum Exploration and Production Technology*, 10, 3389-3397.

Alcázar-Vara, L. A., Cortés-Monroy, I. R., 2018. Drilling fluids for deepwater fields: An overview. *Recent Insights in Petroleum Science and Engineering*, 71.

Alem, N., Erni, R., Kisielowski, C., Rossell, M. D., Gannett, W., Zettl, A. J. P. R. B., 2009. Atomically thin hexagonal boron nitride probed by ultrahigh-resolution transmission electron microscopy. *Physical review B*, 80(15), 155425.

Al-Khdheewi, E. A., Mahdi, D. S., 2019. Apparent viscosity prediction of water-based muds using empirical correlation and an artificial neural network. *Energies*, 12(16), 3067.

Al-Muntasheri, G. A., Hussein, I. A., Nasr-El-Din, H. A., Amin, M. B., 2007. Viscoelastic properties of a high temperature cross-linked water shut-off polymeric gel. *Journal of Petroleum Science and Engineering*, 55(1-2), 56-66.

Al-Yasiri, M. S., Al-Sallami, W. T., 2015. How the drilling fluids can be made more efficient by using nanomaterials? *American Journal of Nano Research and Applications*, 3(3), 41-45.

Amani, M., Al-Jubouri, M., Shadravan, A., 2012. Comparative study of using oil-based mud versus water-based mud in HPHT fields. *Advances in Petroleum Exploration and Development*, 4(2), 18-27.

Amani, M., Al-Jubouri, M., 2012. The effect of high pressures and high temperatures on the properties of water based drilling fluids. *Energy Science and Technology*, 4(1), 27-33.

Amanullah, M., Al-Tahini, A. M., 2009. Nanotechnology-its significance in smart fluid development for oil and gas field application. In *SPE Saudia Arabia Section Technical Symposium*. Society of Petroleum Engineers.

Ambreen, T., Kim, M. H., 2020. Influence of particle size on the effective thermal conductivity of nanofluids: A critical review. *Applied Energy*, 264, 114684.

Aminfar, H., Motallebzadeh, R., 2012. Investigation of the velocity field and nanoparticle concentration distribution of nanofluid using Lagrangian-Eulerian approach. *Journal of dispersion science and technology*, 33(1), 155-163.

Anoop, K. B., Sundararajan, T., Das, S. K., 2009. Effect of particle size on the convective heat transfer in nanofluid in the developing region. *International journal of heat and mass transfer*, 52(9-10), 2189-2195.

Anoop, K., Sadr, R., Al-Jubouri, M., Amani, M., 2014. Rheology of mineral oil-SiO₂ nanofluids at high pressure and high temperatures. *International Journal of thermal sciences*, 77, 108-115.

Anoop, K., Sadr, R., Yrac, R., Amani, M., 2016. High-pressure rheology of alumina-silicone oil nanofluids. *Powder technology*, 301, 1025-1031.

Anoop, K., Sadr, R., Yrac, R., Amani, M., 2019. Rheology of a colloidal suspension of carbon nanotube particles in a water-based drilling fluid. *Powder technology*, 342, 585-593.

Apaleke, A. S., Al-Majed, A., Hossain, M. E., 2012. Drilling fluid: state of the art and future trend. In *SPE North Africa Technical Conference and Exhibition* (pp. SPE-149555). SPE.

Aranganathan, N., Bijwe, J., Khatri, D. S., 2016. Role of combination of hexagonal boron nitride and graphite in NAO friction material. *Proceedings of the*

Institution of Mechanical Engineers, Part J: Journal of Engineering Tribology, 230(9), 1107-1112.

Ardila, L. H. Q., 2021. Rheological and thermal characterization of the effects of high pressure and high temperature on the properties of water-based drilling fluids with xanthan gum (Master's thesis, Universidade Tecnológica Federal do Paraná).

Armin, K., 2013. Advanced functional fillers for thermally conductive compounds: Key technology for cost reduction in electronic thermal management.

Asadi, A., Asadi, M., Siahmargoi, M., Asadi, T., Andarati, M. G., 2017. The effect of surfactant and sonication time on the stability and thermal conductivity of water-based nanofluid containing Mg (OH) 2 nanoparticles: An experimental investigation. International Journal of Heat and Mass Transfer, 108, 191-198.

Asme, 2005. Drilling fluids processing handbook. Elsevier.

Aybar, H. Ş., Sharifpur, M., Azizian, M. R., Mehrabi, M., Meyer, J. P., 2015. A review of thermal conductivity models for nanofluids. Heat Transfer Engineering, 36(13), 1085-1110.

Baer, D. R., Artyushkova, K., Richard Brundle, C., Castle, J. E., Engelhard, M. H., Gaskell, K. J., ... Smentkowski, V. S., 2019. Practical guides for x-ray photoelectron spectroscopy: First steps in planning, conducting, and reporting XPS measurements. Journal of Vacuum Science & Technology A, 37(3).

Bao, J., Jeppson, K., Edwards, M., Fu, Y., Ye, L., Lu, X., Liu, J., 2016. Synthesis and applications of two-dimensional hexagonal boron nitride in electronics manufacturing. Electronic Materials Letters, 12(1), 1-16.

Bardhan, A., Vats, S., Prajapati, D. K., Halari, D., Sharma, S., Saxena, A., 2024. Utilization of mesoporous nano-silica as high-temperature water-based drilling fluids additive: Insights into the fluid loss reduction and shale stabilization potential. Geoenery Science and Engineering, 232, 212436.

Barnes, H. A., Hutton, J. F., Walters, K., 1989. An introduction to rheology. Elsevier, vol. 3, rheology series.

Barnes, H. A., 1995. A review of the slip (wall depletion) of polymer solutions, emulsions and particle suspensions in viscometers: its cause, character, and cure. Journal of Non-Newtonian Fluid Mechanics, 56(3), 221-251.

Barrett, T. R., Robinson, S., Flinders, K., Sergis, A., Hardalupas, Y., 2013. Investigating the use of nanofluids to improve high heat flux cooling systems. *Fusion Engineering and Design*, 88(9-10), 2594-2597.

Behi, M., Mirmohammadi, S. A., 2012. Investigation on thermal conductivity, viscosity and stability of nanofluids. Master of Science Thesis EGI-2012, Royal Institute of Technology (KTH), School of Industrial Engineering and Management, Department of Energy Technology, Division of Applied Thermodynamics and Refrigeration, Stockholm, Sweden.

Benyounes, K., Mellak, A., Benchabane, A., 2010. The effect of carboxymethylcellulose and xanthan on the rheology of bentonite suspensions. *Energy Sources, Part A: Recovery, Utilization, and Environmental Effects*, 32(17), 1634-1643.

Bicerano, J., 2008. Drilling fluid, drill-in fluid, competition fluid, and work over fluid additive compositions containing thermoset nanocomposite particles; and applications for fluid loss control and wellbore strengthening. U.S. Patent Application 12/178,785.

Bird, R. B., Armstrong, R. C., Hassager, O., 1987. Dynamics of polymeric liquids. Vol. 1: Fluid mechanics.

Blkoor, S. O., Norddin, M. N. A. M., Ismail, I., Oseh, J. O., Risal, A. R., Basaleh, S. S., Yahya, M. N., 2023. Enhanced cutting transport performance of water-based drilling muds using polyethylene glycol/nanosilica composites modified by sodium dodecyl sulphate. *Geoenergy Science and Engineering*, 230, 212276.

Born, K., Langendorff, V., Boulenger, P., Steinbüchel, A., 2002. *Biopolymers Online*.

Bourdet, D., 2002. Well test analysis: the use of advanced interpretation models. Elsevier.

Breit, D., 2017. Existence theory for generalized Newtonian fluids. Academic Press.

Bretas, R., D'Ávila, M. A., 2005. *Reologia de polímeros fundidos*. 2a. edição. Editora: Edufscar. São Carlos.

Bui, B., Saasen, A., Maxey, J., Ozbayoglu, M. E., Miska, S. Z., Yu, M., Takach, N. E., 2012. Viscoelastic properties of oil-based drilling fluids. *Annu. Trans. Nord. Rheol. Soc*, 20, 33-47.

Caenn, R., Chillingar, G. V., 1996. Drilling fluids: State of the art. *Journal of petroleum science and engineering*, 14(3-4), 221-230.

Caenn, R., Darley, H. C., Gray, G. R., 2011. *Composition and properties of drilling and completion fluids*. Gulf professional publishing.

Callet, F., Milas, M., & Rinaudo, M., 1989. On the role of thermal treatments on the properties of xanthan solutions. *Carbohydrate Polymers*, 11(2), 127-137.

Camero, C. B., 2000. Drilling fluids design and field procedures to meet the ultra deepwater drilling challenge. In *Nigerian annual international conference and exhibition*. OnePetro.

Cao, G., 2004. *Nanostructures & nanomaterials: synthesis, properties & applications*. Imperial college press.

Cao, L., Emami, S., Lafdi, K., 2014. Large-scale exfoliation of hexagonal boron nitride nanosheets in liquid phase. *Materials Express*, 4(2), 165-171.

Carico, R. D., Bagshaw, F. R., 1978. Description and use of polymers used in drilling, workovers, and completions. In *SPE Production Technology Symposium* (pp. SPE-7747). SPE.

Carlsen, L. A., Nygaard, G., Nikolaou, M., 2013. Evaluation of control methods for drilling operations with unexpected gas influx. *Journal of Process Control*, 23(3), 306-316.

Casas, J. A.; Santos, V. E.; García-Ochoa, F., 2000. Xanthan gum production under several operational conditions: molecular structure and rheological properties. *Enzyme and microbial technology*, v. 26, p. 282-291.

Chai, Y. H., Yusup, S., Chok, V. S., Irawan, S., 2018. Bio-Based Oil Drilling Fluid Improvements through Carbon-Based Nanoparticle Additives. *Drilling*, 65.

Chen, L., Xie, H., Li, Y., Yu, W. , 2008. Nanofluids containing carbon nanotubes treated by mechanochemical reaction. *Thermochimica acta*, 477(1-2), 21-24.

Cheng, W. C., Hsieh, Y. T., Liu, W. R., 2020. Enhanced Thermal Conductivity of Silicone Composites Filled with Few-Layered Hexagonal Boron Nitride. *Polymers*, 12(9), 2072.

Chhabra, R. P., 2010. *Non-Newtonian fluids: an introduction*. Rheology of complex fluids, 3-34.

Chhabra, R. P., Richardson, J. F., 2011. *Non-Newtonian flow and applied rheology: engineering applications*. Butterworth-Heinemann.

Civan, F., 2023. Reservoir formation damage: fundamentals, modeling, assessment, and mitigation. Gulf Professional Publishing.

Coleman, J. N., Lotya, M., O'Neill, A., Bergin, S. D., King, P. J., Khan, U., ... Nicolosi, V., 2011. Two-dimensional nanosheets produced by liquid exfoliation of layered materials. *Science*, 331(6017), 568-571.

Corcioni, M., 2011. Empirical correlating equations for predicting the effective thermal conductivity and dynamic viscosity of nanofluids. *Energy conversion and management*, 52(1), 789-793.

Coussot, P., Bertrand, F., Herzhaft, B., 2004. Rheological behavior of drilling muds, characterization using MRI visualization. *Oil & gas science and technology*, 59(1), 23-29.

Da Silva, W. M., Ribeiro, H., Neves, J. C., Calado, H. D. R., Garcia, F. G. Silva, G., 2014. Multi-walled carbon nanotubes functionalized with triethylenetetramine as fillers to enhance epoxy dimensional thermal stability. *Journal of Thermal analysis and calorimetry*, 115(2), 1021-1027.

Da Silva, W. M., Monteiro, G. A. A., Gastelois, P. L., de Sousa, R. G., de Almeida Macedo, W. A., Sousa, E. M. B., 2018. Efficient sensitive polymer-grafted boron nitride nanotubes by microwave-assisted process. *Nano-Structures & Nano-Objects*, 15, 186-196.

Das, S. K., Choi, S. U., Yu, W., Pradeep, T., 2007. *Nanofluids: science and technology*. John Wiley & Sons.

Davoodi, S., SA, A. R., Soleimani, A., Jahromi, A. F., 2019. Application of a novel acrylamide copolymer containing highly hydrophobic comonomer as filtration control and rheology modifier additive in water-based drilling mud. *Journal of Petroleum Science and Engineering*, 180, 747-755.

Decol, M., Pachekoski, W. M., Segundo, E. H., Pinheiro, L. A., Becker, D., 2020. Effects of processing conditions on hybrid filler selective localization, rheological, and thermal properties of poly (ϵ -caprolactone)/poly (lactic acid) blends. *Journal of Applied Polymer Science*, 137(20), 48711.

Deshpande, A. P., 2010. Oscillatory shear rheology for probing nonlinear viscoelasticity of complex fluids: Large amplitude oscillatory shear. *Rheology of complex fluids*, 87-110.

Divoux, T., Grenard, V., Manneville, S., 2013. Rheological hysteresis in soft glassy materials. *Physical review letters*, 110(1), 018304.

Dowell, I., Mills, A., Ridgway, M., Mitchell, R. F., 2006. Petroleum Engineering Handbook, Volume II: Drilling Engineering.

Ebnesajjad, S., Ebnesajjad, C., 2013. Surface treatment of materials for adhesive bonding. William Andrew.

Echt, T., Plank, J., 2019. An improved test protocol for high temperature carrying capacity of drilling fluids exemplified on a sepiolite mud. Journal of Natural Gas Science and Engineering, 70, 102964.

Eia, U., 2016. Trends in US oil and natural gas upstream costs. US Energy Information Administration.

Eichler, J., Lesniak, C., 2008. Boron nitride (BN) and BN composites for high-temperature applications. Journal of the European Ceramic Society, 28(5), 1105-1109.

Elkatatny, S., Kamal, M. S., Alakbari, F., Mahmoud, M., 2018. Optimizing the rheological properties of water-based drilling fluid using clays and nanoparticles for drilling horizontal and multi-lateral wells. Applied rheology, 28(4), 201843606.

Engler, M., Lesniak, C., Damasch, R., Ruisinger, B., Eichler, J., 2007. Hexagonal boron nitride (hBN): applications from metallurgy to cosmetics. In CFI. Ceramic forum international (Vol. 84, No. 12). Göller.

Ertuğ, B., 2013. Powder preparation, properties and industrial applications of hexagonal boron nitride. Sintering Applications, 33.

Esfe, M. H., Esfandeh, S., Afrand, M., Rejvani, M., Rostamian, S. H., 2018. Experimental evaluation, new correlation proposing and ANN modeling of thermal properties of EG based hybrid nanofluid containing ZnO-DWCNT nanoparticles for internal combustion engines applications. Applied Thermal Engineering, 133, 452-463.

Ezell, R.G., Ezzat, A.M., Horton (Halliburton), D., Partain, E., The DOW Chemical Company, 2010. State of art Polymers fulfill the need for high temperature clay free drill in and completion fluids. Paper AADE-10-DF-HO-01. In: Presented at the AADE Fluids Conference and Exhibition. Houston, TX, 6–7 April.

Farag, W. A., Helal, M., 2023. Exploring key aspects: Structure, properties, production, and oil & gas applications of graphene and its nanoribbons– A comprehensive review. Geoenergy Science and Engineering, 212416.

Faraldos, M., Goberna, C., 2021. Técnicas de análisis y caracterización de materiales. *Técnicas de análisis y caracterización de materiales*, 1-1052.

Fazelabdolabadi, B., Khodadadi, A. A., Sedaghatzadeh, M., 2015. Thermal and rheological properties improvement of drilling fluids using functionalized carbon nanotubes. *Applied Nanoscience*, 5, 651-659.

Feng, Y., Gray, K. E., 2017. Review of fundamental studies on lost circulation and wellbore strengthening. *Journal of Petroleum Science and Engineering*, 152, 511-522.

Ferraro, J. R., Basile, L. J., 2012. *Fourier transform infrared spectra: applications to chemical systems*. Academic press.

Ferry, J. D., 1980. *Viscoelastic properties of polymers*. John Wiley & Sons.

Fuskele, V., Sarviya, R. M., 2017. Recent developments in nanoparticles synthesis, preparation and stability of nanofluids. *Materials Today: Proceedings*, 4(2), 4049-4060.

Galindo, K. A., Zha, W., Zhou, H., Deville, J. P., 2015. High temperature, high performance water-based drilling fluid for extreme high temperature wells. In *SPE international symposium on oilfield chemistry*. OnePetro.

Garcia-Ochoa, F., Santos, V. E., Casas, J. A., Gómez, E., 2000. Xanthan gum: production, recovery, and properties. *Biotechnology advances*, 18(7), 549-579.

Garg, P., Alvarado, J. L., Marsh, C., Carlson, T. A., Kessler, D. A., Annamalai, K., 2009. An experimental study on the effect of ultrasonication on viscosity and heat transfer performance of multi-wall carbon nanotube-based aqueous nanofluids. *International Journal of Heat and Mass Transfer*, 52(21-22), 5090-5101.

Gates-Rector, S., Blanton, T., 2019. The powder diffraction file: a quality materials characterization database. *Powder Diffraction*, 34(4), 352-360.

Gavrilov, A. A., Finnikov, K. A., Podryabinkin, E. V., 2017. Modeling of steady Herschel–Bulkley fluid flow over a sphere. *Journal of Engineering Thermophysics*, 26, 197-215.

Ghanbari, A., Mousavi, Z., Heuzey, M. C., Patience, G. S., Carreau, P. J., 2020. Experimental methods in chemical engineering: Rheometry. *The Canadian Journal of Chemical Engineering*, 98(7), 1456-1470.

Giannelis, E. P. (1998). Polymer-layered silicate nanocomposites: Synthesis, properties and applications. *Applied organometallic chemistry*, 12(10-11), 675-680.

Glory, J., Bonetti, M., Helezen, M., Mayne-L'Hermite, M., Reynaud, C., 2008. Thermal and electrical conductivities of water-based nanofluids prepared with long multiwalled carbon nanotubes. *Journal of applied physics*, 103(9).

Golberg, D., Bando, Y., Huang, Y., Terao, T., Mitome, M., Tang, C., Zhi, C., 2010. Boron nitride nanotubes and nanosheets. *ACS nano*, 4(6), 2979-2993.

Gonçalves, I., Souza, R., Coutinho, G., Miranda, J., Moita, A., Pereira, J. E., ... Lima, R., 2021. Thermal conductivity of nanofluids: A review on prediction models, controversies and challenges. *Applied Sciences*, 11(6), 2525.

Gorbachev, R. V., Riaz, I., Nair, R. R., Jalil, R., Britnell, L., Belle, B. D., ... Blake, P., 2011. Hunting for monolayer boron nitride: optical and Raman signatures. *Small*, 7(4), 465-468.

Gowda, R., Sun, H., Wang, P., Charmchi, M., Gao, F., Gu, Z., Budhlall, B., 2010. Effects of particle surface charge, species, concentration, and dispersion method on the thermal conductivity of nanofluids. *Advances in Mechanical Engineering*, 2, 807610.

Gowthaman, N. S. K., Lim, H. N., Sreeraj, T. R., Amalraj, A., Gopi, S., 2021. Advantages of biopolymers over synthetic polymers: Social, economic, and environmental aspects. In *Biopolymers and Their Industrial Applications* (pp. 351-372). Elsevier.

Guo, B., Liu, G., 2011. *Applied drilling circulation systems: hydraulics, calculations and models*. Gulf Professional Publishing.

Hackley, V. A., 2001. The use of nomenclature in dispersion science and technology (Vol. 960, No. 3). US Department of Commerce, Technology Administration, National Institute of Standards and Technology.

Halim, M. C., Hamidi, H., Akisanya, A. R., 2021. Minimizing formation damage in drilling operations: A critical point for optimizing productivity in sandstone reservoirs intercalated with clay. *Energies*, 15(1), 162.

Hall, P. L., 1987. Clays: their significance, properties, origins and uses. *A Handbook of Determinative Methods in Clay Mineralogy*, 1, 1-25.

Hamed, S. B., Belhadri, M., 2009. Rheological properties of biopolymers drilling fluids. *Journal of Petroleum Science and Engineering*, 67(3-4), 84-90.

Harris, A., Kazachenko, S., Bateman, R., Nickerson, J., Emanuel, M., 2014. Measuring the thermal conductivity of heat transfer fluids via the modified transient plane source (MTPS). *Journal of Thermal Analysis and Calorimetry*, 116, 1309-1314.

Hermoso, J., Jofore, B. D., Martínez-Boza, F. J., Gallegos, C., 2012. High pressure mixing rheology of drilling fluids. *Industrial & engineering chemistry research*, 51(44), 14399-14407.

Herschel, W. H., Bulkley, R., 1926. Konsistenzmessungen von gummi-benzollösungen. *Kolloid-Zeitschrift*, 39, 291-300.

Herzhaft, B., Peysson, Y., Isambourg, P., Delepouille, A., Abdoulaye, T., 2001. Rheological properties of drilling muds in deep offshore conditions. In *SPE/IADC drilling conference*. Society of Petroleum Engineers.

Higiro, J., Herald, T. J., Alavi, S., Bean, S., 2007. Rheological study of xanthan and locust bean gum interaction in dilute solution: Effect of salt. *Food Research International*, 40(4), 435-447.

Hod, O. 2012. Graphite and hexagonal boron-nitride have the same interlayer distance. Why? *Journal of chemical theory and computation*, 8(4), 1360-1369.

Hong, J., Kim, D., 2012. Effects of aggregation on the thermal conductivity of alumina/water nanofluids. *Thermochimica acta*, 542, 28-32.

Hossain, M. E., Al-Majed, A. A., 2015. *Fundamentals of sustainable drilling engineering*. John Wiley & Sons.

Hu, Y., Yue, Q., Liu, S., Fu, Z., Liang, S., 2011. Research on deepwater synthetic drilling fluid and its low temperature rheological properties. *Petroleum Science*, 8(4), 485-489.

Huang, J., Mohammed, S. M., Alsaikhan, F., Mahdi, M. H., Adil, M., Khudair, S. A., Rushchitc, A. A., 2023. DFT study of D-Penicillamine adsorption on Al and Ga doped boron nitride (Al-B₁₁N₁₂ and Ga-B₁₁N₁₂) nanoclusters as drug delivery agents. *Journal of Molecular Liquids*, 383, 122056.

Hunter, R. J., 2013. *Zeta potential in colloid science: principles and applications* (Vol. 2). Academic press.

Huynh, H. T., Roussel, N., Coussot, P., 2005. Aging and free surface flow of a thixotropic fluid. *Physics of fluids*, 17(3).

Hwang, Y. J., Ahn, Y. C., Shin, H. S., Lee, C. G., Kim, G. T., Park, H. S., Lee, J. K., 2006. Investigation on characteristics of thermal conductivity enhancement of nanofluids. *Current Applied Physics*, 6(6), 1068-1071.

Hwang, Y., Lee, J. K., Lee, J. K., Jeong, Y. M., Cheong, S. I., Ahn, Y. C., Kim, S. H., 2008. Production and dispersion stability of nanoparticles in nanofluids. *Powder Technology*, 186(2), 145-153.

Ibrahim, M. A., Jaafar, M. Z., Yusof, M. A. M., Chong, A. S., Idris, A. K., Yusof, S. R. M., Radzali, I., 2023. The effect of surface properties of silicon dioxide nanoparticle in drilling fluid on return permeability. *Geoenergy Science and Engineering*, 227, 211867.

Ilhan, B., Kurt, M., Ertürk, H., 2016. Experimental investigation of heat transfer enhancement and viscosity change of hBN nanofluids. *Experimental Thermal and Fluid Science*, 77, 272-283.

Ilyas, S. U., Narahari, M., Theng, J. T. Y., Pendyala, R., 2019. Experimental evaluation of dispersion behavior, rheology and thermal analysis of functionalized zinc oxide-paraffin oil nanofluids. *Journal of Molecular Liquids*, 294, 111613.

Irgens, F., 2014. *Rheology and non-newtonian fluids*. New York: Springer International Publishing.

Ismail, A. A., van de Voort, F. R., Sedman, J., 1997. Fourier transform infrared spectroscopy: principles and applications. In *Techniques and instrumentation in analytical chemistry* (Vol. 18, pp. 93-139). Elsevier.

Jain, R., Mahto, V., Sharma, V. P., 2015. Evaluation of polyacrylamide-grafted-polyethylene glycol/silica nanocomposite as potential additive in water based drilling mud for reactive shale formation. *Journal of Natural Gas Science and Engineering*, 26, 526-537.

Jana, S., Salehi-Khojin, A., Zhong, W. H., 2007. Enhancement of fluid thermal conductivity by the addition of single and hybrid nano-additives. *Thermochimica acta*, 462(1-2), 45-55.

Jang, H. Y., Zhang, K., Chon, B. H., Choi, H. J., 2015. Enhanced oil recovery performance and viscosity characteristics of polysaccharide xanthan gum solution. *Journal of Industrial and Engineering Chemistry*, 21, 741-745.

Jangir, A. K., Sethy, P., Verma, G., Bahadur, P., Kuperkar, K., 2021. An inclusive thermophysical and rheology portrayal of deep eutectic solvents (DES)

for metal oxides dissolution enhancement. *Journal of Molecular Liquids*, 332, 115909.

Jansson, P. E., Kenne, L., Lindberg, B., 1975. Structure of the extracellular polysaccharide from *Xanthomonas campestris*. *Carbohydrate research*, 45(1), 275-282.

Jeong, J., Li, C., Kwon, Y., Lee, J., Kim, S. H., Yun, R., 2013. Particle shape effect on the viscosity and thermal conductivity of ZnO nanofluids. *International journal of refrigeration*, 36(8), 2233-2241.

Joni, I. M., Balgis, R., Ogi, T., Iwaki, T., Okuyama, K., 2011. Surface functionalization for dispersing and stabilizing hexagonal boron nitride nanoparticle by bead milling. *Colloids and Surfaces A: Physicochemical and Engineering Aspects*, 388(1-3), 49-58.

Joseph, E., Singhvi, G., 2019. Multifunctional nanocrystals for cancer therapy: a potential nanocarrier. *Nanomaterials for drug delivery and therapy*, 91-116.

Kalhuri, N., Mousavi-Kamazani, M., Hormozi, F., 2023. Effect of CeVO₄/Al₂O₃/rGO nanocomposite on rheological properties and thermal conductivity of water-based drilling fluid. *Geoenergy Science and Engineering*, 221, 111312.

Kamibayashi, M., Ogura, H., Otsubo, Y., 2008. Shear-thickening flow of nanoparticle suspensions flocculated by polymer bridging. *Journal of colloid and interface science*, 321(2), 294-301.

Karthikeyan, N. R., Philip, J., Raj, B., 2008. Effect of clustering on the thermal conductivity of nanofluids. *Materials Chemistry and Physics*, 109(1), 50-55.

Katende, A., Boyou, N. V., Ismail, I., Chung, D. Z., Sagala, F., Hussein, N., Ismail, M. S., 2019. Improving the performance of oil based mud and water based mud in a high temperature hole using nanosilica nanoparticles. *Colloids and surfaces a: physicochemical and engineering aspects*, 577, 645-673.

Kaufmann, E. N., 2003. *Characterization of Materials*, 2 Volume Set (p. 1392).

Kawakami, K., Norisuye, T., 1991. Second virial coefficient for charged rods: sodium xanthan in aqueous sodium chloride. *Macromolecules*, 24(17), 4898-4903.

Kebllinski, P., Prasher, R., Eapen, J., 2008. Thermal conductance of nanofluids: is the controversy over? *Journal of Nanoparticle research*, 10(7), 1089-1097.

Kemp, J. W., Hmeidat, N. S., Compton, B. G., 2020. Boron nitride-reinforced polysilazane-derived ceramic composites via direct-ink writing. *Journal of the American Ceramic Society*, 103(8), 4043-4050.

Kennedy, J. F., Bradshaw, I. J., 1984. Production, properties and applications of xanthan. *Progress in industrial microbiology*, 19, 319-371.

Kermani, A. A., Aggarwal, S., Ghanbarpour, A., 2023. Advances in X-ray crystallography methods to study structural dynamics of macromolecules. In *Advanced Spectroscopic Methods to Study Biomolecular Structure and Dynamics* (pp. 309-355). Academic Press.

Khodja, M., Khodja-Saber, M., Canselier, J. P., Cohaut, N., Bergaya, F., 2010. Drilling fluid technology: performances and environmental considerations. *Products and services; from R&D to final solutions*, 227-256.

Kim, J. H., Bang, I. C., Buongiorno, J., Venerus, D. C., Prabhat, N., McKrell, T., ... Zhou, S. Q., 2009. A benchmark study on the thermal conductivity of nanofluids.

Kim, J., Lee, S., Uhm, Y. R., Jun, J., Rhee, C. K., Kim, G. M., 2011. Synthesis and growth of boron nitride nanotubes by a ball milling–annealing process. *Acta Materialia*, 59(7), 2807-2813.

Kim, J. H., Pham, T. V., Hwang, J. H., Kim, C. S., Kim, M. J., 2018. Boron nitride nanotubes: synthesis and applications. *Nano convergence*, 5(1), 1-13.

Kolle, G., Mesel, R., 1998. *Brønnvæsker: for VK1 brønnteknikk*. Nesbru: Vett & viten.

Kostoglou, N., Polychronopoulou, K., Rebholz, C., 2015. Thermal and chemical stability of hexagonal boron nitride (hBN) nanoplatelets. *Vacuum*, 112, 42-45.

Krečmarová, M., Andres-Penares, D., Fekete, L., Ashcheulov, P., Molina-Sánchez, A., Canet-Albiach, R., ... Sánchez-Royo, J. F., 2019. Optical contrast and Raman spectroscopy techniques applied to few-layer 2D hexagonal boron nitride. *Nanomaterials*, 9(7), 1047.

Krishnan, J. M., Deshpande, A. P., Kumar, P. S., 2010. *Rheology of complex fluids*. New York: Springer.

Kurt, M., 2014. Experimental investigation of thermal and rheological behavior of hexagonal boron nitride nanofluids (Master's thesis, Fen Bilimleri Enstitüsü).

Kuvandykova, D., Bateman, R., 2013. A new transient method to measure thermal conductivity of asphalt. *Thermal Conductivity* 31.

Lai, Y., Al-Musawi, T. J., Hussein, U. A. R., Waleed, I., Ahmed, H. H., Khallawi, A. Q., Alsaab, H. O., 2023. A first-principal study of pure and encapsulation boron nitride cluster with alkaline metals as the metformin drug carrier. *Journal of Molecular Liquids*, 122260.

Leffler, W. L., Pattarozzi, R., Sterling, G., 2011. Deepwater petroleum exploration & production: a nontechnical guide. PennWell Corp.

Lin, S., Chui, Y., Li, Y., Lau, S. P., 2017. Liquid-phase exfoliation of black phosphorus and its applications. *FlatChem*, 2, 15-37.

Lin, Y., Connell, J. W., 2012. Advances in 2D boron nitride nanostructures: nanosheets, nanoribbons, nanomeshes, and hybrids with graphene. *Nanoscale*, 4(22), 6908-6939.

Lipp, A., Schwetz, K. A., Hunold, K., 1989. State of the art hexagonal boron nitride: and applications* fabrication, properties. *J Eur Ceram Soc*, 5, 3-9.

Liu, W., Norisuye, T., 1988. Order–Disorder conformation change of xanthan in 0.01 M aqueous sodium chloride: Dimensional behavior. *Biopolymers: Original Research on Biomolecules*, 27(10), 1641-1654.

Liu, Y., Ye, L., Lu, H., Liu, J., 2019. Effect of Boron Nitride Particle Geometry on the Thermal Conductivity of a Boron Nitride Enhanced Polymer Composite Film. In 2019 25th International Workshop on Thermal Investigations of ICs and Systems (THERMINIC) (pp. 1-5). IEEE.

Lu, Y., Waleed, I., Al-Bahrani, M., Mutlak, D. A., Khaddour, F. A., Koka, N. A., Alwehaibi, H. M., 2023. Computational simulation of organic pollutant removal from wastewater by different porous boron nitride (PBN) nanoclusters. *Journal of Molecular Liquids*, 382, 121850.

Machado, J. C. V., 2002. Reologia e escoamento dos fluidos: ênfase na indústria do petróleo. Interciência.

Mackay, M. E., Tuteja, A., Duxbury, P. M., Hawker, C. J., Van Horn, B., Guan, Z., ... Krishnan, R. S., 2006. General strategies for nanoparticle dispersion. *Science*, 311(5768), 1740-1743.

McLean, B., J.Paga, A., 2023. Boron Nitride Nanomaterials: Properties, Fabrication and Applications. Jenny Stanford.

Macosko, C. W., 1994. Rheology principles. Measurements and Applications.

Magzoub, M. I., Kiran, R., Salehi, S., Hussein, I. A., Nasser, M. S., 2021. Assessing the relation between mud components and rheology for loss circulation prevention using polymeric gels: A machine learning approach. *Energies*, 14(5), 1377.

Mansoor, H. H. A., Devarapu, S. R., Samuel, R., Sharma, T., Ponmani, S., 2021. Experimental investigation of aloe-vera-based CuO nanofluid as a novel additive in improving the rheological and filtration properties of water-based drilling fluid. *SPE Drilling & Completion*, 36(03), 542-551.

Martin, C., 2022. Innovative drilling muds for High Pressure and High Temperature (HPHT) condition using a novel nanoparticle for petroleum engineering systems (Doctoral dissertation).

Martin, C., Nourian, A., Babaie, M., Nasr, G. G., 2023. Environmental, health and safety assessment of nanoparticle application in drilling mud—Review. *Geoenergy Science and Engineering*, 211767.

Mewis, J., Wagner, N. J., 2009. Thixotropy. *Advances in colloid and interface science*, 147, 214-227.

Mewis, J., Wagner, N. J., 2012. Colloidal suspension rheology. Cambridge university press.

Mezger, T., 2020. The rheology handbook: for users of rotational and oscillatory rheometers. European Coatings.

Mi Swaco, 2001. Engineering Drilling Fluids Manual, 1 ed.

Miri, T., 2011. Viscosity and oscillatory rheology. Practical food rheology: An interpretive approach, 7-28.

Mishra, N. S., Chandra, S., Saravanan, P., 2023. Solvent free synthesis of carbon modified hexagonal boron nitride nanorods for the adsorptive removal of aqueous phase emerging pollutants. *Journal of Molecular Liquids*, 369, 120969.

Mitchell, R. F., Miska, S., 2011. Fundamentals of drilling engineering.

Moreno, J., Lopez, M. J., Vargas-Garcia, C., Vazquez, R., 1998. Use of agricultural wastes for xanthan production by *Xanthomonas campestris*. *Journal of industrial microbiology and biotechnology*, 21, 242-246.

Morris, E. R., 1996. Rheology of xanthan: suspension of particles and stabilization of emulsions. *Food & Ingredients Journal of Japan*, 167, 31.

Morrison, F. A., 2001. *Understanding rheology*.

Munaro, M. R., Motta, H. N. D., Gulmine, J. V., Tulio, L., Adonis, N. G., Munaro, M., Kowalski, E. L., 2017. Evaluation of different routes of liquid exfoliation for the obtention of hexagonal boron nitride nanosheets. *Química Nova*, 40(9), 1018-1024.

Murshed, S. M. S., Leong, K. C., Yang, C., 2005. Enhanced thermal conductivity of TiO₂—water based nanofluids. *International Journal of thermal sciences*, 44(4), 367-373.

Nabhani, N., Emami, M., 2012. The potential impact of nanomaterials in oil drilling industry. *Nano con*, 201, 23-25.

Naganawa, S., 2015. Optimum Hydraulics Design and Operation for Extended-Reach and Horizontal Geothermal Drilling. In *Proceedings*.

Nasiri, A., Shariaty-Niasar, M., Rashidi, A., Amrollahi, A., Khodafarin, R., 2011. Effect of dispersion method on thermal conductivity and stability of nanofluid. *Experimental thermal and fluid science*, 35(4), 717-723.

Navaneethakrishnan, G., Karthikeyan, T., Saravanan, S., Selvam, V., 2019. Influence of boron nitride on morphological, mechanical, thermal and wear characteristics of epoxy nanocomposites. *Materials Research Innovations*, 24(5), 257-262.

Neff, J. M., 2005. Composition, environmental fates, and biological effect of water based drilling muds and cuttings discharged to the marine environment: A synthesis and annotated bibliography. In Report prepared for the Petroleum Environmental Research Forum (PERF). Washington DC: American Petroleum Institute.

Ng, H. Y., Lu, X., Lau, S. K., 2005. Thermal conductivity of boron nitride-filled thermoplastics: effect of filler characteristics and composite processing conditions. *Polymer Composites*, 26(6), 778-790.

Nguyen, E. P., Daeneke, T., Zhuiykov, S., Kalantar-zadeh, K., 2016. Liquid exfoliation of layered transition metal dichalcogenides for biological applications. *Current protocols in chemical biology*, 8(2), 97-108.

Nicolosi, V., Chhowalla, M., Kanatzidis, M. G., Strano, M. S., Coleman, J. N., 2013. Liquid exfoliation of layered materials. *Science*, 340(6139).

Nikaido, Y., Ichibha, T., Hongo, K., Reboredo, F. A., Kumar, K. H., Mahadevan, P., ... Nakano, K., 2022. Diffusion Monte Carlo Study on Relative Stabilities of Boron Nitride Polymorphs. *The Journal of Physical Chemistry C*, 126(13), 6000-6007.

Niu, L., Coleman, J. N., Zhang, H., Shin, H., Chhowalla, M., Zheng, Z., 2016. Production of two-dimensional nanomaterials via liquid-based direct exfoliation. *Small*, 12(3), 272-293.

Oppong, F. K., Rubatat, L., Frisken, B. J., Bailey, A. E., de Bruyn, J. R., 2006. Microrheology and structure of a yield-stress polymer gel. *Physical Review E*, 73(4), 041405.

Ouyang, J. H., Li, Y. F., Zhang, Y. Z., Wang, Y. M., Wang, Y. J., 2022. High-temperature solid lubricants and self-lubricating composites: A critical review. *Lubricants*, 10(8), 177.

Oseh, J. O., Norddin, M. N. A. M., Ismail, I., Duru, U. I., Gbadamosi, A. O., Agi, A., Risal, A. R., 2023. Rheological and filtration control performance of water-based drilling muds at different temperatures and salt contaminants using surfactant-assisted novel nanohydroxyapatite. *Geoenergy Science and Engineering*, 228, 211994.

Ozbayoglu, M. E., Saasen, A., Sorgun, M., Svanes, K., 2008. Effect of pipe rotation on hole cleaning for water-based drilling fluids in horizontal and deviated wells. In *IADC/SPE Asia Pacific Drilling Technology Conference and Exhibition*. OnePetro.

Pallares-Rusiñol, A., Bernuz, M., Moura, S. L., Fernández-Senac, C., Rossi, R., Martí, M., Pividori, M. I., 2023. Advances in exosome analysis. *Advances in Clinical Chemistry*; Elsevier: Amsterdam, The Netherlands, 112, 69-117.

Parate, N. B., 2021. A review article on drilling fluids, types, properties and criterion for selection. *International Journal of Emerging Technologies and Innovative Research*, 8(9), 463-484.

Parmar, K. P. S., Méheust, Y., Schjelderupsen, B., Fossum, J. O., 2008. Electrorheological suspensions of laponite in oil: rheometry studies. *Langmuir*, 24(5), 1814-1822.

Pelletier, E., Viebke, C., Meadows, J., Williams, P. A., 2001. A rheological study of the order–disorder conformational transition of xanthan gum. *Biopolymers: Original Research on Biomolecules*, 59(5), 339-346.

Piau, J. M., 2007. Carbopol gels: Elastoviscoplastic and slippery glasses made of individual swollen sponges: Meso-and macroscopic properties, constitutive equations and scaling laws. *Journal of non-newtonian fluid mechanics*, 144(1), 1-29.

Placet, V., Passard, J., Perré, P., 2008. Viscoelastic properties of wood across the grain measured under water-saturated conditions up to 135 C: evidence of thermal degradation. *Journal of Materials Science*, 43, 3210-3217.

Ponticorvo, E., Iuliano, M., Cirillo, C., Maiorino, A., Aprea, C., Sarno, M., 2022. Fouling Behavior and Dispersion Stability of Nanoparticle-Based Refrigeration Fluid. *Energies*, 15(9), 3059.

Power, D., Zamora, M., 2003. Drilling fluid yield stress: measurement techniques for improved understanding of critical drilling fluid parameters. In *AADE Technical Conference*, Houston (pp. 1-3).

Philip, J., Shima, P. D., 2012. Thermal properties of nanofluids. *Advances in colloid and interface science*, 183, 30-45.

Prasher, R., Phelan, P. E., Bhattacharya, P., 2006. Effect of aggregation kinetics on the thermal conductivity of nanoscale colloidal solutions (nanofluid). *Nano letters*, 6(7), 1529-1534.

Pryazhnikov, M. I., Minakov, A. V., Rudyak, V. Y., Guzei, D. V., 2017. Thermal conductivity measurements of nanofluids. *International Journal of Heat and Mass Transfer*, 104, 1275-1282.

Qiu, L., Zhu, N., Feng, Y., Michaelides, E. E., Żyła, G., Jing, D., ... Mahian, O., 2020. A review of recent advances in thermophysical properties at the nanoscale: From solid state to colloids. *Physics Reports*, 843, 1-81.

Rajwar, A., Vaswani, P., Naveena, A. H., Bhatia, D., 2022. Designer 3D-DNA nanodevices: Structures, functions, and cellular applications. In *Advances in Protein Molecular and Structural Biology Methods* (pp. 669-676). Academic Press.

Raval, N., Maheshwari, R., Kalyane, D., Youngren-Ortiz, S. R., Chougule, M. B., Tekade, R. K., 2019. Importance of physicochemical characterization of nanoparticles in pharmaceutical product development. In *Basic fundamentals of drug delivery* (pp. 369-400). Academic Press.

Rebello, L. R. B., Nicolini, J. V., Ferraz, H. C., 2023. Nanofluid formulation based on the combined effect of silica nanoparticles and low salinity water for

Enhanced Oil Recovery in sandstones. *Geoenergy Science and Engineering*, 223, 211570.

Reich, S., Ferrari, A. C., Arenal, R., Loiseau, A., Bello, I., Robertson, J., 2005. Resonant Raman scattering in cubic and hexagonal boron nitride. *Physical Review B*, 71(20), 205201.

Reiner, M., 1964. The Deborah number. *Physics today*, 17(1), 62-62.

Riaz, T., Iqbal, M. W., Jiang, B., Chen, J., 2021. A review of the enzymatic, physical, and chemical modification techniques of xanthan gum. *International Journal of Biological Macromolecules*, 186, 472-489.

Rinaudo, M., 2001. Relation between the molecular structure of some polysaccharides and original properties in sol and gel states. *Food Hydrocolloids*, 15(4-6), 433-440.

Rosalam, S., England, R., 2006. Review of xanthan gum production from unmodified starches by *Xanthomonas campestris* sp. *Enzyme and Microbial Technology*, 39(2), 197-207.

Saboori, R., Sabbaghi, S., Kalantariasl, A., 2019. Improvement of rheological, filtration and thermal conductivity of bentonite drilling fluid using copper oxide/polyacrylamide nanocomposite. *Powder Technology*, 353, 257-266.

Sainsbury, T., Satti, A., May, P., Wang, Z., McGovern, I., Gun'ko, Y. K., Coleman, J., 2012. Oxygen radical functionalization of boron nitride nanosheets. *Journal of the American Chemical Society*, 134(45), 18758-18771.

Sajjadian, M., Sajjadian, V. A., Rashidi, A., 2020. Experimental evaluation of nanomaterials to improve drilling fluid properties of water-based muds HP/HT applications. *Journal of Petroleum Science and Engineering*, 190, 107006.

Salehnezhad, L., Heydari, A., Fattahi, M., 2019. Experimental investigation and rheological behaviors of water-based drilling mud contained starch-ZnO nanofluids through response surface methodology. *Journal of Molecular Liquids*, 276, 417-430.

Shah, S. N., Shanker, N. H., Ogugbue, C. C., 2010. Future challenges of drilling fluids and their rheological measurements. In *AADE fluids conference and exhibition*, Houston, Texas.

Shi, Y., Hamsen, C., Jia, X., Kim, K. K., Reina, A., Hofmann, M., ... Kong, J., 2010. Synthesis of few-layer hexagonal boron nitride thin film by chemical vapor deposition. *Nano letters*, 10(10), 4134-4139.

Singh, S., Ahmed, R., Growcock, F., 2010. Vital Role of Nanopolymers in Drilling and Stimulation Fluid Applications. In Paper SPE 130413 presented at the SPE Annual Technical Conference and Exhibition, Florence, Italy, pp. 19-22

Souza, G. S. D., Luporini, S., Rigoli, I. C., 2017. Rheological characterization of bentonite dispersions with xanthan for oil well drilling fluids. *Materials Research*, 20, 159-166.

Stevie, F. A., Donley, C. L., 2020. Introduction to x-ray photoelectron spectroscopy. *Journal of Vacuum Science & Technology A*, 38(6).

Stenger, I., Schué, L., Boukhicha, M., Berini, B., Plaçais, B., Loiseau, A., Barjon, J., 2017. Low frequency Raman spectroscopy of few-atomic-layer thick hBN crystals. *2D Materials*, 4(3), 031003.

Sutherland, I. W., 2005. Microbial exopolysaccharides. *Polysaccharides: structural diversity and functional versatility*, 431-458.

Suri, A., Sharma, M. M., 2004. Strategies for sizing particles in drilling and completion fluid. *SPE Journal*, 9(01), pp.13-23.

Taha Tijerina, J., 2013. Multifunctional Nanofluids with 2D Nanosheets for Thermal Management and Tribological Applications (Doctoral dissertation).

Taha-Tijerina, J., Peña-Paras, L., Narayanan, T. N., Garza, L., Lapray, C., Gonzalez, J., Ajayan, P. M., 2013. Multifunctional nanofluids with 2D nanosheets for thermal and tribological management. *Wear*, 302(1-2), 1241-1248.

Taha-Tijerina, J. J., 2018. Thermal transport and challenges on nanofluids performance. *Microfluidics and Nanofluidics*, 1, 215-256.

Taha-Tijerina, J., Ribeiro, H., Aviña, K., Martínez, J. M., Godoy, A. P., Cremonuzzi, J. M. D. O., ... Castro, S., 2020. Thermal conductivity performance of 2D h-BN/MoS₂-hybrid nanostructures used on natural and synthetic esters. *Nanomaterials*, 10(6), 1160.

Tahr, Z., Ali, J. A., Mohammed, A. S., 2023. Sustainable aspects behind nano-biodegradable drilling fluids: A critical review. *Geoenergy Science and Engineering*, 211443.

Tanner, R. I., Walters, K., 1998. *Rheology: an historical perspective (Vol. 7)*. Elsevier.

Tay, R. Y., 2018. Chemical Vapor Deposition Growth and Characterization of Two-Dimensional Hexagonal Boron Nitride. In *ASM Handbook*.

Timofeeva, E. V., Routbort, J. L., Singh, D., 2009. Particle shape effects on thermophysical properties of alumina nanofluids. *Journal of applied physics*, 106(1).

Thomas, J. E., Triggia, A. A., Correia, C. A., Verotto Filho, C., Xavier, J., Machado, J., 2001. *Fundamentos de Engenharia de Petróleo*. ed. Interciência: Petrobrás, Rio de Janeiro, Brasil.

Thomas, S., Muller, R., Abraham, J., 2016. (Eds.). *Rheology and Processing of Polymer Nanocomposites*. John Wiley & Sons.

Urbaniak, W., Majewski, T., Powązka, I., Śmigielski, G., Petelska, A. D., 2022. Study of nano h-BN impact on lubricating properties of selected oil mixtures. *Materials*, 15(6), 2052.

Vahedi, A., Lahidjani, M. H. S., 2017. Tunable thermal conductivity along graphene/hexagonal boron-nitride polycrystalline heterostructures. *The European Physical Journal Plus*, 132(10), 1-7.

Vargas, R. P., M Costa, C., S Fonseca, B., F Naccache, M., de Souza Mendes, P. R., 2019. Rheological characterization of carbopol® dispersions in water and in water/glycerol solutions. *Fluids*, 4(1), 3.

Vargas, P. R., Azevedo, P. E., Fonseca, B. S., de Souza Mendes, P. R., Naccache, M. F., Martins, A. L., 2020. Immiscible liquid-liquid displacement flows in a Hele-Shaw cell including shear thinning effects. *Physics of Fluids*, 32(1), 013105.

Vendruscolo, C. T., Moreira, A. D. S., Souza, A. D. S., Zambiasi, R., Scamparini, A. R. P., 2000. Heteropolysaccharides produced by *Xanthomonas campestris* pv *pruni* C24. In *Hydrocolloids* (pp. 187-191). Elsevier Science.

Vinogradov, G. V., Malkin, A. Y., 1980. *Rheology of polymers: viscoelasticity and flow of polymers* (pp. 105-121). Moscow: Mir.

Vryzas, Z., Kelessidis, V. C., 2017. Nano-based drilling fluids: A review. *Energies*, 10(4), 540.

Wamkam, C. T., Opoku, M. K., Hong, H., Smith, P., 2011. Effects of pH on heat transfer nanofluids containing ZrO₂ and TiO₂ nanoparticles. *Journal of Applied Physics*, 109(2).

Wang, J., Bai, R. Y., Joseph, D. D., 2004. Nanoparticle-laden tubeless and open siphons. *Journal Of Fluid Mechanics*, 516, 335-348.

Wang, Y., Shi, Z., Yin, J., 2011. Boron nitride nanosheets: large-scale exfoliation in methanesulfonic acid and their composites with polybenzimidazole. *Journal of Materials Chemistry*, 21(30), 11371-11377.

Wasan, D. T., Nikolov, A. D., 2003. Spreading of nanofluids on solids. *Nature*, 423(6936), pp. 156-159

Wightman, R., 2022. An overview of cryo-scanning electron microscopy techniques for plant imaging. *Plants*, 11(9), 1113.

William, J. K. M., Ponmani, S., Samuel, R., Nagarajan, R., Sangwai, J. S., 2014. Effect of CuO and ZnO nanofluids in xanthan gum on thermal, electrical and high pressure rheology of water-based drilling fluids. *Journal of Petroleum Science and Engineering*, 117, 15-27.

Williams, P. A., Day, D. H., Langdon, M. J., Phillips, G. O., Nishinari, K., 1991. Synergistic interaction of xanthan gum with glucomannans and galactomannans. *Food Hydrocolloids*, 4(6), 489-493.

Xie, S., Istrate, O. M., May, P., Barwich, S., Bell, A. P., Khan, U., & Coleman, J. N., 2015. Boron nitride nanosheets as barrier enhancing fillers in melt processed composites. *Nanoscale*, 7(10), 4443-4450.

Xu, J., Yu, B., Zou, M., Xu, P., 2006. A new model for heat conduction of nanofluids based on fractal distributions of nanoparticles. *Journal of Physics D: Applied Physics*, 39(20), 4486.

Xu, G., Fu, J., Dong, B., Quan, Y., Song, G., 2019. A novel method to measure thermal conductivity of nanofluids. *International Journal of Heat and Mass Transfer*, 130, 978-988.

Xue, S., Yan, J. N., Du, Y. N., Jiang, X. Y., Xu, S. Q., Wu, H. T., 2021. Synergistic gelation in the hybrid gel of scallop (*Patinopecten yessoensis*) male gonad hydrolysates and xanthan gum. *Journal of food science*, 86(5), 2024-2034.

Yang, J., Jiang, G., Wang, G., Yang, L., He, Y., Dong, T., Yuan, X., 2023. Performance evaluation of polymer nanolatex particles as fluid loss control additive in water-based drilling fluids. *Geoenergy Science and Engineering*, 223, 211462.

Yang, Y., Li, Y., Yao, J., Zhang, K., Iglauer, S., Luquot, L., Wang, Z., 2019. Formation damage evaluation of a sandstone reservoir via pore-scale X-ray computed tomography analysis. *Journal of Petroleum Science and Engineering*, 183, 106356.

Ysiwata-Rivera, A. P., Hernández-Hernández, E., Cadenas-Pliego, G., Ávila-Orta, C. A., González-Morones, P., Velásquez-de Jesús, J. A., ..., Mata-Padilla, J. M., 2020. Effect of modified hexagonal boron nitride nanoparticles on the emulsion stability, viscosity and electrochemical behavior of nanostructured acrylic coatings for the corrosion protection of AISI 304 stainless steel. *Coatings*, 10(5), 488.

Yu, W., Xie, H., 2012. A review on nanofluids: preparation, stability mechanisms, and applications. *Journal of nanomaterials*, 2012, 1-17.

Zakani, B., Grecov, D., 2020. Yield stress analysis of cellulose nanocrystalline gels. *Cellulose*, 27, 9337-9353.

Zakaria, F. M., Mostafavi, V., Hareland, G., Husein, M., 2011. Design and application of novel nano drilling fluids to mitigate circulation loss problems during oil well drilling operations. In *World Nano Conference and Expo (Vol. 2011, pp. 13-16)*.

Zamora, M., Broussard, P. N., Stephens, M. P., 2000. The top 10 mud-related concerns in deepwater drilling operations. In *SPE International Petroleum Conference and Exhibition in Mexico. OnePetro*.

Zhou, K. G., Mao, N. N., Wang, H. X., Peng, Y., Zhang, H. L., 2011. A mixed-solvent strategy for efficient exfoliation of inorganic graphene analogues. *Angewandte Chemie*, 123(46), 11031-11034.

Zhou, W., Ikuhara, Y. H., Zheng, Z., Wang, K., Cao, B., Chen, J., 2023. Transmission electron microscopy (TEM) studies of functional nanomaterials. In *Modeling, Characterization, and Production of Nanomaterials (pp. 467-512)*. Woodhead Publishing.

Zyla, G., Witek, A., Gizowska, M., 2015. Rheological profile of boron nitride–ethylene glycol nanofluids. *Journal of Applied Physics*, 117(1), 014302.